CHALMERS
UNIVERSITY OF TECHNOLOGY

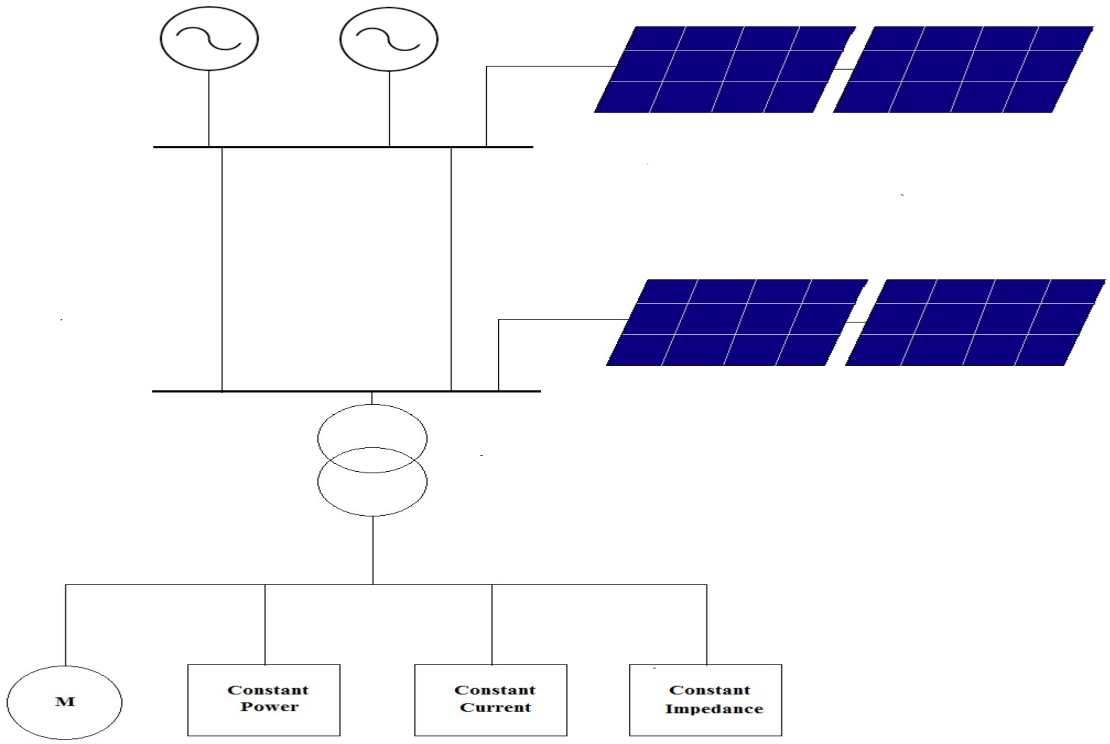

Impacts of Large-Scale Integration of Solar Photovoltaics and Load Characteristics on Power System Voltage Stability

Master's Thesis in the program of Electric Power Engineering

Baheej Alghamdi
Mohammed Alamri

Department of Energy & Environment
Division of Electric Power Engineering
CHALMERS UNIVERSITY OF TECHNOLOGY
Gothenburg, Sweden 2015

Impacts of Large-Scale Integration of Solar Photovoltaics and Load Characteristics on Power System Voltage Stability

Baheej Alghamdi &
Mohammed Alamri

In partial fulfilment for the award of Master of Science degree in Electric Power Engineering, in the Department of Environment and Energy, Division of Electric Power Engineering, Chalmers University of Technology, Göteborg, Sweden.

Supervisor & Examiner: Tuan Anh Le

Division of Electric Power Engineering

Chalmers University of Technology SE-

412 96 Göteborg

Sweden

Impacts of Large-Scale Integration of Solar Photovoltaics and Load Characteristics on Power System Voltage Stability
Master's Thesis within the Master's program, Electric Power Engineering
BAHEEJ ALGHAMDI
MOHAMMAD ALAMRI

Department of Energy and Environment
Division of Electric Power Technology
Chalmers University of Technology
SE-412 96 Gothenburg
Sweden
Telephone: + 46 (0)31-772 1000
Fax:+46 (0)31-7721633

Cover: Symbolic single line diagram that shows the interconnection of large scale photovoltaics to an existing grid with different load characteristics.

Chalmers Bibliotek , Reproservice
Gothenburg, Sweden 2015

Impacts of Large-Scale Integration of Solar Photovoltaics and Load Characteristics on Power System Voltage Stability

Master's thesis in Electric Power Engineering

Baheej Alghamdi
Mohammed Alamri

Department of Energy & Environment
Division of Electric Power Engineering
Chalmers University of Technology

Abstract

In this thesis work, the voltage stability and post disturbance voltage recovery times are investigated for the Nordic 32 test system for different load combinations with and without large scale integration of solar PV power plants. In addition, the mitigation of the voltage stability and voltage recovery time phenomena through various Dynamic Var Compensators are investigated.

The study is commenced with detailed analysis of the Nordic-32 test system that mimics the Swedish power grid through a Power System Simulation Software (PSS/E). The dynamic analysis was then done through PSS/E dynamic simulation capability to investigate the fault induced VRT (Voltage Recovery Time) through different load combinations in the system. It has been found that the voltage recovery time when induction motor loads are introduced beside complex (constant impedance and constant current) loads is significantly higher than that of the case when having complex loads only. Moreover, the system is more likely to have a voltage collapse with less number of cascaded disturbances in the case when having induction motors in the system. Also, if induction motor loads are dispersed throughout the weak buses in the system instead of being concentrated into a single bus, the voltage recovery time increases even more and the system becomes much more prone to a voltage collapse.

The improvement of the voltage stability of the system has been done through the installation of Dynamic Var Compensators at the point of common coupling with the induction motor loads. The performance of various Dynamic Var Compensators such as Static Var Compensators (SVC) and Static Synchronous Compensators (STATCOM) has been investigated in the mitigation of the voltage recovery time with different load combinations and it has been found that the STATCOM was superior to the SVC in reducing the voltage recovery time and postponing the voltage collapse. The base case with the induction motor loads was able to withstand N-1 contingency. SVCs and STATCOMs are installed at the induction motor load buses with the same rating of 300 Mvar capacitive power for both devices such that the minimum voltage sag induced due to the fault doesn't decrease below 0.8 p.u. It has been noticed that the system was able to withstand N-2 contingency for both compensators cases. For the case with SVC the voltage recovery time was reduced from 0.9 seconds in the base case to 0.665 seconds which corresponds to a reduction of 26% of voltage recovery time with a minimum voltage sag of 0.8 p.u. However, for the case with STATCOM, the voltage recovery time was reduced to 0.364 seconds that corresponds to a reduction of 60% of voltage recovery time with a minimum voltage sag of 0.87 p.u.

The effects of large scale solar PV plants penetration has been investigated. It has been found that the maximum allowable solar PV penetration is 30% of the total generation for the base case due to the limits imposed by the Nordic Grid Code for frequency deviations due to the lack of inertia for PV plants. It has been also found that the voltage stability gets worse due to the increase in the voltage recovery time in the case of 30% PV penetration, this is because the time constant for the exciter models of the conventional generating units in PSS/E is less than that of the PV model. Adding to that, the significant reactive power losses in the transmission lines since the PV plants located far away from the load center. The effect of irradiance changes with load profile changes throughout year has been investigated. It has been found that the system was more prone to a voltage instability if the share of the PV plants to the total generation of the system is significant.

Key words: Voltage Recovery Time (VRT), Photovoltaic (PV), Induction motor, Distance Relay, Voltage Collapse, Static Var Compensator (SVC), Static Synchronous Compensator (STATCOM), Irradiance, Load Profile, Voltage Stability Improvement, PSS/E.

Acknowledgments

We would like to express our deep gratitude to Dr. Tuan Le and everyone within the electric power engineering department who has helped and guided us with our master thesis without hesitation. Also, special thanks to all our loved ones who have been supporting and encouraging us during our study at Chalmers University of Technology. Thanks to the monarchy of our country, Saudi Arabia for providing unlimited support and assistance to all of the Saudi citizens who are pursuing their studies abroad.

We would also like to thank the two global companies, ABB and Saudi Aramco for granting us the scholarships to pursue the Master's Degree program and providing us with a generous support.

To all our loved ones

Table of Contents

Abstract iv

Acknowledgments vi

List of Figures xi

List of Tables xiii

List of Acronyms xiv

Chapter 1: Introduction 1

1.1 Background 1

1.2 Objective 2

1.3 Tasks 2

1.4 Overall Methodology of the Voltage Stability Analysis 2

1.5 Thesis Layout 3

Chapter 2: Background on Voltage Stability 5

2.1 Concept and Classes of Voltage Stability 5

2.1.1 Dynamic analysis 6

2.1.2 Static analysis 6

2.2 PV Curve and Voltage Stability 7

2.3 Load Characteristics 8

2.3.1 Static load models 9

2.3.2 Dynamic load models 10

2.4 Induction Motors 10

2.5 Flexible AC Transmission Systems FACTS 11

2.5.1 Static var compensator (SVC) 12

2.5.2 Static synchronous compensation (STATCOM) 12

2.6 Photovoltaic Solar Cells 13

2.6.1 Components 13

2.6.2 Characteristics 14

2.7 Literature Review of Voltage Stability 15

2.7.1 Impacts of load characteristics on voltage sag shape 15

2.7.2 Impacts of load characteristics on voltage recovery time 15

2.7.3 Impacts of connecting large scale PV arrays on voltage stability 16

Chapter 3: Modelling of the Components in PSS/E 19
3.1 Overview on the Modeled Components 19
3.2 Generator Models 19
3.2.1 Solar PV models. 19
3.2.2 Synchronous generators models 20
3.3 Load Characteristics and Models 20
3.3.1 ZIP static loads 21
3.3.2 Induction motor loads 22
3.4 Tap Changer Model 23
3.5 FACTS Models 24
3.5.1 Static Var compensators (SVC) 24
3.5.2 Static synchronous compensators (STATCOM) 27
3.6 Protective Relays: Distance Relays 29
Chapter 4: Steady State Analysis of Nordic-32 Bus Test System 31
4.1 Overview on Nordic 32 Test System 31
4.2 Steady State Analysis of the Nordic 32 System 31
4.3 Identification of the Weak Buses in the System 31
Chapter 5: Effects of Load Characteristics on Voltage Stability 37
5.1 Dynamic Voltage Analysis Setup 37
5.2 Voltage Recovery Analysis with ZIP Loads 37
5.3 Voltage Recovery Analysis with ZIP Loads Along with 20% IM on a Single Bus (1041) 40
5.4 Voltage Recovery Analysis with ZIP Loads Along with 30% & 100% IM on a Single Bus (1041) 41
5.5 Voltage Recovery Analysis with Induction Motors on All of the Weak Buses. 45
Chapter 6: Improvement of Voltage Stability 49
6.1 Improvement of Voltage Stability Through SVC 49
6.1.1 SVC rating and location 49
6.1.2 Voltage recovery time analysis with and without SVCs 51
6.2 Improvement of Voltage Stability Through STATCOM. 55
6.2.1 STATCOM rating and location 55
6.2.2 Voltage recovery time analysis with and without STATCOM 56
Chapter 7: Impacts of Large Scale Integration of Solar PV Plants on Voltage Stability 61
7.1 Solar PV Plant Location 61
7.2 Modifications to Nordic 32 System. 63
7.3 Solar PV Sizing Methodology. 64

7.4 Determination of Maximum Allowable Solar PV Penetration. 64
7.4.1 Dynamic simulation to determine the maximum PV penetration 64
7.4.2 P-V Curve analysis with different solar PV penetration levels 65
7.5 Impacts of Load Profile and Irradince Changes on Voltage Stability 66
7.5.1 Solar PV plant output power in relation to irradiance 68
7.5.2 Dynamic simulation to investigate the impacts of load profile and irradince changes on voltage stability. 68
7.6 Voltage Recovery Time Analysis with Large Scale PV Penetration 76
Chapter 8: Conclusion and Future work 81
8.1 Conclusions 81
8.2 Future work 82
References 83
Appendix A 87
Appendix B 88
Appendix C 93
Appendix D 95
Appendix E 97
Appendix F 98

List of Figures

Figure 1.1:The methodology of the voltage stability analysis 3
Figure 2.1: Thevenin equivalent circuit 7
Figure 2.2: PV curve 8
Figure 2.3: Induction motor equivalent circuit 11
Figure 2.4: The layout of an SVC 12
Figure 2.5: The layout of a STATCOM 13
Figure 2.6: Symbolic representation of a PV plant 13
Figure 3.1: The interaction between PV modules 20
Figure 3.2: Changing the characteristics of static loads through PSS/E 22
Figure 3.3: Equivalent circuit of double cage motor 22
Figure 3.4: The interface of the IMD program of PSS/E 23
Figure 3.5: Tap changer single line diagram 24
Figure 3.6: The SVC layout 25
Figure 3.7: The system's thevenin equivalent circuit with the SVC 25
Figure 3.8: SVC characteristics for given system conditions 26
Figure 3.9: The SVC CSSCST model block diagram 27
Figure 3.10: STATCOM equivalent circuit 27
Figure 3.11: The V-I characteristics of STATCOMS 28
Figure 3.12: The block diagram of STATCOM CSTCNT model 28
Figure 3.13: Distance relay protective zones 30
Figure 4.1: The layout of the Nordic 32 system 32
Figure 4.2: Load flow summary for the base case 33
Figure 4.3: P-V Curve analysis for the base case of the system at bus 4044. 34
Figure 4.4: P-V analysis for different disturbances at bus 4044 35
Figure 5.1: Voltage, consumed active and reactive power at bus 1042 38
Figure 5.2: Extended time frame for the voltage (1041 and 4044) and the consumed active and reactive power (1041) 39
Figure 5.3: Apparent impedance of the transmission line at 4041-4044 40
Figure 5.4: Bus 1041 voltage profile in two cases: with ZIP loads only (black) and with ZIP + induction (blue) 41
Figure 5.5: Bus 1041 voltage profile for ZIP, 20%, 30% and 100% induction motors 42
Figure 5.6: Bus 1041 voltage, reactive power and induction motor slip at 100% induction motor load at bus 1041 42
Figure 5.7: OLTC 4044 -1044 voltage profile and the power flow through at 100% IM loading at bus 1041 43
Figure 5.8 Apparent impedance of the transmission line at 4041-4044 (100% IM loading of bus 1041)..... 44
Figure 5.9: Terminal and field voltage, Active and reactive power of generator 1043 at 100% IM loading at bus 1041 44
Figure 5.10: Bus 1041 voltage profile for 0%, 10% and 20% IM loading at the weakest buses. 45
Figure 5.11: Apparent impedance of the transmission line at 4042-4044 (20% IM loading of the five weakest buses) 46
Figure 5.12: Apparent impedance of the transmission line at 4041-4044 (20% IM loading of the five weakest buses) 47
Figure 6.1: The voltage and reactive power consumption at bus 1041 50
Figure 6.2: The voltage recovery times with different SVC ratings. 51
Figure 6.3: The VRT with different load combination with and without SVC at T= 29-33 seconds 52
Figure 6.4: The slip of the induction motor load and voltages at bus 1041 at T=130 seconds. 53
Figure 6.5: The voltage profile at bus 1041 at T= 229-231 seconds 54

Figure 6.6: The characteristics of the distance relay at the transmission line 4042-4044. 55
Figure 6.7: Voltages at bus 1041 with STATCOMs and SVCs 56
Figure 6.8: The induction motor slip and voltages at bus 1041. 57
Figure 6.9: The slip and voltages at bus 1041. 58
Figure 6.10: The loading of the critical lines 59
Figure 7.1: Solar irradiance map according to JRC 62
Figure 7.2: Nordic-32 bus system with PV plants buses 63
Figure 7.3: Frequency deviation for 0%, 10%, 25% and 30% PV penetration when tripping 4051-1G 65
Figure 7.4: Power-voltage (P-V) curves for Nordic-32 systems with different PV penetration 66
Figure 7.5: Load profile of the Nordic-32 system during the specified hours 67
Figure 7.6: Irradiance values changes at the specified hours 67
Figure 7.7: Active power production of PV plants and conventional generators during the specified hours .. 68
Figure 7.8: The voltage profile at 6 a.m. for all of the months... 69
Figure 7.9: The voltage profile at 9 a.m. for all of the months... 70
Figure 7.10: The voltage profile at 12 a.m. for all of the months... 71
Figure 7.11: The voltage profile at 15 a.m. for all of the months... 72
Figure 7.12: The voltage profile at 18 a.m. for all of the months... 73
Figure 7.13: The voltage profile at 21 a.m. for all of the months... 74
Figure 7.14: Reactive power production at PV plant 102 for two different hours 75
Figure 7.15: Bus 1041 voltage for 0% and 30% PV penetration during the first fault..................................... 76
Figure 7.16: Bus 1041 voltage for 0% and 30% PV penetration during the first fault (extended)................... 77
Figure 7.17: Frequency deviation due to the first fault 77
Figure 7.18: Bus 1041 voltage for 0% and 30% PV penetration during the second fault 78
Figure 7.19: Bus 1041 voltage for 0% and 30% PV penetration during the second fault (extended).............. 78
Figure 7.20: Frequency deviation during the second fault 79
Figure 7.21: Voltage at bus 1041 of the 0% PV penetration system in the duration (270s-440s)..................... 79
Figure 7.22: Frequency deviation of the 0% PV penetration system in the duration (270s-440s) 80

List of Tables

Table 4.1: Loadings of the critical transmission lines 33
Table 4.2: The buses with lowest voltages. 35
Table 5.1: Timings of the distance relays that operated 40
Table 5.2: Timings of the distance relays that operated 46
Table 6.1: the parameters of the SVC controller 51
Table 6.2: The voltage recovery time for different load combinations 52
Table 6.3: The timings of distance relay operation 54
Table 6.4: The timings of distance relay operation 56
Table 6.5: The timings of the distance relay operation 58
Table 7.1: the generation of each of the solar PV penetration level 64
Table 7.2: Losses in the transmission lines for different hours 70

List of Acronyms and Symbols

PSS/E:	Power System Simulator for Engineers.
VRT:	Voltage recovery time.
IM:	Induction Motor.
ZIP:	Constant current, constant current and constant power loads.
PV:	Photovoltaic.
P-V:	Power-Voltage curves.
FACTS:	Flexible Alternating Current Transmission System.
SVC:	Static Var Compensator.
STATCOM:	Static Synchronous Compensator.
OLTC:	On-Load Tap Changer.
USRMDL:	User Defined Model.
x:	System state vector
V_B:	Bus voltage
I:	Injected current
Y_N:	Admittance matrix
***dP*:**	Change in active power
***dQ*:**	Change in reactive power
***dV* :**	Change in voltage magnitude
dr:	Change in voltage angle
J:	Jacobean matrix and A11, A12, A21 and A22 are the elements of the Jacobean matrix.
V:	Load voltage
E:	Thevenin equivalent source voltage
X:	Thevenin equivalent reactance
P :	Active power
Q:	Reactive power
n_s:	Synchronous speed in revolution per minute (rpm).
f:	System frequency.
NP:	Number of rotor poles.
n_s:	Synchronous speed of the motor
n_r:	Motor operating speed
R_1:	Stator resistance.
X_1:	Stator leakage reactance.
R_2:	Rotor resistance.
X_2:	Rotor leakage reactance.

S:	Rotor slip.
R_{c}:	Resistance of the magnetic core.
X_m:	Reactance of the magnetic core.
G:	The solar power density (W/m^2).
A:	The effective area of the solar array (m^2).
μ_1:	The efficiency of the PV array.
μ_1:	The efficiency of the inverter.
G_{max}:	the maximum solar power density in the whole day (at noon if the location at the equator).
σ:	the standard deviation of the distribution function.
i_D:	The current through the diode (A).
v_d:	The diode voltage (V).
I_s:	Leakage current (A).
η:	A constant that represent emission coefficient.
H :	Inertia constant (s),
w_m:	Rotor mechanical speed (rad/s),
w_s:	Synchronous mechanical speed (rad/s),
T_e :	Electrical torque in p.u.,
T_L :	Mechanical load-torque in p.u.
K:	Steady state gain.
T1-T4:	Parameters that influence the closed loop response of the SVC.
T5:	The time delay of the thyristor valves.
V_{OV} :	Voltage override
P_{nom}:	Nominal active power.
U:	Actual voltage.
U_{nom}:	Nominal voltage.
Q_{nom}:	Nominal reactive power.
a, b & c:	Fractions that add up to 1.

1

Introduction

This chapter introduces the goals and the main tasks of studying the implications of load characteristics and solar photovoltaic (PV) on voltage stability in the Nordic-32 system. It starts with a background that discusses the need and importance of conducting this study followed by clearly stating the objective of it. The main tasks are then defined with the required functions that are needed to accomplish each task. Finally, this chapter ends with the thesis layout that indicates the associated chapter of each task.

1.1 Background

Governments around the globe are shifting toward renewable energy resources due to economic, political and environmental issues. As a consequence, many sustainable alternatives to fossil fuel are being utilized especially solar power. Solar power is becoming an attractive choice for many countries around the globe because of the advances that have been made in the photovoltaic industry that resulted in the development of low operational cost and high efficiency PV panels. That would lead many countries to adopt large scale implementation of this sustainable energy resource in their grids which recent studies have indicated that such scenario would happen [1].

Large scale PV power plants have many components such as power electronic devices that are represented in the DC/AC converters and the maximum power point tracking that make such a system nonlinear and dependent on environmental conditions. Therefore, large scale integration of solar PV will have a significant impact on the power system stability as it has been suggested by recent studies [2]. Hence, investigation and verification of large scale implementation of solar PV generation units is one of the top priorities of electric utilities around the world.

The major element that contributes to power interruption, according to [3], and the one that will be heavily affected by the integration solar PV is the voltage instability. Voltage instability occurs when the system is heavily stressed and reactive power compensation is insufficient. Unlike synchronous machines, solar PV generation units lack the inertia associated with the rotor and that would result in significant frequency deviation if a disturbance occurs. Also, large scale PV generation units are usually located in remote areas that require long transmission lines and the voltage profile of these transmission lines will be affected. Hence the location of the PV plants will also play a significant role in the voltage stability of the system.

In addition, the power system’s load characteristics are another significant factor that affects voltage stability. It has been shown by some studies [4] that a power grid where induction motors represent a significant portion of its loads will suffer from sever post disturbance voltage recovery time. The greater the duration of the voltage recovery time, the more likelihood that some generation units both on the transmission level and the distribution level would trip and that will increase the risk of voltage stability. Consequently, the voltage profile of the system must be maintained through the utilization of various Dynamic Var Compensators. Therefore, the role of large scale implementation of solar PV on the voltage recovery time needs to be investigated.

In order to investigate the role of load characteristics and large scale solar PV implementation on voltage instability, a software based modelling tools will be utilized due to their effectiveness in simulating power oscillations. Among these modelling tools and the one that is recognized by many utilities is the power system simulator for engineers (PSS/E). It's capable of performing dynamic simulation studies of stability issues of large grids flawlessly and hence, PSS/E will be the simulation software to be used in this thesis work.

1.2 Objective

The objective of this thesis is to investigate the role of the load characteristics and the solar PV generating units on the voltage stability and the voltage recovery time along with developing mitigation procedures that involve the utilization of Dynamic Var Compensating devices and comparing their performances through the Power System Simulation Software PSS/E.

1.3 Tasks

This research investigates the role of load characteristics and solar PV units on voltage instability and voltage recovery time by fulfilling the following tasks:

- Conducting a literature review of the voltage instability and what have been done regarding this study.
- Setting up the Nordic32 bus system in PSS/E and generate a set of scenarios that involve varying the load characteristics of the system with distance protection that would lead to voltage instability of the system and ultimately voltage collapses.
- Developing a mitigation procedure for each scenario through the implementation of Dynamic Var Compensating devices and compare the performance of each of them.
- Studying the effects of large scale implementation of PV generation units on voltage stability and voltage recovery time and make a comparison of the results with the previous cases.

1.4 Overall Methodology of the Voltage Stability Analysis

The methodology of how the study is carried out is shown in Figure 1.1. In chapter 4, P-V curve analysis are made on the Nordic 32 system to identify the weakest busses of the system at which the induction motor loads will be installed in order to mimic the worst case scenario. Chapter 5 mainly focuses on the voltage stability analysis of the system with different load combinations while chapter 6 focuses on improving the voltage stability of the system through SVCs and STATCOMs and a comparison between the performance of these devices in improving the voltage stability of the system. Chapter 7 highlights the effects of large scale integration of solar photovoltaics on the voltage stability of the system through the investigation of the changes in the solar irradiance and the load profile of the system. Also, in chapter 7, the effects of the large scale integration of photovoltaics on the voltage recovery time is investigated. Finally, chapter 8 concludes the study.

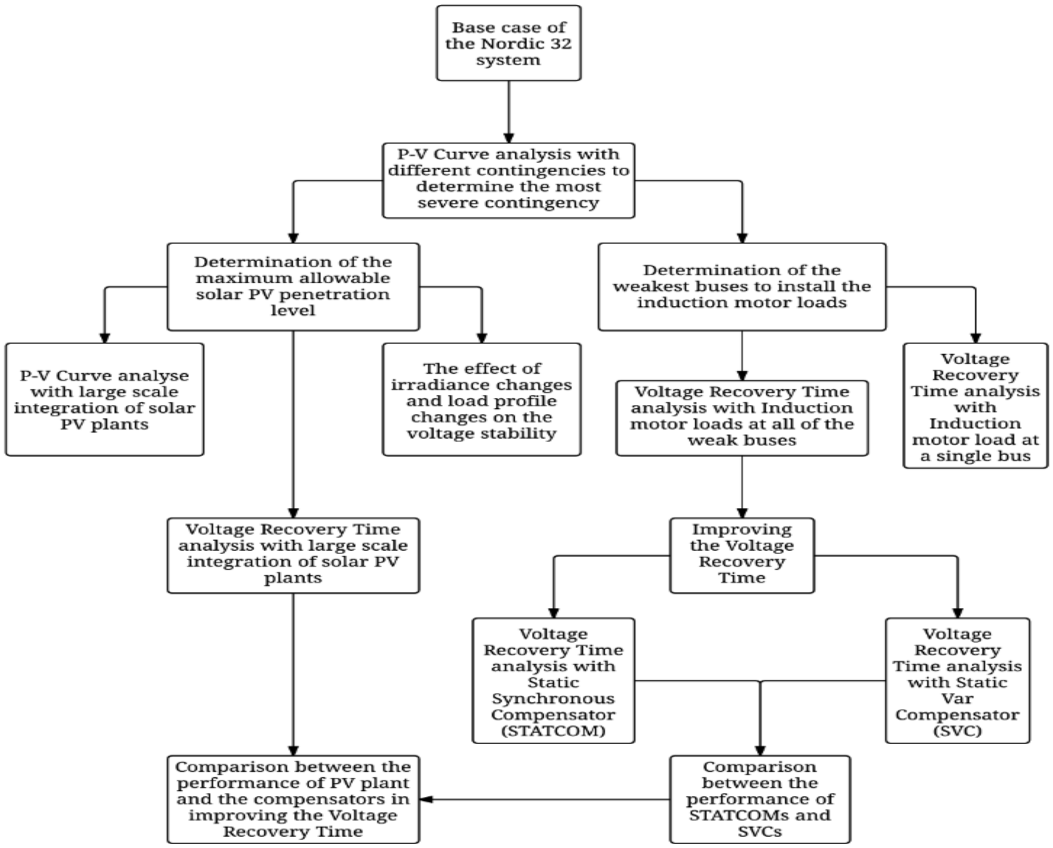

Figure 1.1: The methodology of the voltage stability analysis

1.5 Thesis Layout

The chapters of this report were designed in an order that makes the reader be able to easily connect different parts of the report and follow up with the results. The following points summarize the contents of the eight chapters:

- The second chapter of the thesis includes general review of voltage instability in literature along with the methods which are used to mitigate it and the up to date work done to investigate the voltage stability with different load characteristics and renewable energy sources.
- The third chapter highlights the important aspects of the simulation and will include the important components to be modeled in the simulation and brief literature review about them.
- The fourth chapter includes information about the Nordic-32 system, the methodology of the voltage stability analysis and steady state voltage stability analysis of the base case of the system.
- The fifth chapter explains the impacts of load characteristics on voltage stability through performing dynamic analysis in PSS/E.
- The sixth chapter discusses the mitigation of the voltage instability and the voltage recovery time through compensators.
- The seventh chapter highlights the effects of large scale implementation of solar PV plants on voltage instability and voltage recovery time.

- The eighth chapter concludes the research work with the results obtained in the previous chapters and suggests the future work that would be built on this research.

2

Background on Voltage Stability

This chapter discusses the theory part of the voltage stability. It starts with voltage stability concept and the two analysis methods (static and dynamic) that are used for deciding whether a system is stable or instable. Then, the power-voltage (PV) curve is discussed from different aspects such as how this curve is generated and how to judge on the system stability from such a curve. After that, the concept of load characteristics is highlighted with more discussion about the specifications of load types. Flexible AC Transmission Systems (FACTS) concept and its main types are also discussed with the components and the circuit diagram of each. The photovoltaic (PV) solar cell array system is then explained in terms of components, operation and output power. Finally, the impacts of load characteristics and solar PV on voltage stability is discussed based on previous researches.

2.1 Concept and Classes of Voltage Stability

According to [3], a power system is said to be a voltage stable if it succeeds to maintain voltages at all buses within an acceptable steady range under all conditions. These conditions can be classified to under normal operation and after disturbances conditions. The system is said to be voltage unstable if it fails to maintain the voltage profile within an acceptable range either during normal operation or following a disturbance. According to [3], voltage stability/instability is related to meeting the reactive power demand at system buses. Therefore, a power system is said to be voltage stable if, for every bus, the voltage magnitude increases when increasing the injected reactive power. On the other hand, it is said to be voltage unstable if the voltage magnitude decreases when increasing the injected reactive power at least at one of the buses.

According to the size of the disturbance that could lead to voltage stability, the voltage stability can be classified to two classes: Large-disturbance voltage stability and small-disturbance voltage stability. Large disturbances such as loss of big generation unit or loss of heavily loaded transmission line require performing studies of sub-transient and transient nature. Voltage stability in this case tests the system ability to maintain bus voltages after such major disturbances. For an operator, it is required to perform nonlinear dynamic analysis with time frame ranging from few seconds to tens of minutes. In this time range, the operation of on load tap changers, generator field current limiters and transmission protection can be noticed. The type of analysis used here is dynamic analysis [3].

Small-disturbance voltage stability is more related to static nature where the effect of the disturbance here on voltage stability is not as harm as the large disturbances. Examples of small disturbances are small incremental in system load or losing small distribution generator. The type of analysis used here is steady state or static analysis where the change in voltage due to such small disturbances is examined at buses. Below sections discusses both dynamic analysis and static analysis [3].

2.1.1 Dynamic analysis

Dynamic analysis is modelled using algebraic and differential equations as functions of time. These huge computations do not measure the degree of voltage instability but it explains the mechanism of the voltage stability, how the voltage changes with respect to time after large disturbance, and whether the system is able to maintain the voltage or a collapse will happen [5].

According to [3], the differential equation and the algebraic equation that are used in dynamic analysis are according to equations (2.1) and (2.2):

$$\dot{x} = f(x, V_B) \tag{2.1}$$

$$I(x, V_B) = Y_N V \tag{2.2}$$

These equations are presented in matrices including all network buses where:

x: System state vector

V_B: Bus Voltage

I: Injected current

Y_N: Admittance matrix

2.1.2 Static analysis

Voltage stability static analysis can be achieved through two study methods: Load Flow Feasibility (LFF) and Steady-state Stability (SSS). The first method, LFF, examines if the voltage profile is acceptable or not after running power flow. It is more related to the transmission lines capacity to transfer the power within the network. On the other hand, SSS method examines if the system is operating at a stable point or not when that system is represented by algebraic and differential equations. These equations are linearized around the operating point in order to obtain the steady state [5].

According to [3], one of the steady state analysis approaches is the V-Q sensitivity. This method depends on the network constraints which can be represented according to equations (2.3) and (2.4):

$$\begin{bmatrix} dP \\ dQ \end{bmatrix} = [J] \begin{bmatrix} dV \\ dr \end{bmatrix} \tag{2.3}$$

$$\begin{bmatrix} dP \\ dQ \end{bmatrix} = \begin{bmatrix} \mathrm{A11} & \mathrm{A12} \\ \mathrm{A21} & \mathrm{A22} \end{bmatrix} \begin{bmatrix} dV \\ dr \end{bmatrix} \tag{2.4}$$

where:

dP: change in active power

dQ: change in reactive power

dV : change in voltage magnitude

dr: change in voltage angle

J: Jacobean matrix and A11, A12, A21 and A22 are the elements of the Jacobean matrix.

By keeping the active power constant at all operating points and evaluating the change in voltage due to a change in reactive power, equations (2.5) and (2.6) show the new relation matrix:

$$dQ = J_R \, dV \tag{2.5}$$

$$dV = [J_R]^{-1} \, dQ \tag{2.6}$$

where J_R is the reduced Jacobean matrix. The diagonal elements of $[J_R]^{-1}$ represents the V-Q sensitivity. A positive sensitivity is an indication of stability but a negative one is an indication of instability [3].

2.2 PV Curve and Voltage Stability

PV curve can be used to measure the system stability. At a load bus, PV curve can be achieved by increasing the active power absorbed by the load and monitor what happen to the voltage. Then the voltage is plotted versus power to obtain a shape which is sometimes called “nose curve” [6].

In order to understand the relation between voltage and power, the system Thevenin equivalent circuit is presented in Figure 2.1. It consists of the equivalent voltage source (E), equivalent reactance (X) and the load by considering a lossless network [7].

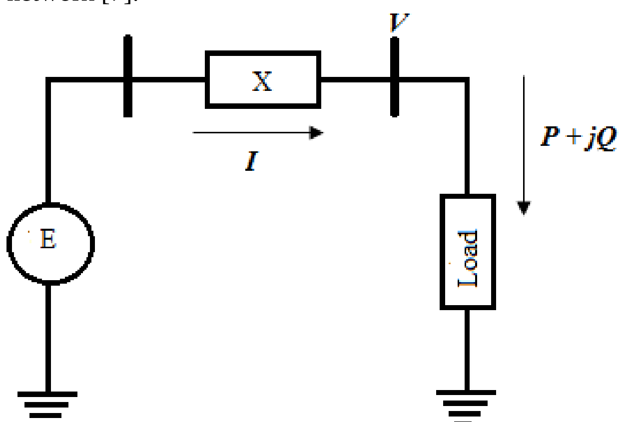

Figure 2.1: Thevenin equivalent circuit

The stability can be determined from Figure 2.2, which shows the P-V curve for 0.9 inductive power factor. The knee point of this curve is the critical point at which the voltage collapse would occur if the active power is continuously increased beyond it. The mathematical relation between the voltage and power is given according to equation (2.7) [6]:

$$V = \sqrt{\frac{E^2}{2} - QX \pm \sqrt{\frac{E^2}{4} - X^2P^2 - XEQ}} \tag{2.7}$$

where:

V: Load voltage
E: Thevenin equivalent source voltage
X: Thevenin equivalent reactance
P & Q: Active and reactive power absorbed by the load

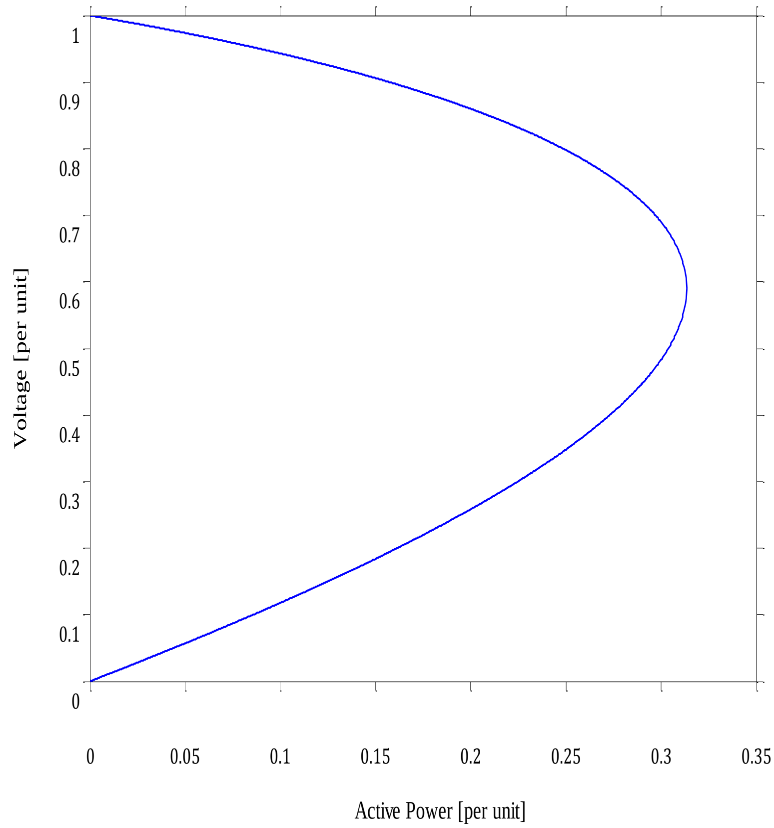

Figure 2.2: P-V curve [3]

2.3 Load Characteristics

There are different physical characteristics for different loads that make each type behave differently during transient stages. According to [8], there are mainly three types under which loads can be classified as:

- Fast dynamic response loads in terms of both: electrical and mechanical characteristics (induction motors),
- Voltage sensitive loads (discharge lighting), and
- Slow dynamic response loads (electric heating).

An example of fast dynamic response loads is the induction motors that consumes significant amount of the total power system energy. These loads almost require constant torque at all operation stages (transients and steady states). They are the most loads that contribute to voltage stability and on steady state they operate as constant power during steady state. More elaboration about induction motors and their specifications is introduced in section 2.4. In contrast, the slow dynamic loads that are mostly found in residential areas such as electric heating. These loads behave as constant resistance during transients so that when a voltage dip happens, the temperature in the electric heater (for example) will not change immediately. This is the reason why these loads are called slow dynamic loads. However, during steady state, these loads acts as constant power loads when the current and voltage are almost constants. The loads that are sensitive to voltage variations such as lighting loads that operates based on electric discharge. During voltage dips, such lighting types can distinguish at 80% voltage [8].

According to [9], loads can be represented mathematically during transients according to the relationship between power and voltage/frequency. Based on this, loads can be classified to static loads and dynamic loads as can be seen in the below sections.

2.3.1 Static load models

According to [10], a static load model represents the active and reactive powers in terms of frequency or voltage at the same moment (in this study, voltage variations are only considered). This model does not depend on previous time values of the parameters. The below models are commonly used to represent static loads according to [9].

Constant power
In this model, power does not depend on voltage changes. When voltage reduces, current increases in order to maintain constant power. The mathematical expressions for this model are shown by equations (2.8) and (2.9):

$$\frac{P}{P_0} = \left(\frac{V}{V_0}\right)^0 = 1 \tag{2.8}$$

$$\frac{Q}{Q_0} = \left(\frac{V}{V_0}\right)^0 = 1 \tag{2.9}$$

Constant impedance
In this model, power changes according to the voltage square. Therefore, when voltage reduces due to a fault, there will be severe impact on the output of such loads. The mathematical expressions for this model are shown by equations (2.10) and (2.11):

$$\frac{P}{P_0} = \left(\frac{V}{V_0}\right)^2 \tag{2.10}$$

$$\frac{Q}{Q_0} = \left(\frac{V}{V_0}\right)^2 \tag{2.11}$$

Constant current
In this model, power changes linearly according to the voltage. The active or reactive power percentage of change is the same as the voltage percentage of change. The mathematical expressions for this model are shown by equations (2.12) and (2.13):

$$\frac{P}{P_0} = \left(\frac{V}{V_0}\right) \tag{2.12}$$

$$\frac{Q}{Q_0} = \left(\frac{V}{V_0}\right) \tag{2.13}$$

2.3.2 Dynamic load models

According to [10], dynamic load model represents the active and reactive powers in terms of frequency or voltage at the past and current instants of time (in this study, voltage variations are only considered). Usually, differential equations are used in order to represent and solve this model. An example of dynamic load models is the induction motor model which is shown with more elaborations in chapter 3.

2.4 Induction Motors

Induction motors are also called rotating transformers that consumes both active and reactive power. Induction motor consists of two main components: stator and rotor. The stator is connected to the source and it is composed of stationary copper coils wounded in a special way to induce rotating flux. The rotor is the rotating part and it is composed of copper coils (or squirrel cage copper pieces) that are wounded around a poles that are connected a shaft [11].

Operation principle

As explained in [11], current flows from the power source towards the stator where the wounded coils exist which generate rotating flux. As a result of induction, another flux is generated at the rotor which is in reverse to the direction of the original flux. The resultant torque of the two fluxes makes the operation of the rotor shaft. When the induction motor is started, induction motor draws high starting current that may reach to six times its normal operating current. This is because that the motor electrical loading is almost purely reactance when the speed is zero when starting the motor. The current is then reduces while the speed increases until reaching the operating point which is slightly below the synchronous speed that is given by equation (2.14):

$$n_s = \left(\frac{120\,f}{NP}\right) \tag{2.14}$$

where:

n_s: Synchronous speed in revolution per minute (rpm).

f: System frequency.

NP: Number of rotor poles.

The equivalent circuit for the induction motor can be represented as in Figure 2.3. In the Figure: where R_1, R_2 and R_c are the resistances of the stator, rotor and magnetic core respectively and X_1, X_2 & X_m are the reactances of the stator, rotor and magnetic core respectively. The term (s) represents the slip of the motor which is given by equation (2.15) [11]:

$$s = \left(\frac{n_s - n_r}{n_s}\right) \tag{2.15}$$

where n_s is the synchronous speed and n_r is the motor operating speed.

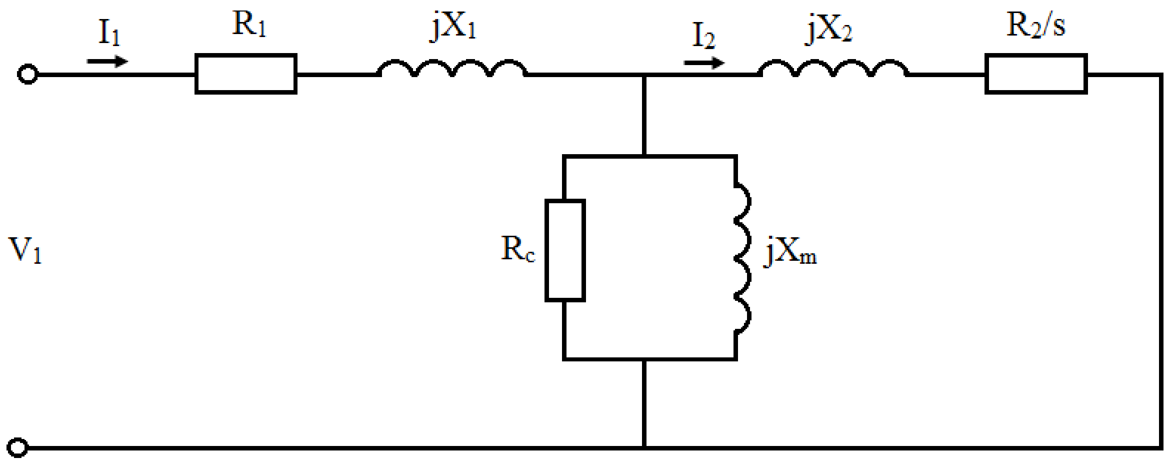

Figure 2.3: Induction motor equivalent circuit [11]

where:

R_1: Stator resistance.
X_1: Stator leakage reactance.
R_2: Rotor resistance.
X_2: Rotor leakage reactance.
S: Rotor slip.
R_c: Resistance of the magnetic core.
X_m: Reactance of the magnetic core.

2.5 Flexible AC Transmission Systems (FACTS)

FACTS are flexible AC transmission systems that are able to change some grid parameters that control the transmission lines operation. The parameters that can be changed are mainly the series and shunt impedances and as a result, the values of voltage and current will change consequently. FACTS does this function automatically without need of any mechanical operation. The change that FACTS does in system parameters offer more operation flexibility such as increasing the maximum line transfer capacity, increasing the voltage profile at system buses and reducing the transmission line losses [12].

According to [13], FACTS devices are able to control the flow of the active and reactive power and the bus voltage at the same time by their fast and continuous switching power electronics. In addition, FACTS can improve the stability, loadability and reliability of the system since the area under the power angle curve will be increased by using FACTS. This can be done without performing any change in generation schedules or network topology [13].

According to [14], there are three types of FACTS connections. They can be connected in series with a transmission line to inject a voltage in the system, reduce the line impedance and hence reduce losses. Also they can be connected in parallel to the grid at one of the buses in order to inject reactive current and reduce the reactive current flowing in the system lines. Also, FACTS can be connected to the system in combination to ensure having the benefits of series and parallel FACTS together. Figure 2.3 shows the three different connections of FACTS to a power system.

There are two main types of parallel FACTS, static var compensator (SVC) and static synchronous compensation (STATCOM). Below sections explain each of these types.

2.5.1 Static var compensator (SVC)

SVC is composed of parallel combinations of thyristor controlled reactors (TCRs) and thyristor switched capacitors (TSCs). TCR is composed of reactance in series with power electronics (thyristors) in order to do the required switching to adjust the value of the reactor. This device consumes the reactive power and hence, it is used to reduce the voltage in case of having overvoltage condition in the system [3]. On the other hand, TSC is composed of a capacitance that is connected in series with power electronics (thyristors) in order to do the required switching either to switch the capacitor on or off. TSC injects the reactive power to the system and hence, it is used to upgrade the voltage in case of having bus undervoltage [15].

Hence, SVC has the ability to operate based on a control algorithm to keep the voltage stable as shown in Figure 2.4. That means SVC can reduce the voltage at a bus by absorbing reactive power from the system through TCRs and it can upgrade the voltage by injecting reactive power to the system through TSCs [15][16].

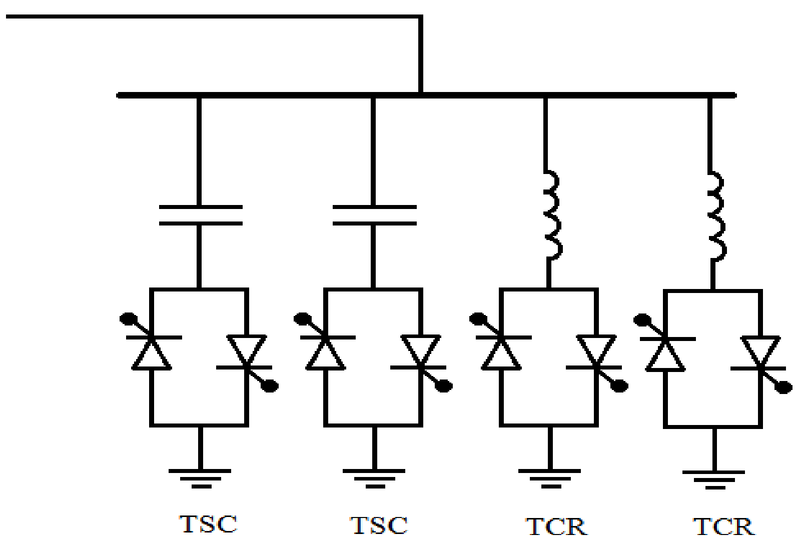

Figure 2.4: The layout of an SVC [12]

2.5.2 Static synchronous compensation (STATCOM)

STATCOM as shown in Figure 2.5, is composed of fixed capacitor and voltage source convertor (VSC) to convert the DC output of the capacitor to AC. The voltage source convertor is composed of power electronics (mainly thyrisotrs) that will do the required switching according to the required pulse width modulation. STATCOM is connected in parallel to the bus where the compensation is required and it can provide active and reactive power to the network which makes it different from SVC [17 & 18].

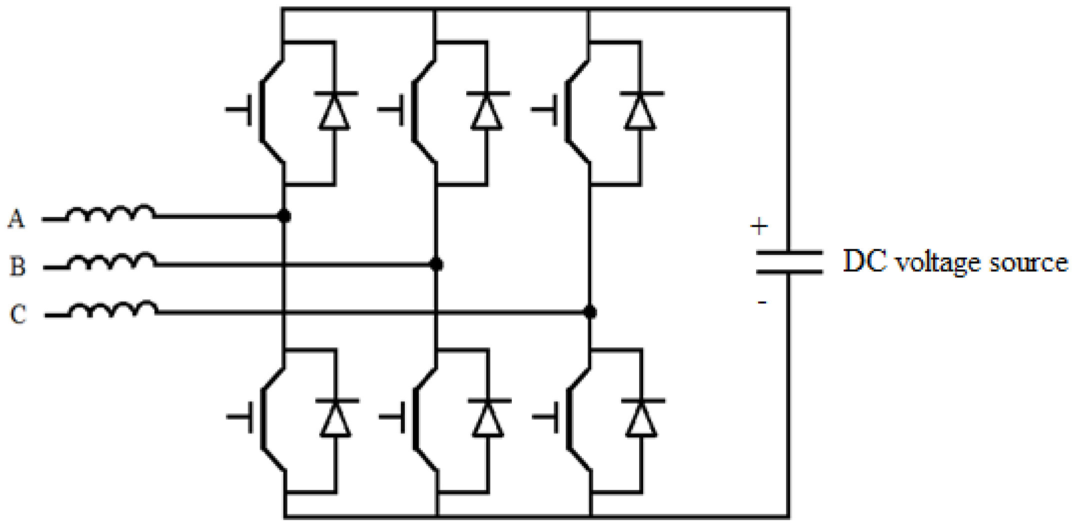

Figure 2.5: The layout of a STATCOM [12]

2.6 Photovoltaic Solar Cells

Grid connected PV has proved several long term benefits related to its lower operation and maintenance cost in addition to producing green electricity without pollution. On the other hand, there are some challenges related to its high capital costs and the optimal utilization of solar power taking in consideration this energy is variable from one hour to another, from day to another and from season to another. To solve the technical part that is related to the varying nature of solar power, a maximum power point tracker (MPPT) is used because of the changing temperature and irradiation to obtain the maximum output power from a solar PV. There are three main systems where the PV arrays are mostly connected: 1) Satellite applications, 2) Remote (isolated) areas and 3) Grid connected applications [19]. In this research, we are more interested in studying the impacts of the grid connected type on voltage stability.

2.6.1 Components

There are two main components as can be seen in Figure 2.6: PV array panel and power electronic converter unit. When sun irradiation hits the photovoltaic units, DC current is generated and transferred by electric wires to the power conditioning unit where the converter inside transforms the power from DC to AC. The produced power can be transferred to the grid or stored in batteries for later use [19].

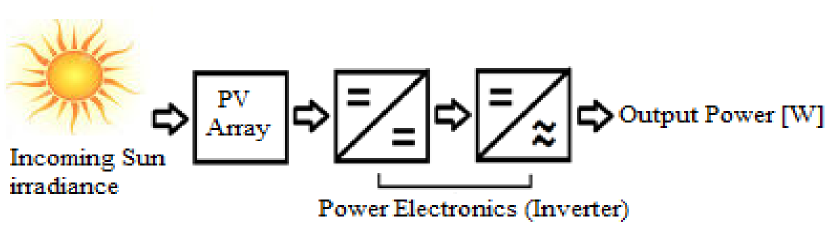

Figure 2.6: Symbolic representation of a PV plant

2.6.2 Characteristics

As shown in [20], the output power of a PV array is intermittent and is dependent on the availability of the solar irradiance. The output power of a PV array can be written as:

$$P_{out} = G \times A \times \mu_1 \times \mu_2 \tag{2.16}$$

where,

G: The solar power density (W/m^2).

A: The effective area of the solar array (m^2).

μ_1: The efficiency of the PV array.

μ_1: The efficiency of the inverter.

The solar power density G can peak to very high values during the day, it could reach a value up to more than 800 W/m^2. If weather conditions are neglected the solar power density can be expressed as a normal distribution function according to [20]:

$$G = G_{max} e^{\frac{-(t-t_o)^2}{2\sigma^2}} \tag{2.17}$$

where,

G_{max}: the maximum solar power density in the whole day (at noon if the location at the equator).

σ: the standard deviation of the distribution function.

A large standard deviation translates into wider area under the normal distribution curve which means more energy will be obtained through the day. However, at high latitudes as in the case of Sweden, the value of the standard deviation becomes smaller in the winter and bigger in the summer. A Solar PV plant would consists of PV arrays, each array has several solar panels and each solar panel has several solar cells. The solar cell can be estimated as a reversed biased diode and a current source and the diode current can be written as follows according to [20]:

$$i_D = I_s \left(e^{\frac{v_d}{\eta V_T}} - 1 \right) \tag{2.18}$$

where,

i_D: The current through the diode (A).

v_d: The diode voltage (V).

I_s: Leakage current (A).

η: A constant that represent emission coefficient.

The load current i_L can be written in terms of the source current (I_C) and diode current (i_D) as:

$$i_L = I_C - i_D = I_C - I_s \left(e^{\frac{v_d}{\eta V_T}} - 1 \right) \tag{2.19}$$

According to [20], when there is no load the open circuit voltage across the solar cell circuit can be written as:

$$V_{OC} = V_T \times \ln \left(\frac{I_c}{I_s} + 1 \right) \tag{2.20}$$

2.7 Literature Review of Voltage Stability

The following sections address some of the up to date researches and studies about the impacts of load characteristics and solar PV integration on voltage stability.

2.7.1 Impacts of load characteristics on voltage sag shape

According to [21], the effect of having induction motors appears clearly in the shape of the sag that can be induced by applying fault as example. Without induction motors the shape of the sag is almost rectangular and defined by sharp drop and rising at the beginning and at the end respectively. But in the case with induction motors, the voltage magnitude drops sharply just after the fault moment and then continues decreasing until fault clearing, voltage collapsing, or reaching deep point if the system is rigid. From the study in [21], it was found that the voltage magnitude in the case with induction motors, does not return immediately to the pre-fault condition after clearing the fault.

The reason why the shape of the sag was not rectangular was interpreted by looking at the values of the active power, reactive power, and current absorbed by one of the induction motors. It was found that the induction motor immediately after the fault turned to be generator and started supplying active and reactive power to the fault instead of consumption. Because of energy conservation law, the energy stored in the trapped flux did not change immediately at the moment of the fault. Moreover, the internal transient induced electromotive force (emf) did not change immediately but forced active and reactive power to flow out of the motor. As mentioned earlier that the voltage with induction motor does not reduce to the deepest point immediately after the fault due to the reactive power contribution of the induction motor. Also, it was found that the voltage at the bus where the induction motor installed is slightly higher that the faulted bus during the fault. The trapped flux energy started decreasing after the first moment of fault as the emf started decaying. On the other hand, a negative electrical torque is induced due to the negative flow of the active power and this resulted in slowing down the motor and increasing the slip [21].

Practical effects on induction motors due to its dynamic nature during sags were presented in [22]. It shows the quantitative effects in the operation of induction motors during voltage dips by applying experiments. The obtained results shows probable damages in the structure of an induction motor such as shafts or bearings. Also, voltage dips could degrade the wires insulation due to heat that results from the increase in current consumed by a motor due to voltage sags. It was found from the experiments that the more frequent occurrence of voltage sags will result in more mechanical damages such as vibrations and may cause loss of an induction motor lifetime [22].

2.7.2 Impacts of load characteristics on voltage recovery time

According to [21], voltage recovery delay was noticed after clearing the fault. It was studied by looking at the electrical and mechanical torques and the speed of the motors. It was found that the voltage recovery time is related to the amount of speed loss during the fault and this depends on the fault clearing time and the characteristics of the mechanical torque. It was found that the mechanical torque with constant characteristics is the most severe case in terms of the delay in recovery time [21].

The contents of [23] explain theoretically why there is a delay in the voltage recovery at a motor bus by the concept of the terminal voltage and back emf. During normal operation the emf voltage is lower than terminal voltage which results in the normal flow of current towards the motor. However, during voltage dip, and because of the sub-transient time constant of the motor, the emf voltage delays to decay which cause the current flow to be out of the motor. At this stage, the rotor speed drops causing further decay in the emf voltage. The emf will continue decaying until it becomes lower than the terminal voltage and the current will flow again towards the motor. The current flow will increase with the decay in emf and motor speed will continue decreasing causing more voltage drops and leading to motor stalling or voltage collapse. At the case when having long dip durations or more induction motor loads, the decay in emf moves faster and deeper causing the emf to become lower than the terminal voltage in a fast manner [23].

In [24], a voltage recovery comparison between three motors having different inertia constants using a dynamic induction motor model along with single phase quadrated power flow model. The inertia constants give an indication about how the motors accelerate or decelerate due to changes in motors characteristics based on equation (2.21) according to [23]:

$$\frac{2H}{w_S}\frac{dw_m}{dt} = T_e - T_L \tag{2.21}$$

where:

H : Inertia constant (s),

w_m: Rotor mechanical speed (rad/s),

w_s: Synchronous mechanical speed (rad/s),

T_e : Electrical torque in p.u.,

T_L : Mechanical load-torque in p.u.

According to [23], when voltage dip occurs, motor deceleration depends on voltage level and on the mechanical load characteristics. Mechanical load characteristics could be constant torque or it may depend on the speed depending on the nature of the process load. For constant mechanical torque, as the voltage sag becomes deeper, T_e becomes smaller causing the deceleration rate higher (more delay in voltage recovery) and vice versa. Also, as the inertia constant increases, it results in smaller deceleration rate which when fault is cleared, the voltage recovers faster [23].

The contents of [25] stress that the relation between transient stability and induction motor response during disturbances is whether the induction motor will be able to re-accelerate after deceleration or it will stall. The impact of fault location was introduced and it was found that the closer the fault location to induction motor bus, the deeper voltage sag. Because the faults durations were selected short, all motors were able to reaccelerate but with deeper voltage sag for the closest fault location as mentioned earlier. The second part of study is to examine the impact of fault duration on the shape of voltage sag. It was found that three induction motors at three different load centres were able to reaccelerate after clearing the fault in 4-5.5 cycles. However, when the fault clearing time increased to 5-6.5 cycles, one of the motors continued deceleration even after clearing the fault which indicates the importance of having compensation devices and fast fault clearing relays.

2.7.3 Impacts of connecting large scale PV arrays on voltage stability

The consequences on static voltage stability due to connecting PV arrays to a grid have not been adequately assessed in [26]. According to this paper, the integration of large scale PV gives good results when doing static analysis where the system losses are reduced and the maximum loading of the transmission lines is increased. Hence, the lines voltage drop will be reduced and in case of a fault, the bus voltages will experience less reduction in existence of PV compared to the system without PV. This is regarding static voltage stability analysis.

According to [27], and in agreement with [26], solar PV can improve static voltage stability but not as much as wind turbine can do. This is due to the fact that wind turbine can support the system with reactive power larger than what solar PV can do. However, when the renewable generation is compared with conventional generation, the difference can be seen by the high capability of conventional generators to support the system with larger amounts of reactive power.

According to [28], the philosophy of solar PV control mode affects the static voltage stability. It is stated that when the control mode is set as current source, the PV model will not generate reactive power during normal operation regardless of the output active power but will absorb the reactive power instead in practical applications. However, when the mode is set as voltage source, the PV model will absorb less amount of reactive power and will not affect the voltage stability as much as current source mode does during normal operation. It was recommended by [28] to install dynamic compensators for both types of mode to improve voltage stability.

However, static voltage stability analysis is performed without taking the constraints in consideration such as excitation limits. This could lead to overestimating the stability margin and giving wrong results about the voltage stability. This is not the case when performing dynamic analysis where the mechanism of voltage stability is shown verses time domain and taking in consideration the effects of non-linear elements such as OLTC and the constraints of the installed devices [29]. This research concluded that the effectiveness of solar PV to impact positively on dynamic voltage stability depends on how controller settings are appropriately selected. Moreover, inappropriate settings will not only inhibit improving the dynamic voltage stability but may negatively affect it. The main factors that may influence dynamic voltage stability are network characteristics, reactive power reserves at generation plants and operational constraints of control equipment.

Paper [30] gives a solution for the stated problem in [29] regarding PV controller settings when it suggested an inverter based control algorithm that provides fast reactive power support and three modes of active power control: fixed output mode, maximum power point tracking (MPPT) mode and automatic switching mode between the two modes. This algorithm can operate effectively for a wider range of weather conditions and for transient operation disturbances.

In [31], transient stability and voltage stability were examined with reconnecting large solar PV plants as a mitigation. The obtained results revealed that the transient stability does not improve by necessity when reconnecting solar PV plants after faults. Moreover, it was found that solar PV generations will lead to deterioration of the transient stability when the ratio of constant impedance loads to constants power loads is high. Regarding voltage stability, it was found that voltage stability will improve with fast reconnection of solar PV in the case when having induction motors.

The distribution voltage stability was discussed in [32] with high PV penetration level without reactive power generation in the IEEE-13 bus system. The obtained results proves that voltage instability takes place when having 40% PV penetration for due to irradiance changes. This ignite in mind the permanent need for conventional generation putting in mind that PV output power may drop from maximum to minimum in seconds due to cloud fluctuations. But the results also show that voltage instability will not mostly happen due to cloud fluctuations when having PV with 20% penetration and also 20% power storage at tiny residential network. From reactive power aspect, when the PV inverter was installed to support the distribution network with reactive power, it improved voltage stability and replaced the installation of compensator devices.

3

Modelling of the Components in PSS/E

PSS/E has the capability to perform both steady state analysis and dynamic analysis. The dynamic simulation is to be utilized since it's capable of simulating the dynamic behavior of every component in the system during a disturbance and post disturbance conditions. PSS/E comes with hundreds of built-in load models, generation models, tap changers models and reactive compensation models which will be discussed in this chapter. Therefore, Proper selection of the built in models to simulate the system to give an accurate details that match real life scenarios is very important.

3.1 Overview on the Modeled Components

The analysis of the system will begin with the base case of the Nordic-32 bus test system. In the base case, the synchronous generators models, the tap changers models are present. Further models will be added to the system as a progress has been achieved with the analysis. The models to be added to the system are: Load models, these include induction motor models and complex load models. Distance Relay models will be added to demonstrate the role of protection devices on voltage instability. Furthermore, Dynamic Var Compensating devices and solar PV models will be added as necessary for the voltage instability analysis. The input parameters of the models will be mainly based on previous publications [33] and [34]. However, some times the input parameters need to be adjusted slightly to avoid causing the PSS/E program becomes unstable. The documentations that come with PSS/E provide useful information on how to set up the models.

3.2 Generator Models

Two generator models to be used in the system are the synchronous generator model and solar PV model to represent the effects of large scale integration of solar PV on the Nordic-32 bus test system.

3.2.1 Solar PV models.

In the beginning of the simulation, synchronous generators will be dominant in the network. Then solar PV units will be added gradually till they represent a huge portion of the generation units as will be illustrated later in chapter 7. This has been done in order to observe the effects of solar PV units on the network. A complete system of a solar PV plant with its components is shown in Figure 3.1.

PSS/E has a built in generic type 4 wind turbine model WT4 that could be configured such that it would behave as a PV plant. The generic wind model WT4 that could be configured as a PV model has four sub modules:

- IRRAD: the solar irradiance profile module.
- PANEL: module of a PV panel output curve.
- PVEU: Electrical control module.
- PVGU: Inverter module.

The inverter module PVGU calculates the active and reactive to be injected to the grid based on the commands of the electrical control module PVEU. The active power control make a comparison between the active power to be supplied to the grid versus the reference power and adjust it accordingly. The reference power is controlled by the amount of DC power coming from the PANEL module. The panel module calculates the DC power from the PV plant at a specified irradiance level. The maximum DC power a panel could produce at a given irradiance level can be specified by the user. The specifications and entry parameters that are used in this research for the four PV models can be found in Appendix D. Figure 3.1 shows the interaction between the modules. Further information can be found in PSS/E documentations [35].

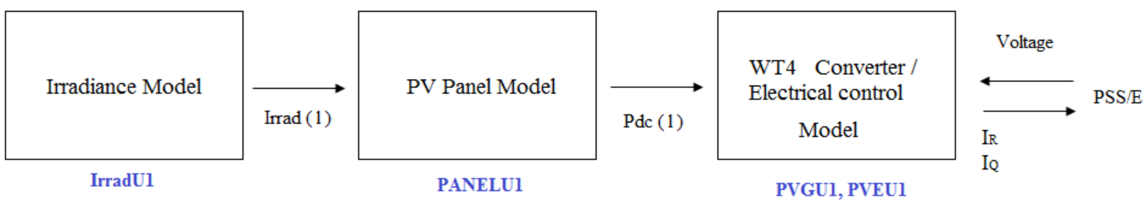

Figure 3.1: The interaction between PV modules in PSS/E [35].

3.2.2 Synchronous generators models

In the Nordic 32 system, generators are either thermal or hydro. Both types have their own characteristics. The hydro generation units are represented by the salient pole model GENSAL while the thermal units are represented by the round rotor machine model GENROU.

For the excitation systems of the generators, a general purpose exciter has been used which SEXS which is useful when the excitation system needs to be modeled but the detailed design is not known. The data for generators, their transformers and ratings including the PSS/E models that have been used to model them are taken from a previous publication [34]. As a progress is made within the thesis, the parameters of the synchronous generators will be modified as necessary for the study. The parameters for generators models, governors, stabilizers and excitation limiters can be found in [34].

3.3 Load Characteristics and Models

In the base case of the Nordic 32 system, all of the loads are modeled as static constant MVA loads. However, these constant MVA loads could be adjusted easily to be either constant impedance, constant current or constant power (ZIP loads). Dynamic loads such as induction motors could also be added easily to the system as necessary for the analysis. Furthermore, complex loads that consist of different types of motors and distribution transformers are also available. The composition of the loads in the network has a significant effect on the voltage stability and the voltage recovery time during post disturbances [3]. Based on loads dynamic response to disturbances, the voltage recovery time, which is considered as an indicator for voltage stability, is affected.

During post disturbance, tap changing transformers attempt to restore the power consumption of the loads and induction motor torque-speed characteristics would change and will draw very high current from the grid. This will ultimately make the generation units and shunt compensation devices hit their maximum reactive power production capacity and the system will be in greater risk of voltage instability [3].

3.3.1 ZIP static loads

ZIP means a load that is composed of constant power, constant current, and constant impedance characteristics. A constant power load doesn't change its power consumption with the variation of the voltage while the power consumption of constant current and constant impedance loads change with the variation of the voltage. These load characteristics are represented by the following functions [35]:

$$P = P_{nom}\left(a\left(\frac{U}{U_{nom}}\right)^{0} + b\left(\frac{U}{U_{nom}}\right)^{1} + c\left(\frac{U}{U_{nom}}\right)^{2}\right) \tag{3.1}$$

$$Q = Q_{nom}\left(a\left(\frac{U}{U_{nom}}\right)^{0} + b\left(\frac{U}{U_{nom}}\right)^{1} + c\left(\frac{U}{U_{nom}}\right)^{2}\right) \tag{3.2}$$

where:

P:	Actual active power.
P_{nom}:	Nominal active power.
U:	Actual voltage.
U_{nom}:	Nominal voltage.
Q:	Actual reactive power.
Q_{nom}:	Nominal reactive power.
a, b & c:	Fractions that add up to 1.

In the dynamic analysis, the characteristics of the static loads will be 100% constant current for the active power consumption and 100% constant impedance for the reactive power consumption. In PSS/E it's relatively easy to change the composition of the existing static loads to any characteristic. This can be done by the load conversion function as shown in Figure 3.2.

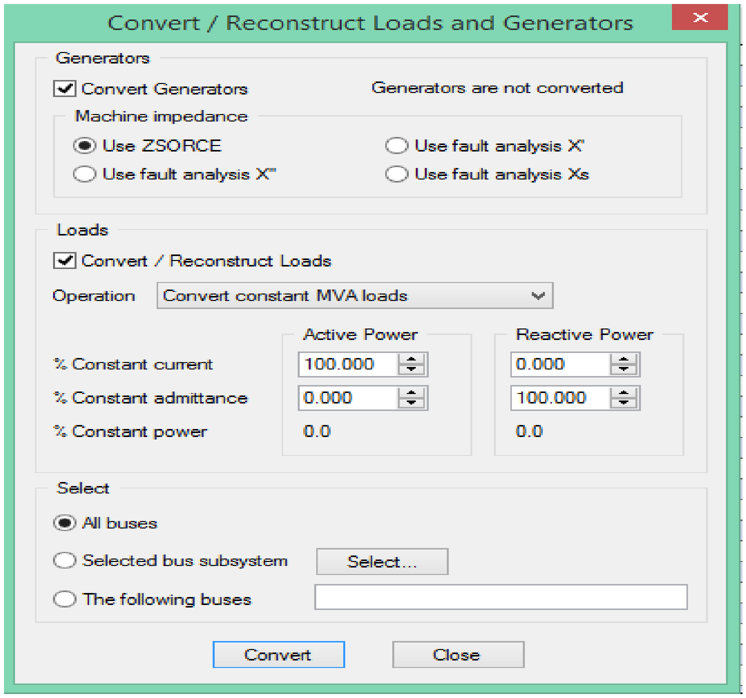

Figure 3.2: Changing the characteristics of static loads through PSS/E

3.3.2 Induction motor loads

In PSS/E, it is possible to model both double cage and single cage induction motors with the rotor flux dynamics. To model the induction motor in PSS/E, they do not need to be installed in the single line diagram. When the induction motor model is loaded onto the dynamic simulation in PSS/E, it converts the existing load power consumption to the motor power consumption and together with the motors circuit parameters, it will calculate the initial slip. To determine the parameters of the equivalent circuit of the induction motor as shown in Figure 3.3, an auxiliary program that comes with PSS/E called IMD must utilized.

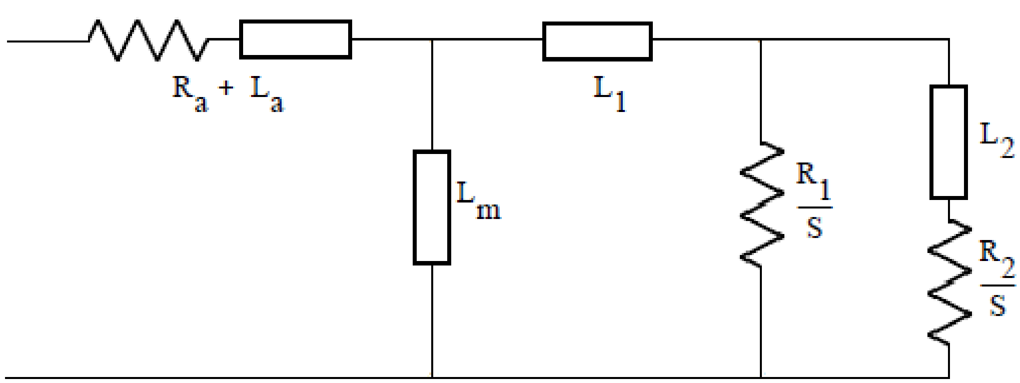

Figure 3.3: Equivalent circuit of double cage motor [35].

The interface of the IMD program is shown in Figure 3.4. The motor power should be set equal to the load bus at which the motor to be used and the power factor should equal to the load bus power factor. Also, the current needs to be 1 p.u. that is done by varying the parameters within the program through an iterative process till the power factor and the current are within the desired values.

Then, once equivalent circuit parameters have been obtained, they will be used to build up the model of the induction motor in the dynamic file. There is only one dedicated induction motor model within PSS/E that has been used in almost all of the studies that are related to voltage stability analysis. The name of the model is **CIM5BL;** the model provides a realistic dynamics of an actual induction machine. The induction motor models will be installed on the weakest buses in the system to represent the worst case scenario [35]. The specifications and entry parameters that are used in this research for the induction motor model can be found in Appendix B.

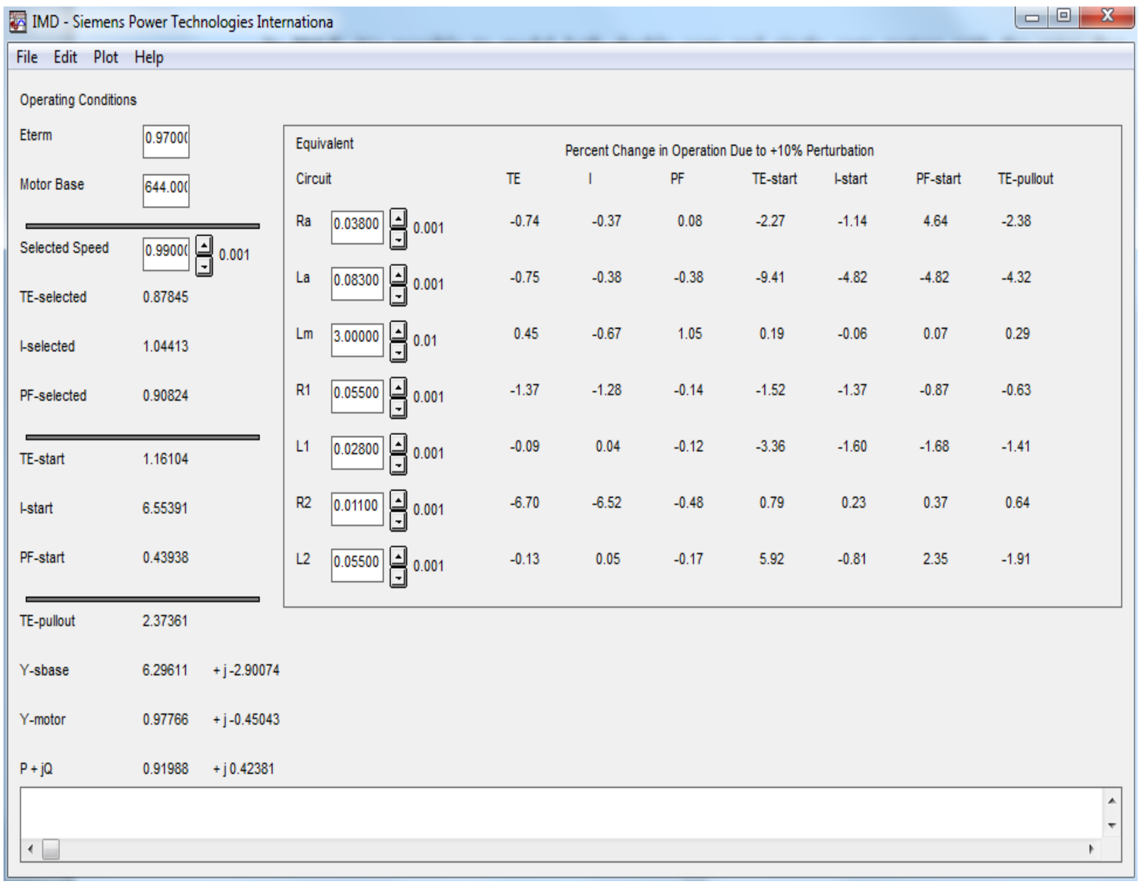

Figure 3.4: The interface of the IMD program of PSS/E

3.4 Tap Changer Model

Tap changers have a great influence on voltage stability [3]. On-load tap changers at substation transformers attempt to restore the distribution level voltages and loads during post disturbance to pre-disturbance level. When tap changers operate, the losses in the high voltage transmission lines increase and that will further increase the voltage drop in the transmission lines and eventually the generators will hit their maximum reactive power capability curve and the system will no longer be able to meet the reactive power demand and a voltage collapse will ultimately occur. The single line diagram of an OLTC (ON-Load Tap Changer) is shown in Figure 3.5.

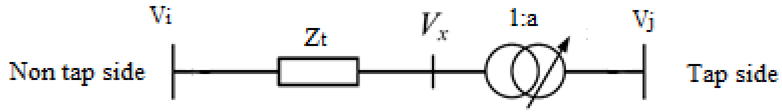

Figure 3.5: Tap changer single line diagram [36]

The built in models in PSS/E that represent OLTC only require parameters that are associated with the control circuitry of the OLTC, the specifications of the OLTCS including the number of steps are entered separately through PSS/E network data. The parameters to be entered are time delay to change the tap ratio, the transformer time constant and the time between subsequent taps all of these parameters have been obtained from an old publication [34] the time delay between each step is considerably long, it might be reduced in the simulation in order to observe the effects of tap changers on voltage stability. The parameters of the OLTC model code can be found in [34].

3.5 FACTS Models

Flexible alternating current transmission system (FACTS) is a power electronic based system with static equipment (capacitors and reactors) that provide reactive power support for the network, hence they have great impact on the voltage stability of the system. FACTS devices can either provide series compensation or shunt compensation, series compensation has only effects on increasing power flow while shunt compensation has the capability of regulating bus voltages and increasing power flow in the transmission lines. Therefore, in this thesis work, shunt compensation will be considered. FACTS devices can further be classified either as voltage source converter based (STATCOM) or Static Var Compensator (SVC). Each of these two types has advantages and disadvantages as it will be seen later [8].

3.5.1 Static Var compensators (SVC)

The static Var compensator is one of the shunt connected FACTS devices that provide continuous reactive power compensation. The device consists of a set of thyristor switched capacitors (TSC), a Thyristor controlled reactor (TCR) and a filter to filter out harmonics. Therefore, it has the capability to generate and absorb reactive power. Hence, the device could be used to mitigate voltage collapses and keeps the voltage profile of the buses nominal. The single line diagram of the device is shown in Figure 3.6.

Thyristors are used to control the value of the reactance since they are high rated switching devices that are able to sustain high current flow more than the other switching devices such as MOSFET (metal oxide semiconductor field effect transistor) or IGBT (Insulated-gate bipolar transistor). In addition, the associated losses with this switching device is considerably lower than other devices. However, this device has slower switching operation than the other switching devices [12].

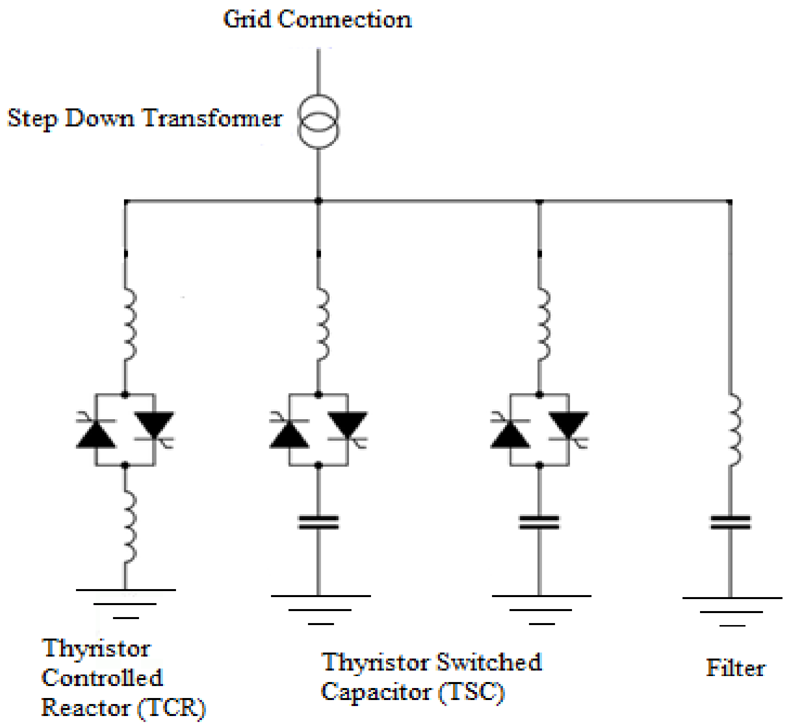

Figure 3.6: The SVC layout [12]

To analyze the performance of an SVC, Thevenin equivalent circuits are utilized with respect to the point of common coupling with the SVC as shown in Figure 3.7. Then, the characteristic equation of the system with SVC could be written as [12]:

$$V_{SVC} = E_{th} - Z_{th} I_{SVC} \tag{3.3}$$

The SVC characteristics within the maximum and minimum voltage control range is defined by the reactance X_{SL} of the SVC:

$$V_{SVC} = V_0 + X_{SL} * I_{SVC} \tag{3.4}$$

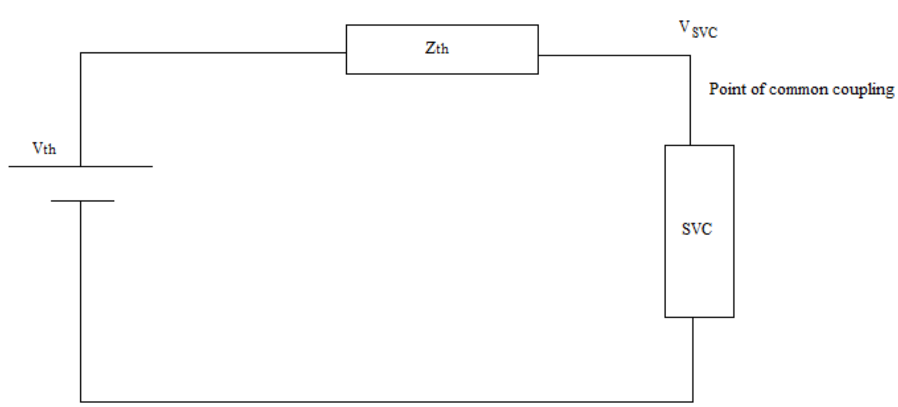

Figure 3.7: The system's Thevenin equivalent circuit with the SVC

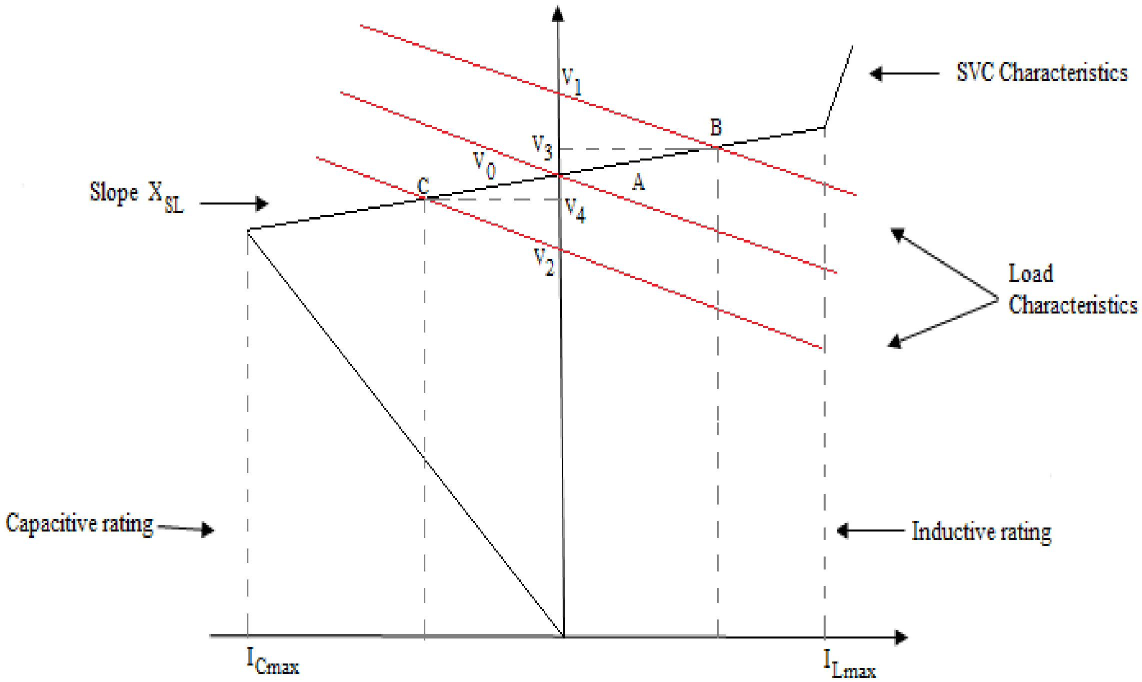

Figure 3.8: SVC characteristics for given system conditions [3]

Then from both equations 3.3 and 3.4, the characteristic of the SVC is drawn in Figure 3.8 for different system conditions. If the system's voltage decreases, the voltage at the point of common coupling (PCC) should decrease to V_2 but if the SVC is utilized and supplied capacitive reactive current, the voltage will settle at V_4. If the system's voltage increase, the voltage at PCC should rise to V_1 but with the SVC the voltage will settle at V_3 by absorbing inductive reactive current. Hence, the rating of the SVC could be determined by calculating the maximum reactive power supplied or absorbed by the following equation [12]:

$$Q_{SVC} = \sqrt{3} V_{SVC} I_{SVC} \tag{3.5}$$

The optimal place to install the SVCs in the system is at the point of common coupling with the dynamic loads especially at the induction motor loads in order to gain the full benefit of the reactive capability of the SVC.

In PSS/E, there is a built-in model called (**CSSCST**) [38] which only require six input parameters and it can represent the dynamic response of an SVC accurately as it has been used in many publications [26]. Therefore, the **CSSCST** is the model to be used in the simulation. In order for the dynamic model of the SVC to work, a switched shunt must be installed at the desired bus in the single line diagram of the system and the control setting of the SVC should be set to continuous voltage control. The model is implemented as an integrator controller and the block diagram of the **CSSCST** is shown in Figure 3.9.

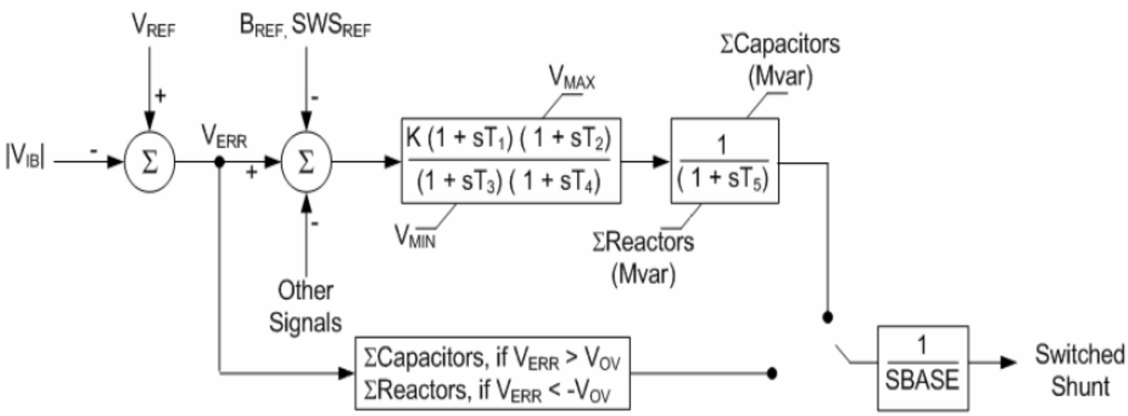

Figure 3.9: The SVC CSSCST model block diagram [38]

where:

K:	Steady state gain.
T1-T4:	Parameters that influence the closed loop response of the SVC.
T5:	The time delay of the thyristor valves.
V_{OV} :	Voltage Override represents the system's voltage deviation that will force SVC to supply its full reactive power compensation.

The specifications and entry parameters that are used in this research for the SVC model (CSSCST) can be found in Appendix F2. The methodology for calculating each of these parameters is based on [39] and [40].

3.5.2 Static synchronous compensators (STATCOM)

According to [12], STATCOMS are used to supply or absorb reactive power just like SVCs. However, unlike the SVCs, they voltage source based converters behind reactance that convert an input DC voltage into an output AC voltage to compensate for the reactive power needs of the system. The circuit diagram of a STATCOM is shown in Figure 3.10.

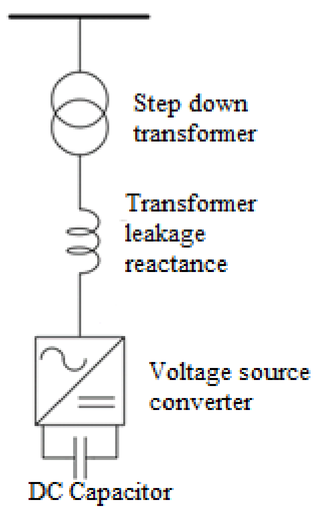

Figure 3.10: STATCOM equivalent circuit [12]

The STATCOM has the advantage of the ability of to supply full reactive power regardless of the system's low voltage which would be much desired in a weak grid where a lot of induction motors are present. Also, a STATCOM always have a symmetrical rating for the inductive and the capacitive compensations as shown in Figure 3.11.

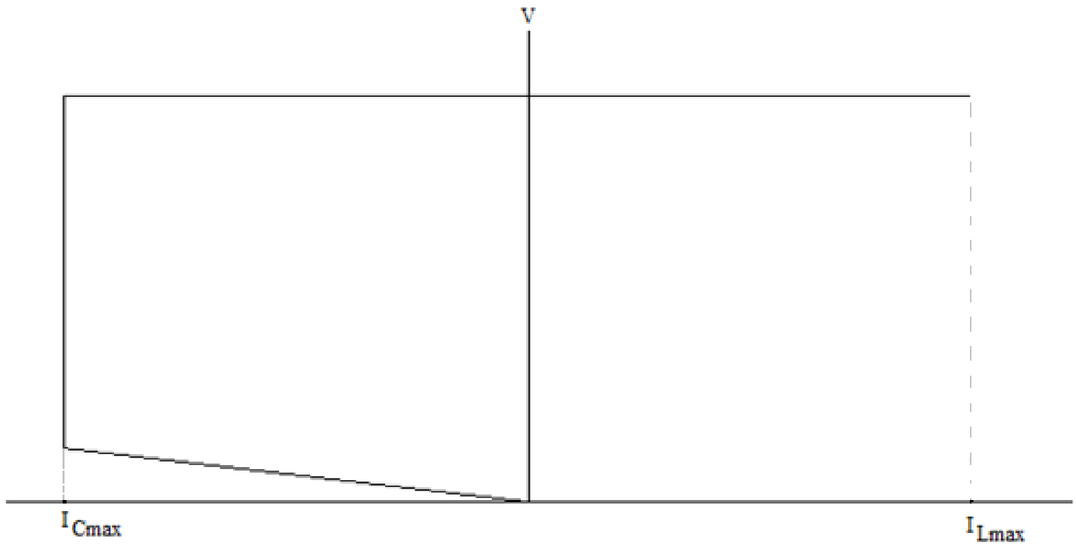

Figure 3.11: The V-I characteristics of STATCOMS [12]

The only disadvantage of this FACTS device is its losses. The losses of a STATCOM could go above 1% that is very high especially if the rating of the device is high. STATCOMs will be used in our system just for comparison with the performance of the SVCs [8]. The implementation of STATCOM in PSS/E dynamic simulation is done through the model **CSTCNT [**35]. The model requires 15 input parameters and the block diagram of the model is shown in Figure 3.12.

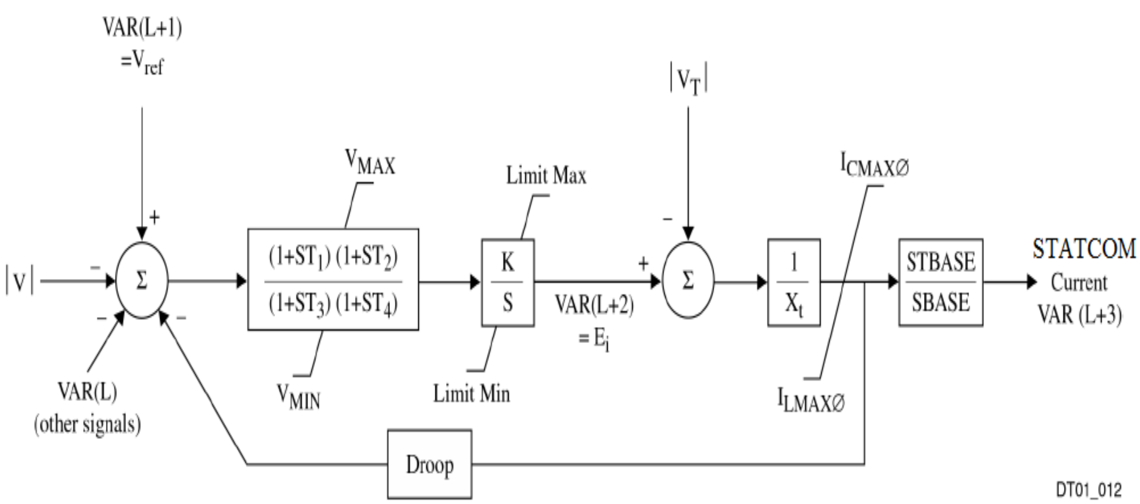

Figure 3.12: The block diagram of STATCOM CSTCNT model [38]

where:
K: The integrator gain.
T1-T4: The time constants that influence the transient gain of the voltage regulator.
Droop: Permits the coordination of voltage control with other generators and STATCOMs.

The output of the model is either positive or negative currents that represent a STATCOM performance as either a reactor or capacitor respectively. The parameters of the model are based on a previous publication [41] and further explanation of the parameters can be found in [41]. The values of these parameters that are used in this research for STATCOM model (CSTCNT) can be found in Appendix F1.

3.6 Protective Relays: Distance Relays

Protection relays play a major role in voltage stability. If a transmission gets overloaded, the relay that protects that line would trip and that will cause a depression in the voltages of the system which will lead to cascaded tripping in several transmission lines and that will ultimately lead to a voltage collapse. Protective relays could also be used to mitigate voltage instability, for example, an under-voltage load shedding relay will disconnect some of the system's loads if the voltage at a load bus goes below minimum threshold. However, in this study, only the distance relay protection will be considered.

Distance relays are used for transmission line protection due to their fast protection and coordination. They are used to protect transmission lines from either faults or overloading. Distance relays measure the ratio of voltage to the current through voltage transformers and current transformers. If the ratio of voltage to current is less than the settings of the relay, the relay will operate and send a signal to trip the circuit breakers. Distance Relays have three protective zones. The first two zones provide primary protection for the protected line and the third zone offers remote backup protection for the adjacent transmission line as shown in Figure 3.13 [3].

The Characteristics of the distance relays for our system have been set as follow according to [3]:

- Zone 1: covers 80% of the protected line with a time delay of 5 cycles.
- Zone 2: covers 100% of the protected line and 20% of the shortest adjacent line with a time delay of 15 cycles.
- Zone 3: covers 100% of the protected line and 120% of the shortest adjacent line with a time delay of 30 cycles.

Therefore, the total fault clearing time will be the protective zone time delay plus the breaker trip time which is five cycles. However, in chapter 6 where the SVCs and STATCOMS are introduced into the system, Zone 1 time delay and the breaker trip times were reduced down to 2.5 cycles in order to make the dynamic model of these devices work. The **DISTR1** distance relay model has been selected for the model library to act as a MHO distance relay. The model requires 24 input parameters, the only important parameters for our case are the data for the three protective zones, their time of operation and the circuit breaker trip time. Distance relays have been installed on all of the 400 kV high voltage lines (at the buses with positive power flow) and the data of each distance relay is presented in Appendix C1 and Appendix C2 includes the dynamic parameters for MHO distance relay.

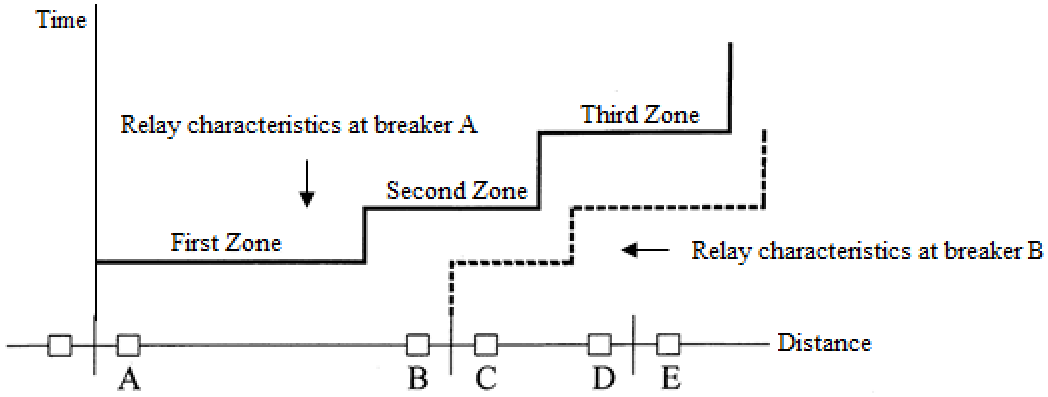

Figure 3.13: Distance relay protective zones [3]

4

Steady State Analysis of Nordic-32 Bus Test System

The chapter begins by introducing the Nordic 32 system and the methodology at which the study will be carried out. Also, steady state analysis will be carried out through performing P-V curve analysis to determine which contingency that will severely affect the voltage stability of the system from which the weakest buses of the system will be determined at which the induction motor loads will be installed in order to mimic the worst case scenario that would affect the voltage stability of the system. The subsequent chapter will deal with the voltage recovery time analysis with different load combinations.

4.1 Overview on Nordic 32 Test System

The Nordic 32 test system which represent Sweden's power grid was developed by Svenska Kraftnät [34] for simulations purposes. The system consists of 32 high voltage buses and 9 low voltage buses. The system is distinguished by two main areas; the northern area is characterized by having a large number of hydro generation units with a few loads while the southern area is heavily populated and hence has a lot of loads and thermal-nuclear generation units. The high voltage transmission system is rated 400 kV while the sub-transmission systems are rated 220 kV and 130 kV respectively and are connected to the high voltage buses through On-load Tap Changers, more details about the system are found in [33] and [34]. The layout of the system is shown in Figure 4.1.

The system has been designed to withstand the N-1 contingency which means that the system will operate normally even if one of the high voltage transmission lines tripped or one of the generating units tripped. The dynamic file of the system only contained the dynamic data of the generators such as the exciter, the turbine governor and the stabilizer. The maximum excitation current limter and the distance relay models had to be added. The SVCs, STATCOMS and the PV Plants will be added later as a progress in the simulation has been achieved.

4.2 Steady State Analysis of the Nordic 32 System

Before proceeding with the dynamic simulation of the system, the system must be ensured to work perfectly in the steady state before and after the introduction of new dynamic loads such as induction motors to the system. This could be determined if the power flow solution converges without any voltage or thermal violations in the system. A summary of the loadflow for the base case is shown in Figure 4.3. which shows the total load, losses and generation for the base case of the Nordic 32 system.

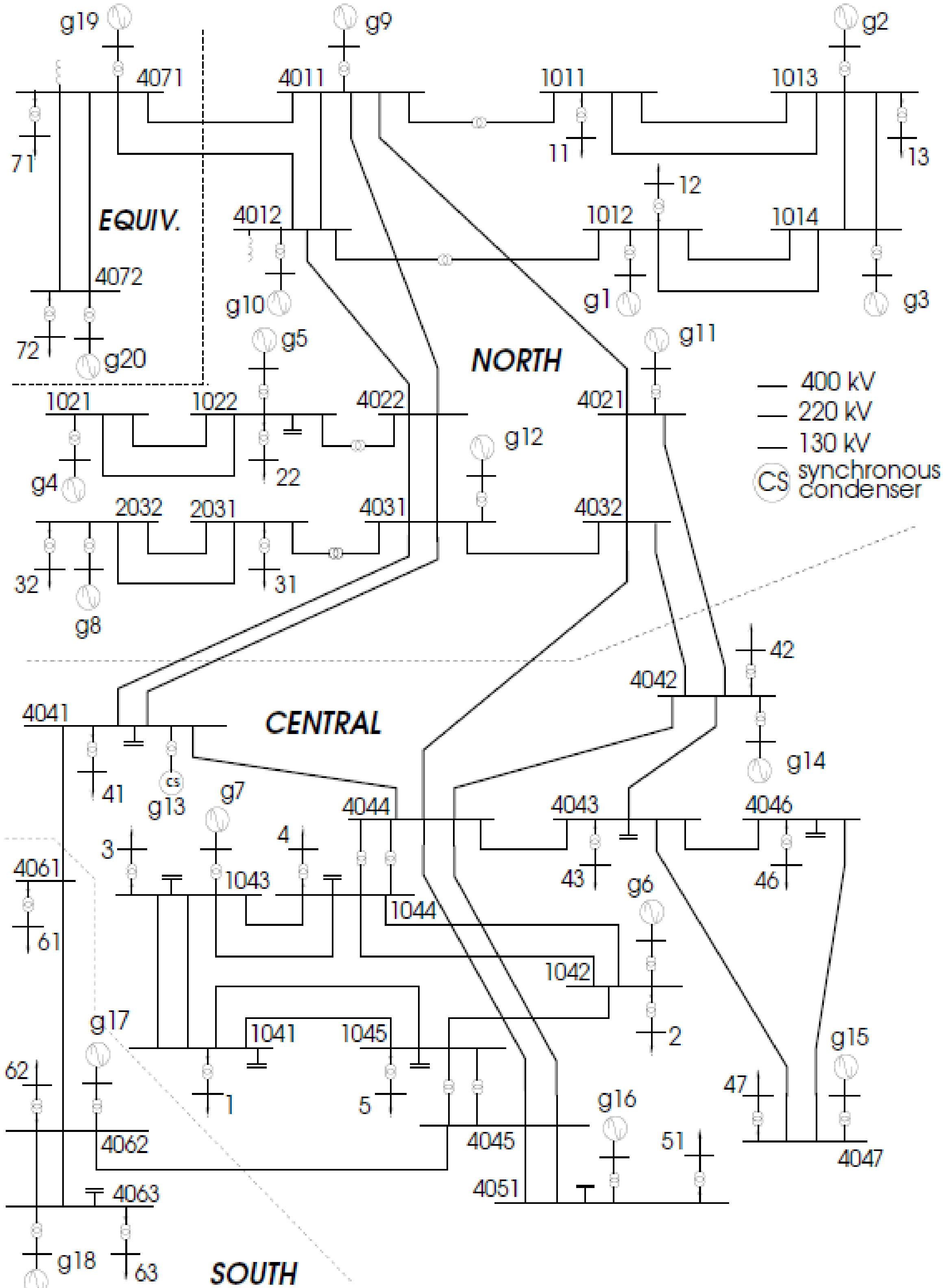

Figure 4.1: The layout of the Nordic 32 system [33]

```
************************  SUMMARY FOR COMPLETE SYSTEM  ************************

                                 SYSTEM SWING BUS SUMMARY
X------ SWING BUS ------X X---- AREA -----X X---- ZONE -----X
  BUS# X-- NAME --X BASKV    # X-- NAME --X    # X-- NAME --X       MW       MVAR   MVABASE
  4011 BUS4011     400.00    1                 1                  452.1     -403.2    1000.0

    41 BUSES        20 PLANTS          23 MACHINES      0 INDUCTION GENS      0 INDUCTION MOTORS
    22 LOADS        11 FIXED SHUNTS     0 SWITCHED SHUNTS
    69 BRANCHES     17 TRANSFORMERS     0 DC LINES      0 FACTS DEVICES       0 GNE DEVICES

                       X------ ACTUAL ------X X----- NOMINAL ------X
                               MW        MVAR         MW        MVAR
FROM GENERATION           11252.1      1043.3    11252.1      1043.3
FROM INDUCTION GENERATORS     0.0         0.0        0.0         0.0
TO CONSTANT POWER LOAD    10940.0      3358.4    10940.0      3358.4
TO CONSTANT CURRENT           0.0         0.0        0.0         0.0
TO CONSTANT ADMITTANCE        0.0         0.0        0.0         0.0
TO INDUCTION MOTORS           0.0         0.0        0.0         0.0
TO BUS SHUNT                  0.0      -879.3        0.0      -900.0
TO FACTS DEVICE SHUNT         0.0         0.0        0.0         0.0
TO GNE BUS DEVICES            0.0         0.0        0.0         0.0
TO LINE SHUNT                 0.0         0.0        0.0         0.0
FROM LINE CHARGING            0.0      4404.2        0.0      4311.0

 VOLTAGE       X----- LOSSES -----X   X-- LINE SHUNTS --X   CHARGING
 LEVEL BRANCHES       MW       MVAR         MW       MVAR       MVAR
 400.0      50    242.51    2475.11        0.0        0.0     4354.6
 220.0       2     15.27     114.50        0.0        0.0        3.5
 130.0      17     54.31     378.85        0.0        0.0       46.1
 TOTAL      69    312.08    2968.46        0.0        0.0     4404.2
```

Figure 4.2: Load flow summary for the base case

The loading of the high voltage critical transmission lines that connect the northern portion of the network to the southern portion of the network for the base case is shown in Table 4.1.

Table 4.1: Loadings of the critical transmission lines

From Bus	To Bus	Voltage Rating (kV)	Circuit	MW	MVAr	Percentage of loading %	Thermal Rating (MVA)
4031	4041	400	1	581.7	-90.3	41	1400
4031	4041	400	2	581.7	-90.3	41	1400
4031	4032	400	1	795.4	-149.9	57	1400
4032	4044	400	1	611.8	-41.3	43	1400
4042	4043	400	1	675.1	-47.1	48	1400
4042	4044	400	1	529.4	-38.5	38	1400

The P-V (Power-Voltage) analysis has been made with generation from the northern part of the network to the loads of the southern part of the network for bus 4044 since it's located at the load centre is shown in Figure 4.4. The purpose of the P-V curve is to show how the addition of loads will affect the voltage stability of the system in order to appropriately size the induction motor loads later without causing voltage instability.

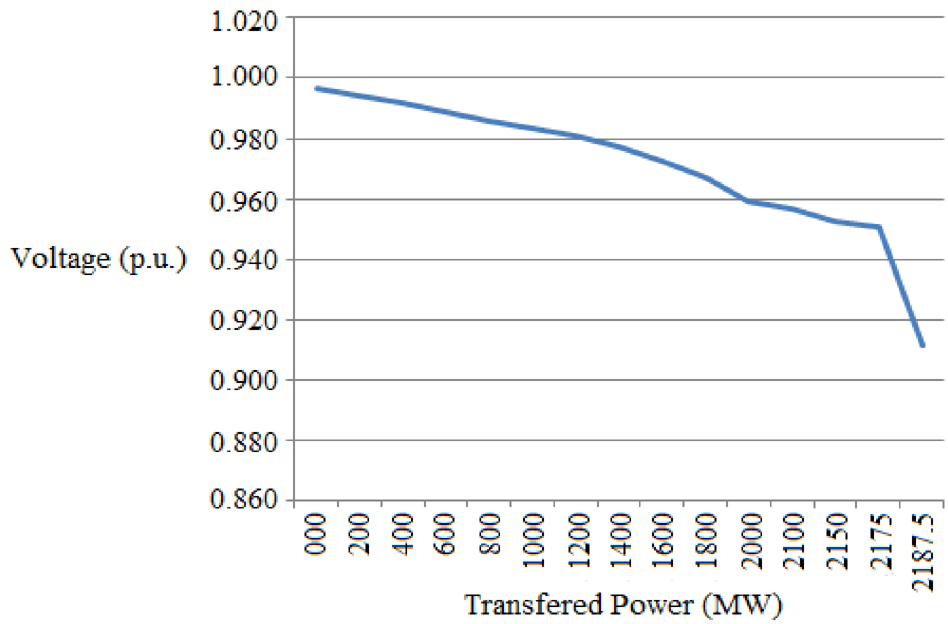

Figure 4.3: P-V Curve analysis for the base case of the system at bus 4044.

It can be seen from Figure 4.3 that the bus voltage continues to decline as the transferred power increases and will ultimately reach the voltage collapse scenario when the transferred power reaches 2186 MW. This will aid in the determination of the number of the dynamic loads to be introduced in the system without causing voltage instability.

4.3 Identification of The Weak Buses in The System

It has been stated earlier that the system was designed for N-1 contingency. In order to commence with the study which is about improving the voltage recovery time during post-disturbance, the system must become stressed. Because in this case the post-disturbacne voltage sag and voltage recovery time become significant. A P-V analysis has been made for different disturbances to determine which disturbance that would bring the system on the stressed level as shown in Figure 4.5. The P-V analysis has been made with OLTCs are allowed to operate in order to obtain the worst case scenario since OLTCs attempt to make the loads as constant MVA loads and that would lead to progressive reduction in the voltages.

From Figure 4.5, it can be seen that the disturbance that would bring the system closer to the critical point of voltage instability is the tripping of the high voltage transmision line that connects buses 4032-4044. A power flow analysis has been made after tripping the transmission line 4032-4044 and the buses with the lowest voltages in the system have been identified. These buses are shown in Table 4.2.

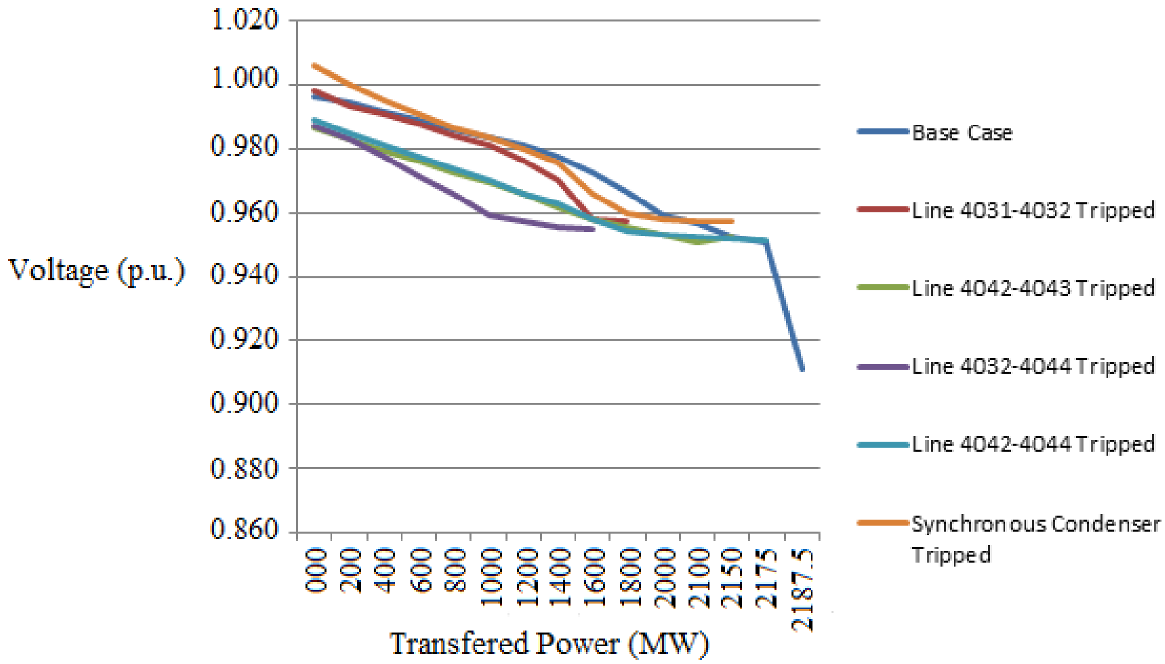

Figure 4.4: P-V analysis for different disturbances at bus 4044

Induction motors will be installed at those buses through an iterative process as necessary to signifiance the voltage recovery phenomena such that when a disturbance occurs in the system, it will not lead to a voltage collapse scenario in order to allow the oppurtunity to observe the voltage recovery phenomena that is affected by the dynamics of the induction motor loads.

Table 4.2: The buses with lowest voltages.

Bus No.	Rating (kV)	Voltage (p.u.)
1041	130	0.9611
61	130	0.9643
46	130	0.9674
43	130	0.9698
62	130	0.9818

5

Effects of Load Characteristics on Voltage Stability

In this chapter, the capability of PSS/E to perform dynamic simulations will be uitlized to study the effect of load characteristics on voltage recovery phenomena (which is an indicator for the voltage stability of the system). In order to proceed with the dynamic simulation, all of the models that resemble the system's components that have been stated it chapter 3 have been written in a text file with with an extension .dyr so that it could be loaded onto PSS/E. The voltage recovery time will be first investigated with constant current, constant power and impedance loads, then the voltage recovery analysis will be made with different proportions of induction motor load installed at one of the weak buses that have been determined in chapter 4. Afterwards, the voltage recovery analysis will be made with the induction motor loads will be installed at all of the weak buses.

5.1 Dynamic Voltage Analysis Setup

The following have been done to prepare the dynamic simulation in PSS/E:

- All of the constant MVA loads in the base case have been converted to ZIP loads that have the characteristics of 100% constant current for the acitve power component and 100% constant impedance for the reactive power components. For motors, CIM5BL model was used as explained in Chapter 3 with its parameters were tuned through the auxiliary program IMD such that its current is equivalent to 1 p.u.

- All of the models that have been stated in chapter 3 are loaded into the dynamic file.

5.2 Voltage Recovery Analysis with ZIP Loads

The voltage recovery time and the voltage collapse scenario will be studied through different load composition of the system. The voltage recovery time is going to be studied first with ZIP loads.

- Line 4032-4044 is set out of service (refer to chapter 4 for the significance of this line).

- The dynamic simulation has been initialzed with all of the induction motors are set as out of service then the simulation is run for 30 seconds.

- At T=30s a three-phase line fault will be introduced into the transmission line that connects buses 4042-4043. This transmission line has been selected because if it tripped , it will not affect the voltage stability greatly as seen from the P-V curves in Figure 4.5, this has been done in order to give the opportunity to observe the voltage recovery phenomena without causing the system to go into voltage collapse directly.

- The simulation is further proceeded till T=130s to allow more time for the tap changers in order to observe their effect on the voltage stability, then the transmission line 4042-4044 is tripped due to a fault at T=130.2 s.

Figure 5.1 shows the voltage, the consumed active power and reactive at bus 1041 along time interval between 29-40 seconds where the the three phase line fault was introduced into line 4042-4043. It can be seen from the Figure that the voltage sags for the duration of the fault which is 0.2 seconds before it's cleared by the distance relay then the voltage recovers almost immediately (0.37 seconds) for the case of ZIP loads.

The whole time interval is shown in Figure 5.2. It can be seen from the Figure the OLTC operation to restore the voltage, the active and reactive power consumption of the loads after the transmission line 4042-4043 tripped. It can be observed that the OLTC attempts to restore the voltages of the low voltage side (bus 1044) to pre-fault conditions. As it does so, the voltages at bus 4044 (high voltage side) decreases. After the line 4042-4044 tripped due to a fault, cascaded tripping has occurred in the transmision line 4041-4044 due to overloading of the transmission line.

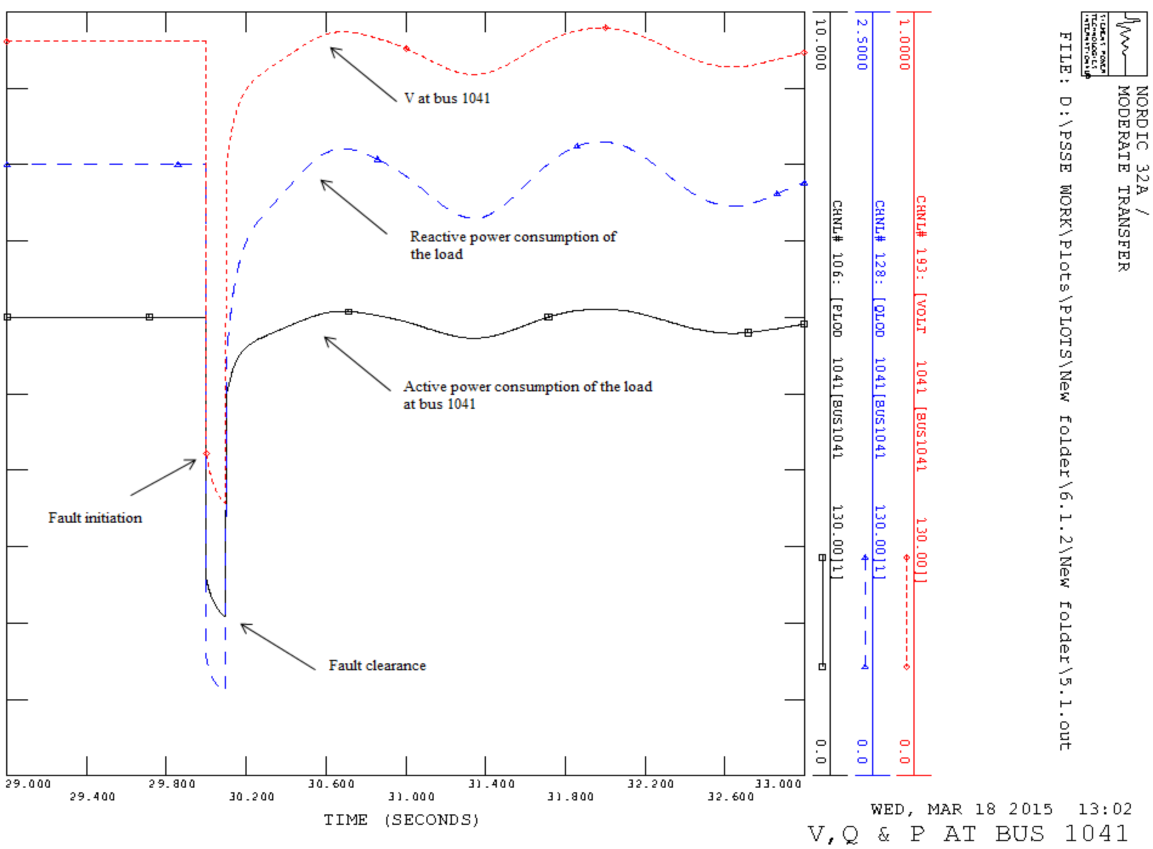

Figure 5.1: Voltage, consumed active and reactive power at bus 1042

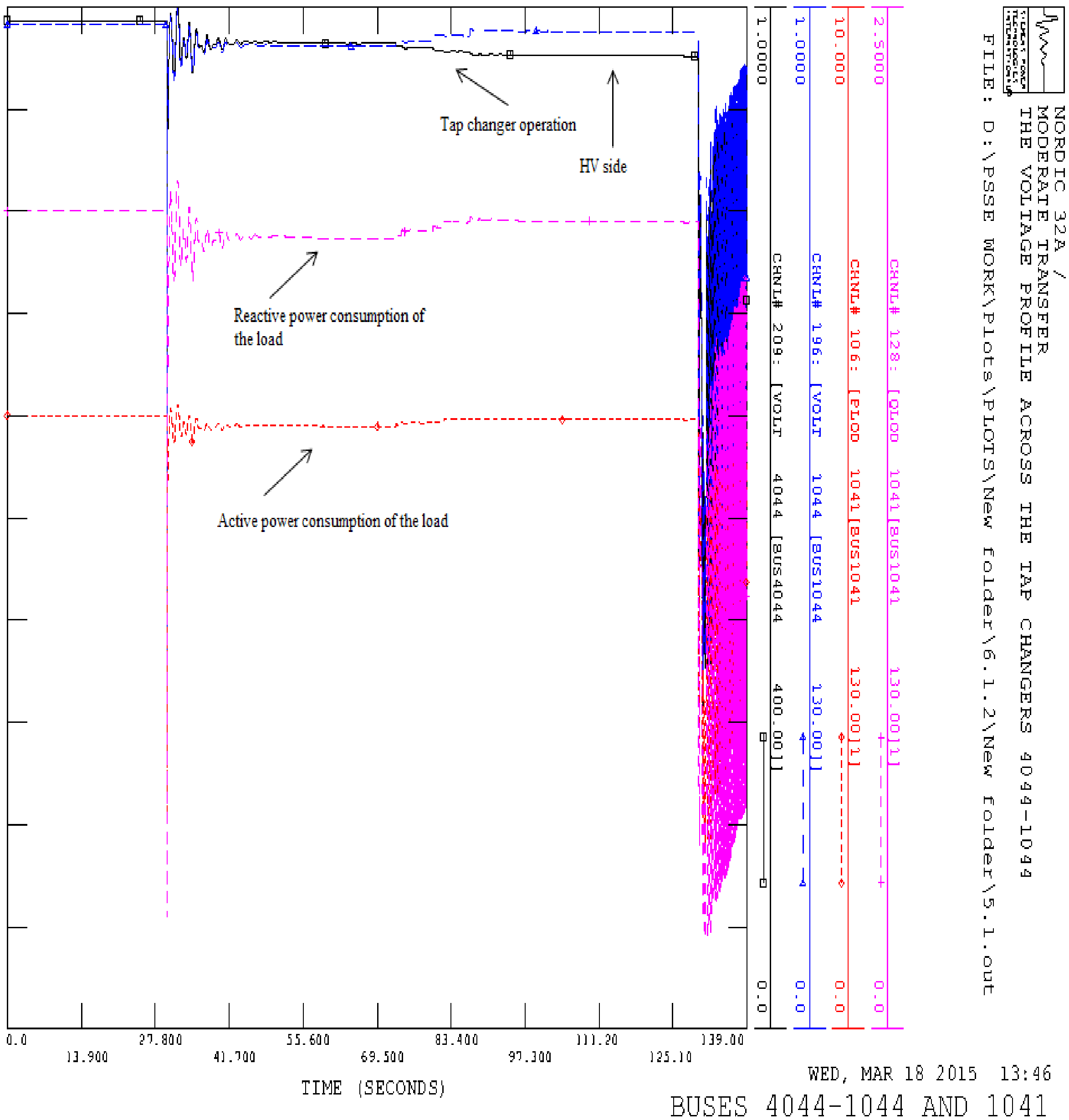

Figure 5.2: Extended time frame for the voltage (1041 and 4044) and the consumed active and reactive power (1041)

The characteristics of the distance relay along with the apparent impedance of the transmission line at 4041-4044 are shown in Figure 5.3. The line impedance decreases as it can be noticed due to the line overloading where the current increased and voltage decreased until the relay tripped.

The black line represent the impedance of the transmision line 4041-4044 and it can be seen that the apparent impedance of the line moved at a constant pace through all of protective zones. The timings of the distance relays that operated are shown in Table 5.1. It can be noted that three lines were tripped at zone 1 of the three relays. Events 1 and 2 were resulted from faults on the lines while event 3 was due to overloading of the line.

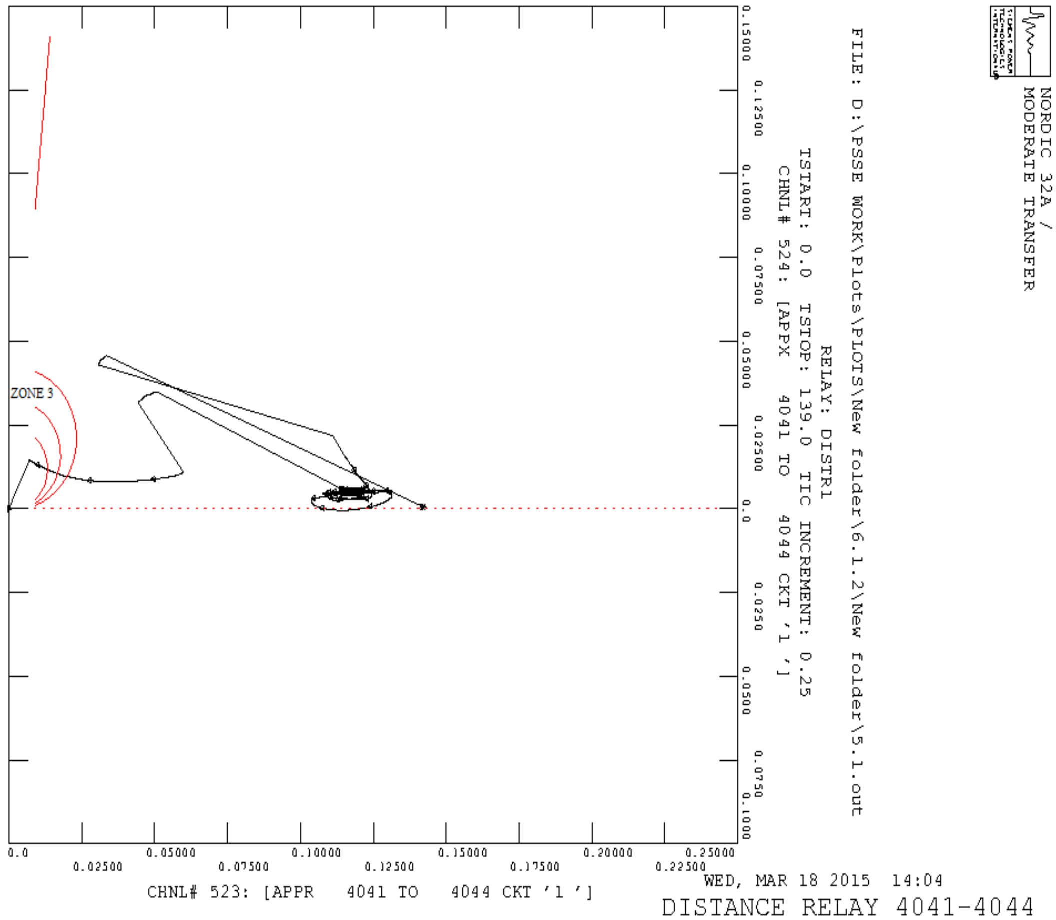

Figure 5.3: Apparent impedance of the transmission line at 4041-4044

Table 5.1: Timings of the distance relays that operated

			Pick up Times (Seconds)			Timed out (Seconds)			
Event No.	**Transmission line**	**Fault initiation time (Seconds)**	**Zone 1**	**Zone 2**	**Zone 3**	**Zone 1**	**Zone 2**	**Zone 3**	**CB operating time (Seconds)**
1	4042-4043	30	30			30.1			30.2
2	4042-4044	130	130			130.1			130.2
3	4041-4044	Cascaded trip	130.7			130.8			130.9

5.3 Voltage Recovery Analysis with ZIP Loads Along with 20% Induction Motors on a Single Bus (1041)

The procedure for doing the analysis is the same as in section 5.2 but in this case aggregated induction motors will be introduced at the weakest bus in the system (bus 1041). The induction motors load represents 20% of the bus load and the rest is ZIP loads.

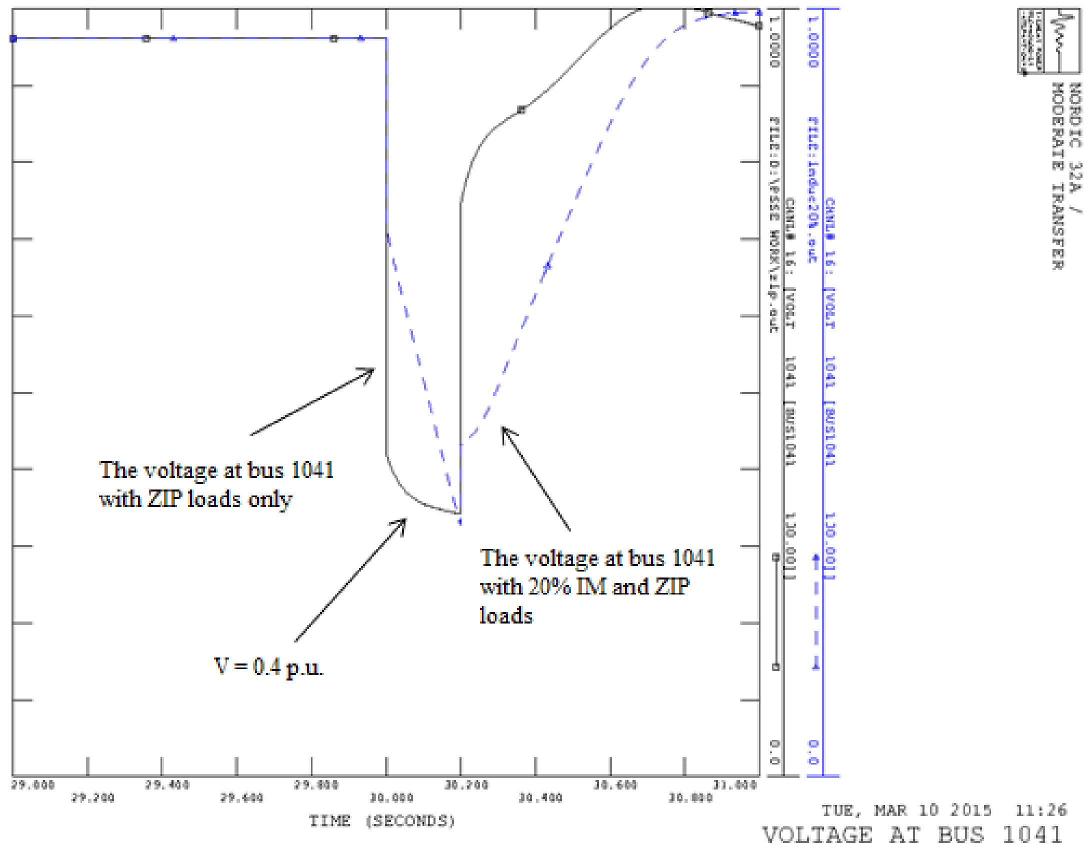

Figure 5.4: Bus 1041 voltage profile in two cases: with ZIP loads only (black) and with ZIP + induction (blue)

Figure 5.4 shows the voltage profile at bus 1041 for two cases: the first case comes with ZIP loads only (represented in the black line) and the second case comes with 20% of the loads at bus 1041 are converted to aggregate motor loads (shown as the dashed blue line). It can be seen from the curves that once the fault (on line 4042-4043) has been cleared, the voltage in the second case (with induction motors) has slower recovery time (0.55 seconds) compared to the first case (0.37 seconds). The slow voltage recovery period is mainly due to the induction motor dynamics as it draws very high current while attempting to reaccelerate.

5.4 Voltage Recovery Analysis with ZIP Loads Along with 30% & 100% Induction Motors on a Single Bus (1041)

With the same simulation procedure mentioned in section 5.2 except in this case the second fault occurred at T= 400 seconds, the induction motors percentage at bus 1041 was increased to 30% and then to 100% to investigate how the voltage behaves during a fault on line 4042-4043 at different levels of induction motor sizes. Figure 5.5 shows the voltages at bus 1041 with different induction motor proportions. It can be seen from the Figure that as the the induction motor percentage increases, the voltage recovery time increases and in the cases of 100%, the voltage never recovers to prefault conditions. Figure 5.6 explains how the induction motor slip behaves and how its reactive power consumption changes during the disturbance. It is clear that as the voltage at bus 1041 decreases the induction motor reactive power consumtion increases since the motor start drawing more current to compenstae the voltage decrease. Meanwhile, the motor speed reduces until reaching stalling condition as the voltage decreases based on the fact that the electrical torque is related to voltage.

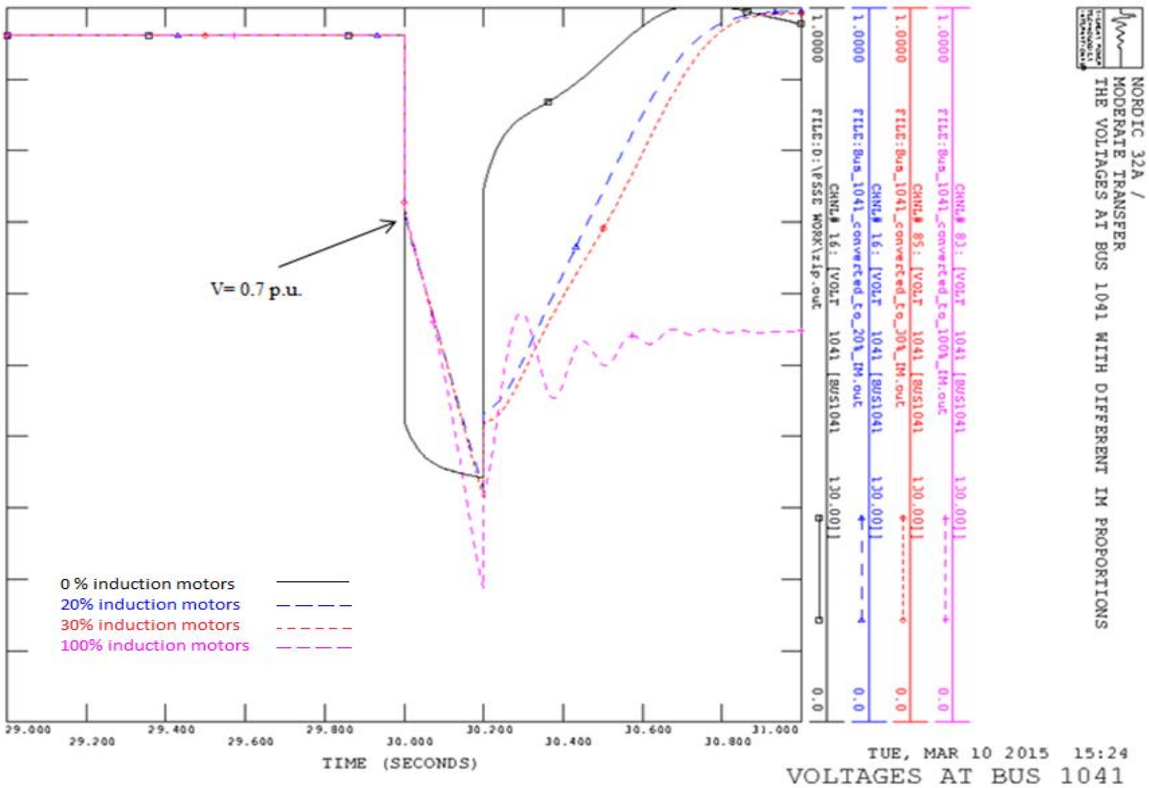

Figure 5.5: Bus 1041 voltage profile for ZIP, 20%, 30% and 100% induction motors

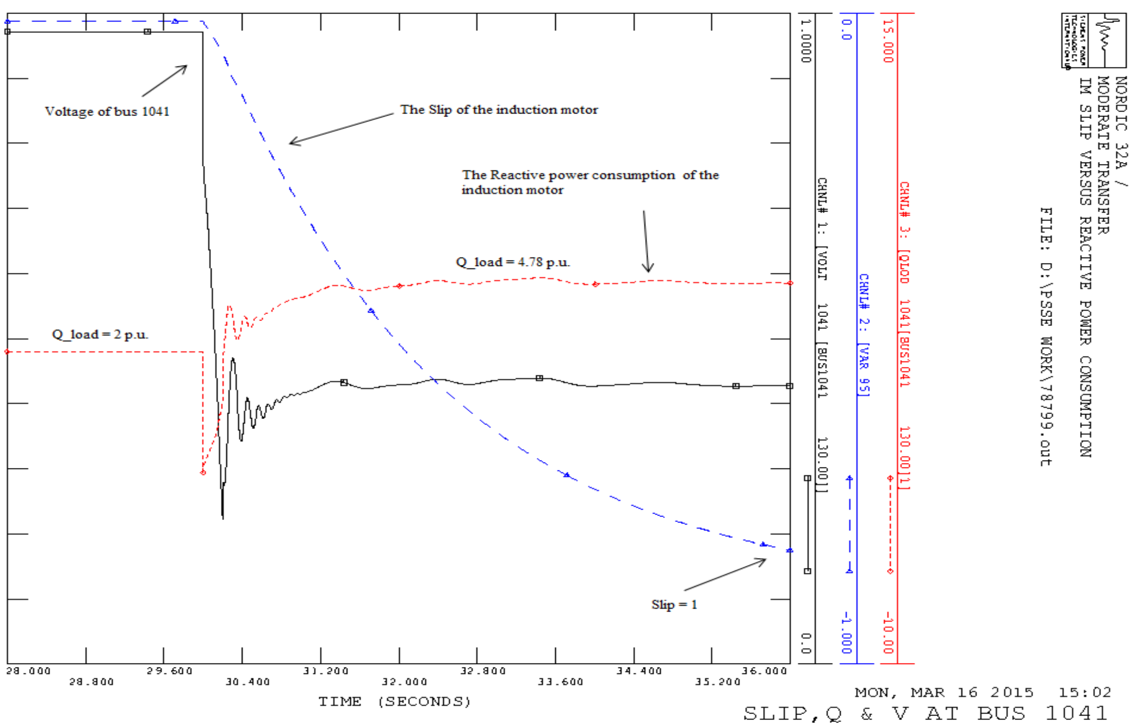

Figure 5.6: Bus 1041 voltage, reactive power and induction motor slip at 100% induction motor load at bus 1041

In the case of 100% induction motor load at bus 1041, the voltage profile of buses 4044 and 1044 where an OLTC exists in between them is shown in Figure 5.7. Also the power flow through the line between the two buses is shown in the Figure. The system was not able to recover the voltages of both buses as can be noted from the Figure. The destabilizing effect of the OLTC can observed through the power flow as shown as the dashed red line as the OLTC attempts to make the loads as constant MVA.

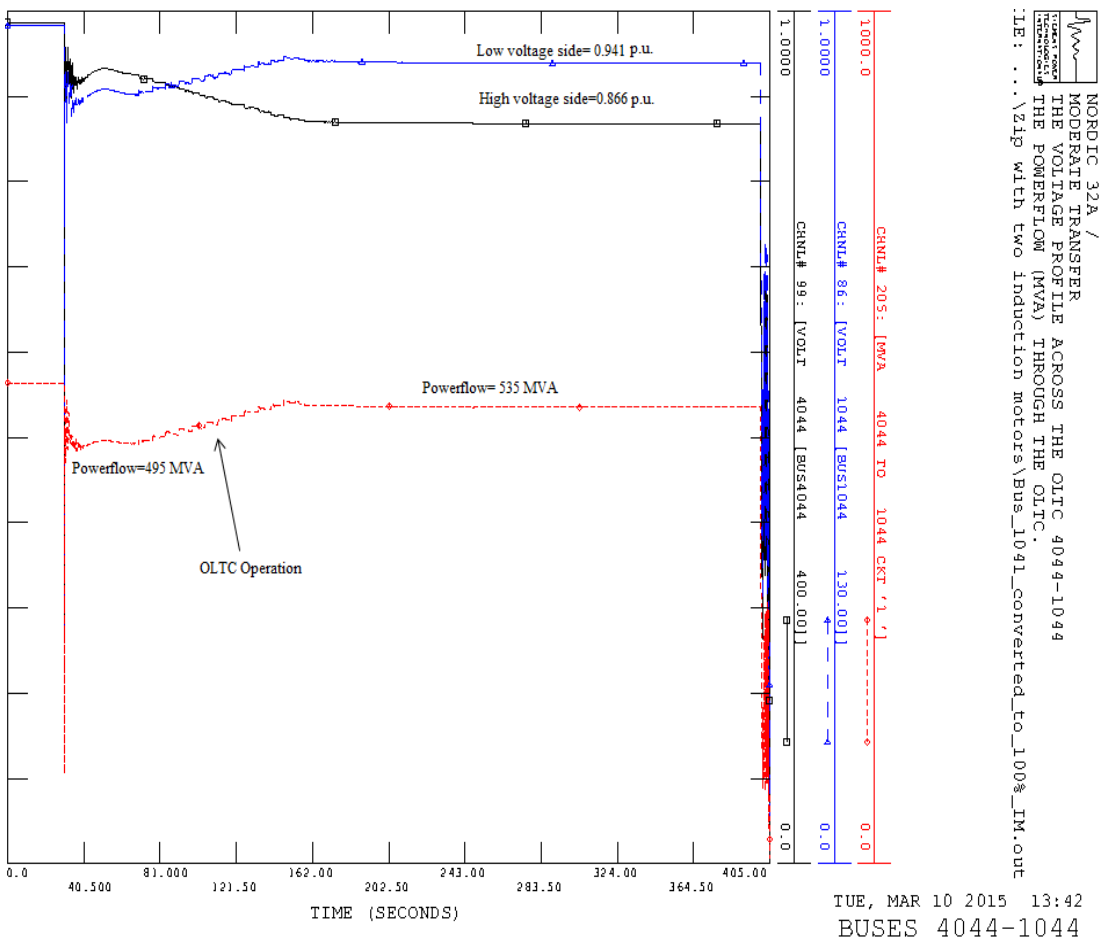

Figure 5.7: OLTC 4044 -1044 voltage profile and the power flow through at 100% IM loading at bus 1041

The characteristics of line 4041-4044 distance relay that tripped due to overloading is shown in Figure 5.8. The aggregated induction motors represent 100% of bus 1041 loads in this case which results in extra overloading on line 4041-4044. Therefore, it can be seen that the apparent impedance transfered through all of the zones within a shorter time frame than the case without induction motor.

Because of the generator's field limitation, its reactive power production is limited. This can be seen in Figure 5.9 where bus 1043 generator's field voltage (EFD) hit its maximum value during the post-fault time interval. Generator 1043 is the closest generator to bus 1041 (100% induction motor loading). After the clearance of the fault, the reactive power production of the generator increased but it was limited when the maximum EFD was reached.

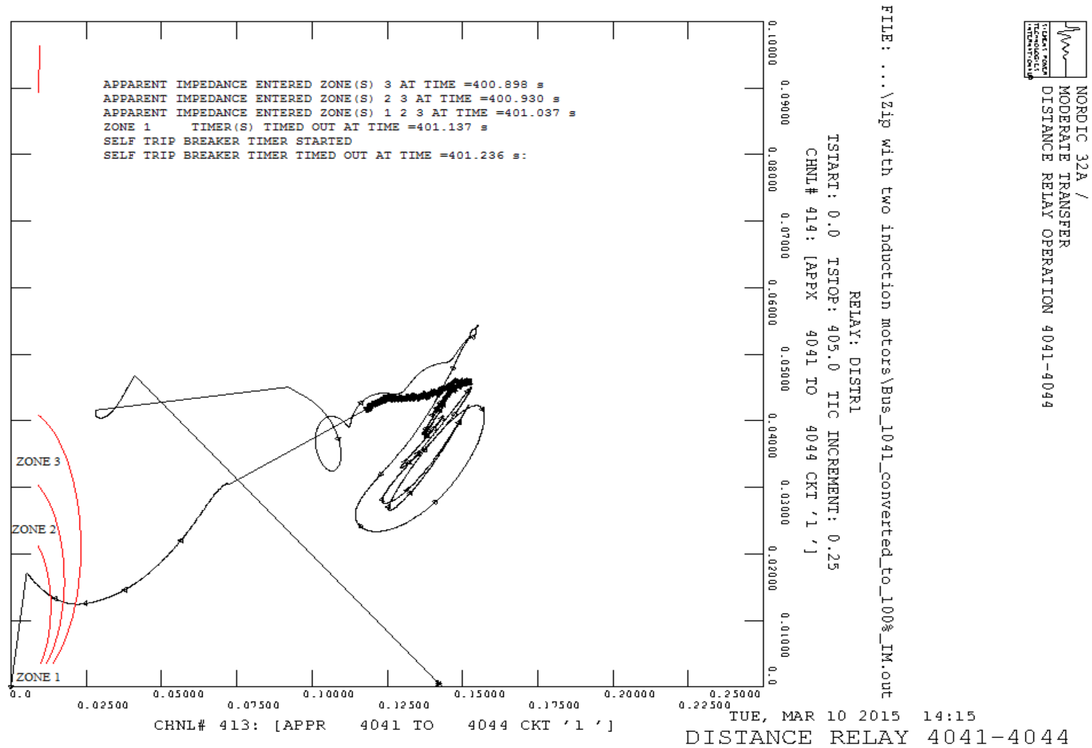

Figure 5.8 Apparent impedance of the transmission line at 4041-4044 (100% IM loading of bus 1041)

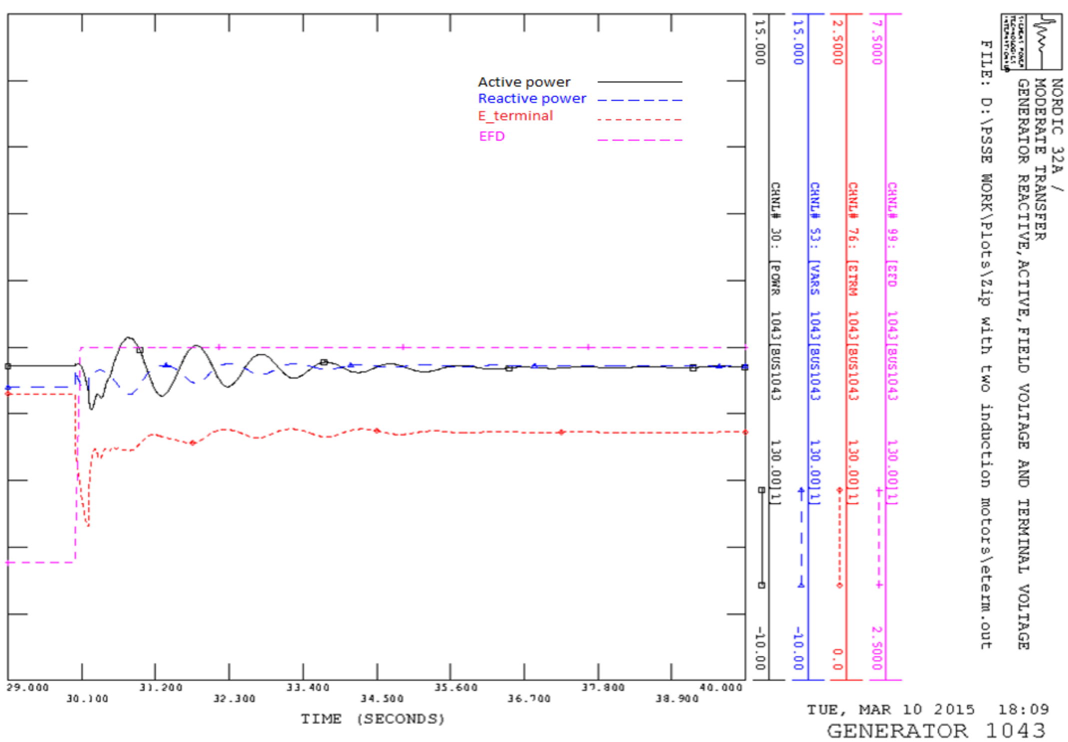

Figure 5.9: Terminal voltage, field voltage, Active and reactive power of generator 1043 at 100% IM loading at bus 1041

5.5 Voltage Recovery Analysis with Induction Motors on All of the Weak Buses

To represent a real case of Sweden's electric power grid which is characterized by having a high penetration of electric heating loads. Induction motor loads have been installed on all of the weak buses (43, 46, 61, 62 and 1041) in the system which has been discussed in chapter 4. A voltage recovery analysis has been made with 10% and 20% of the loads of the mentioned buses converted into induction motors. The analysis has been made with the transmission line 4032-4044 was in service in the sterady state (refere to chapter 4 for the importance of this transmission line) and the steps of the simulation will be as follows:

- The dynamic simulation was initialized and run up to T=30 s where a three phase fault occurred on the line 4032-4044 which caused the line to trip at T=30.2 seconds.
- The simulation is further run up to T=130 s where another fault is applied to the line 4042-4043 which caused the line to trip at 130.2 s which has led to several cascaded trippings and eventually to a voltage collapse at 132 s for the case of 20% induction motor loads at the weak buses.

Bus 1041 voltage recovery analysis is shown in Figure 5.10. It can be seen from the Figure that the voltage recovery time for 10% and 20% induction motor loading (on the five weak buses) has increased significantly than the case without induction motor. This is due to increasing the amount of the aggregated induction motors that absorb more reactive power during faults causing more voltage drop in the feeding lines and leading to slower voltage recovery time (1.15 seconds for the case of 20% IM loading).

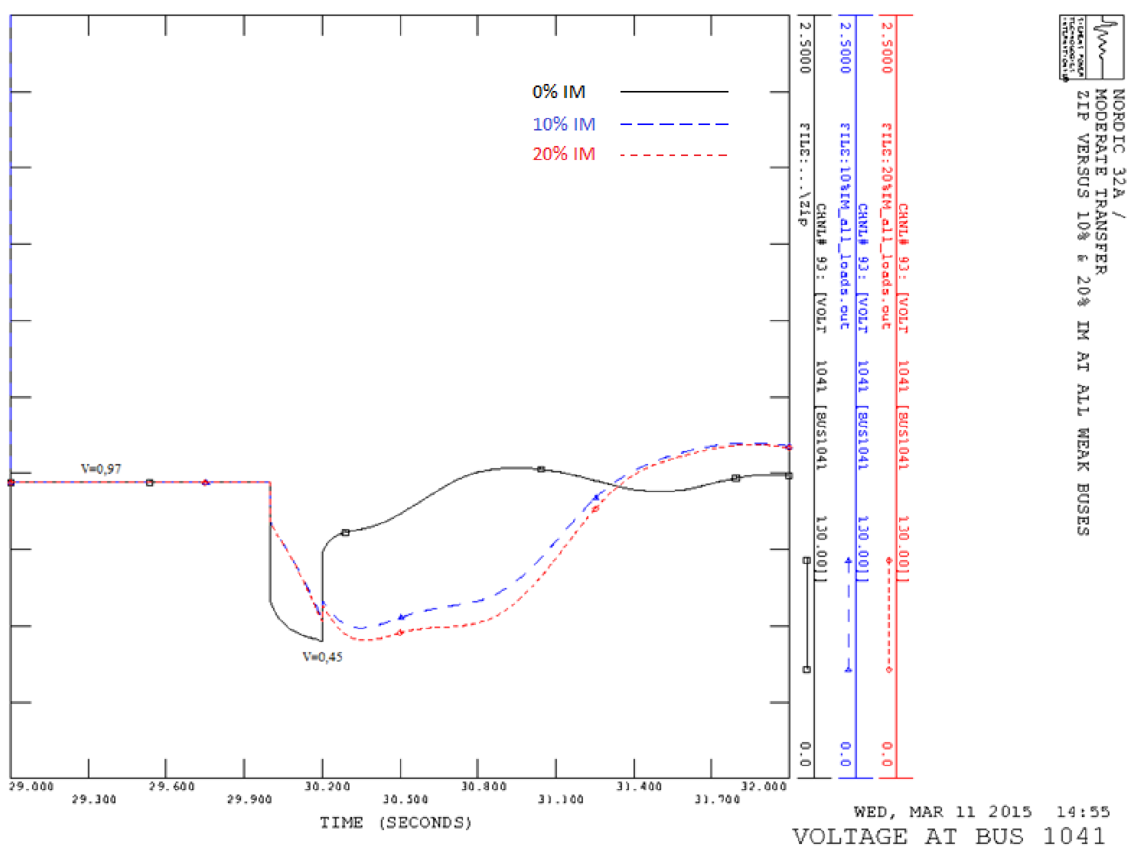

Figure 5.10: Bus 1041 voltage profile for 0%, 10% and 20% IM loading at the weakest buses.

The tripping times of the distance relays and the circuit breakers for the 20% IM loading case are summarized below in Table 5.2. It can be noted that three lines were tripped at zone 1 and one line tripped at zone 3. Events 1 and 2 resulted from faults on the lines while events 3 and 4 occured due to overloading of the lines.

Table 5.2: Timings of the distance relays that operated

			Pick up Times (Seconds)			Timed Out (Seconds)			
Event No.	**Transmission Line**	**Fault initiation time (Seconds)**	**Zone 1**	**Zone 2**	**Zone 3**	**Zone 1**	**Zone 2**	**Zone 3**	**CB operating time (Seconds)**
1	4032-4044	30	30			30.1			30.2
2	4042-4043	130	130			130.1			130.2
3	4042-4044	Cascaded trip			130.2			130.8	130.9
4	4041-4044	Cascaded trip	131.93			132.03			132.13

The characteristics of distance relays that tripped due to overloading operations are shown in Figures 5.11 and 5.12 below. Figure 5.11 shows the distance relay characteristics of line 4042-4044 that operated due overloading in zone 3. Figure 5.12 shows the distance relay characteristics of line 4041-4044 that operated due overloading in zone one.

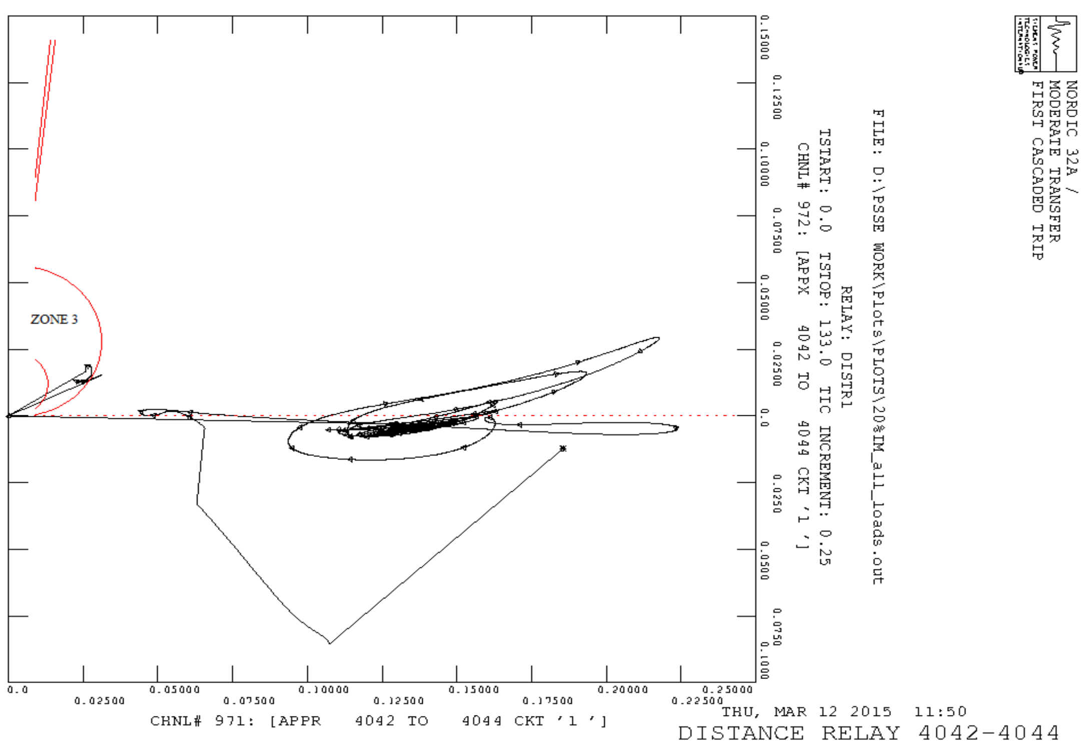

Figure 5.11: Apparent impedance of the transmission line at 4042-4044 (20% IM loading of the five weakest buses)

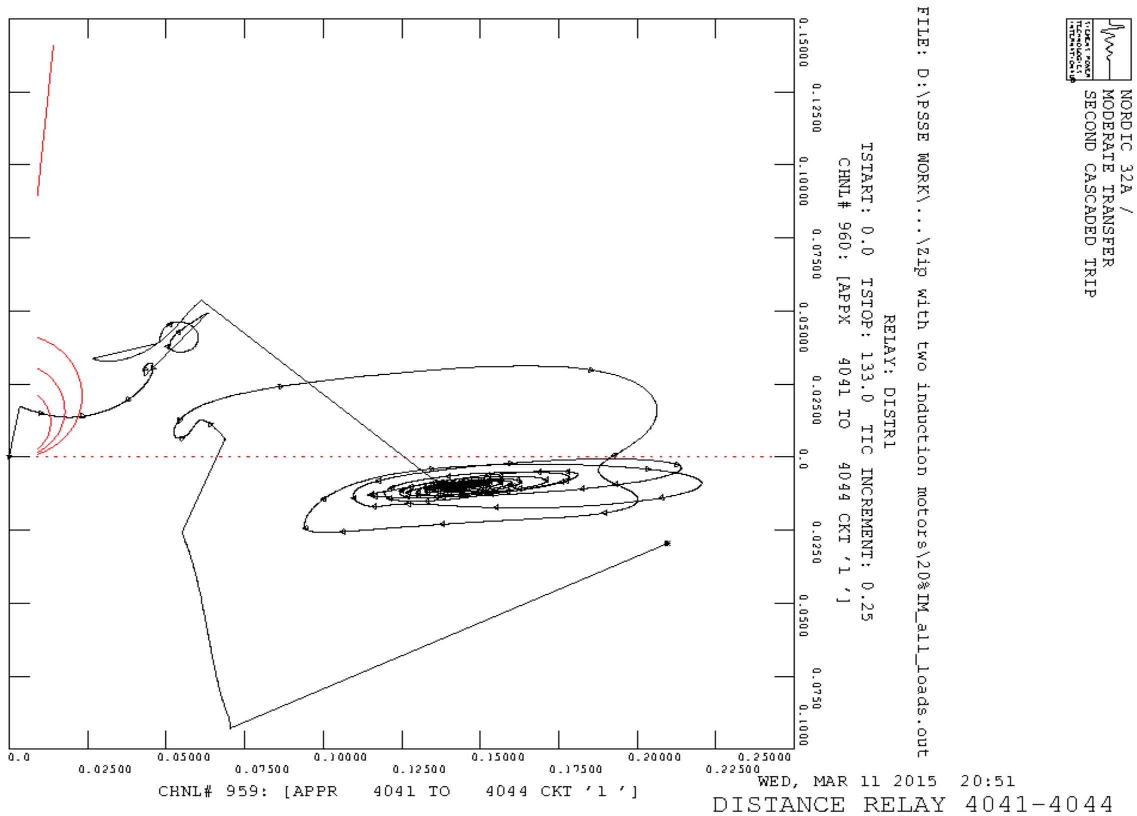

Figure 5.12: Apparent impedance of the transmission line at 4041-4044 (20% IM loading of the five weakest buses)

6

Improvement of Voltage Stability

This chapter will begin by the methodology of improving the voltage stability through mitigating the voltage recovery time phenomena through the use of Dynamic Var Compensators. In addition, the performance of different Dynamic Var Compensators such as Static Var Compensators (SVC) and Static Synchrounous Compensators (STATCOM) in the mitigation of the voltage recovery time will be discussed.

6.1 Improvement of Voltage Stability Through SVC

It has been demostrated before that the cause of the voltage recovery phenomena during the post-fault time interval is due to the induction motor drawing huge amount of reactive power. This could be mitigated through the utilization of Dynamic Reactive Power Compensation: These include the utilization of Static Var Compensators (SVC) and Static Synchrounous Compensators (STATCOM).

The capability of SVC to provide dynamic reactive power compensation would prove to be useful to mitigate voltage dips that occur due to disturbances. However, the voltage recovery time will have an inverse proportional relation with the capacitive rating of the SVC. As the capacitive rating of the SVC increases , the cost of the SVC increases. Therefore, the minimum capacitive rating of the SVC along with the minimum number of SVCs to be installed in our system must be found in order to reduce the post-disturbance voltage recovery time such that the induction motor under-voltage protection should not trip [4]. According to the IEEE C37.96 [42], induction motor loads should trip if the voltage goes below 70%-85% of the rated voltage for more than 15 cycles. However, in this study, the threshold will be set as 80% of the rated voltage.

6.1.1 SVC rating and location

It has been shown before that the cause of the slow voltage recovery phenomena is due to the induction motor load drawing too much reactive power during the post-fault time interval. This can be observed from Figure 6.1 that the maximum power consumption of the IM load at bus 1041 is 2.168 p.u. while the nominal reactive power consumption during the pre-fault time interval is 0.4476 p.u., which corresponds to an increase in reactive power consumption of 1.72 p.u. which is equivalent to 172 Mvar. Therefore, Dynamic reactive power compensation devices must be utilized to mitigate the problem of the prolonged voltage recovery times.

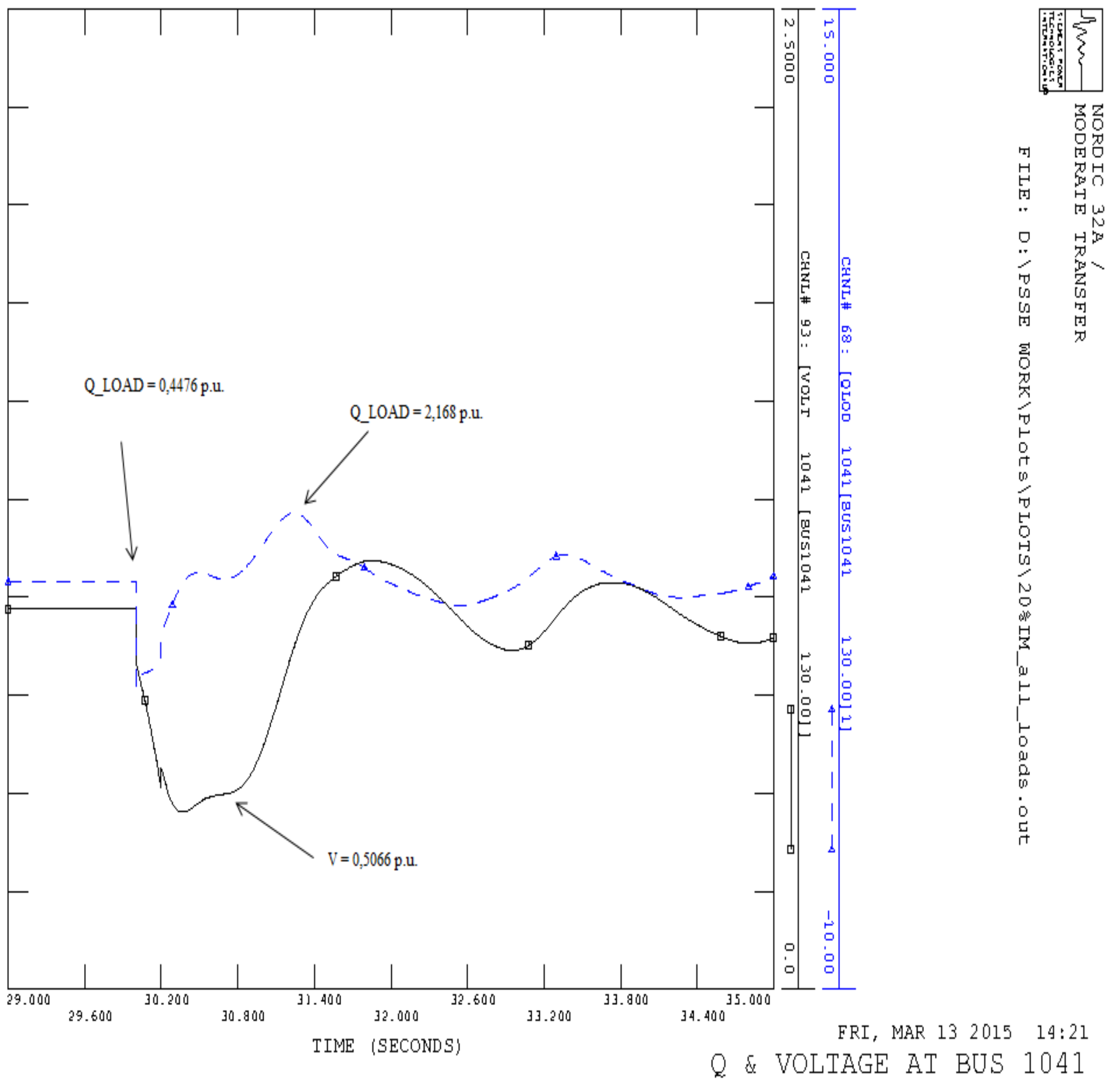

Figure 6.1: The voltage and reactive power consumption at bus 1041

To gain the full effects of SVCs on the voltage recovery phenomena, they must be connected at the point of common coupling (PCC) with the induction motor since the reactive power drawn from remote generation units would cause a huge voltage drop over the transmission lines. The rating of the SVCs is calculated through the trial and error approch which was proposed in the publication [4] till the IEEE requirements have been satisfied [42].

Figure 6.2 shows the voltage recovery times with different SVC ratings at each of the five weak buses at which the induction motor loads were installed. It can be observed from the Figure that the minimum voltage sag and the voltage recovery times improve after the clearance of the faults as the rating of the SVC is increased. According to the IEEE standard C37.96 which states that for the under-voltage protection of induction motors, the voltage should not go below 0.8 p.u. for more than 15 cycles. The 250 Mvar rating has satisfied the IEEE requirements but the 300 Mvar will be considered in our subsequent studies as a saftey margin.

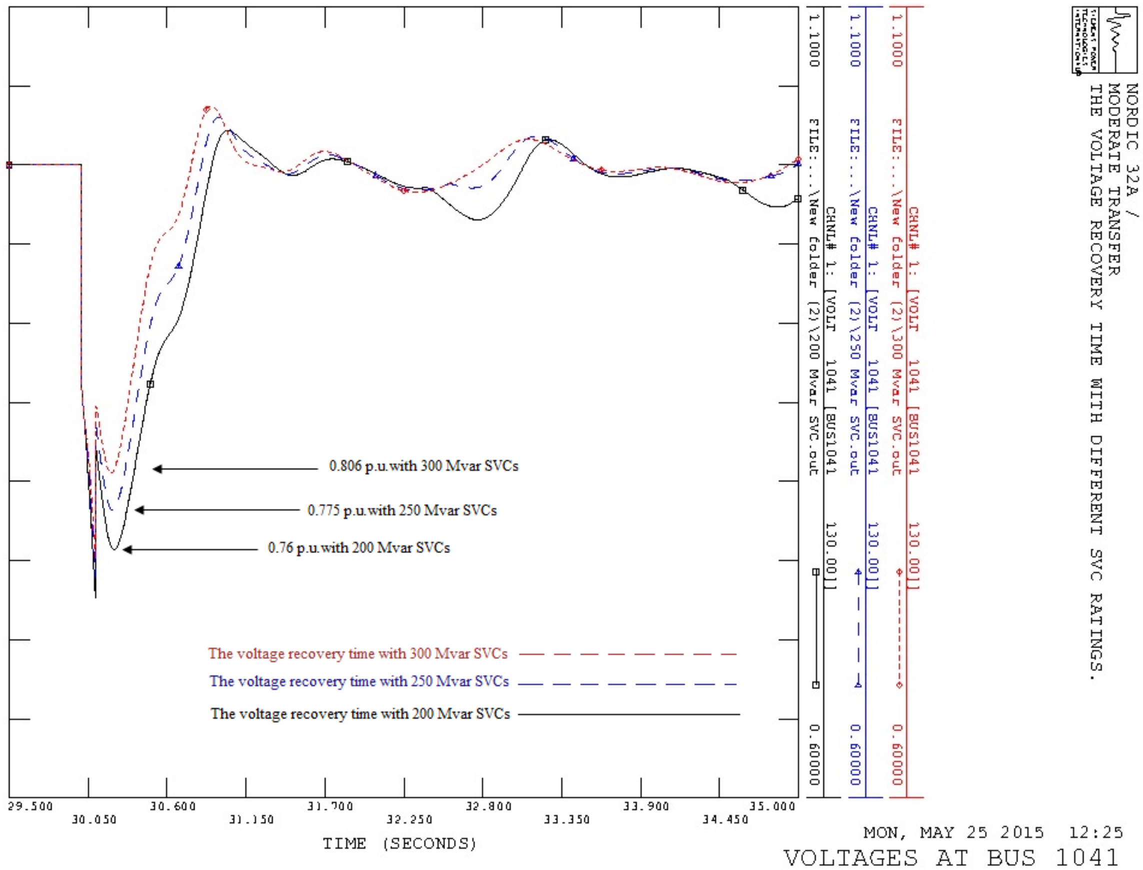

Figure 6.2: The voltage recovery times with different SVC ratings

Table 6.1: the parameters of the SVC controller [39]

	The parameters of the SVC controller (CSSCST)						
SVC Rating (Mvar)	**T1 (s)**	**K (Mvar/p.u.)**	**T2 (s)**	**T3 (s)**	**T4 (s)**	**T5 (s)**	**Vov**
+300/-50	0	30000	0	2.4	0	0.01	2

The explanation of the SVC controller parameter was shown in chapter 3. The parameters for SVC dynamic model code can be found in Appendix F2.

The distance relay protection system must also be modified so that it adopts with the new added SVC devices into the grid. The reactive power generated from SVCs would increase the fault current significantly as they attempt maintain a uniform voltage profile across the buses. Therefore, the total fault clearing time of ZONE 1 plus the circuit breaker was reduced down to 0.1 seconds (previously it was 0.2 seconds) in order to make the SVC model to work.

6.1.2 Voltage recovery time analysis with and without SVCs

The SVCs were installed at all of the induction motor buses which are considered the weakest among all of the buses. The simulation procedure was the same as section 5.5 with adding a third fault on the line 4031-4041-2. Figure 6.3 below shows the post-fault voltage recovery time during the time interval 29-33 seconds with different combinations of loads and SVCs. It can be seen from the Figure that the SVC managed to reduce the voltage sag from 0.71 p.u. to 0.8 p.u. which improved the voltage recovery and satisfied the minimum requirement that was proposed by IEEE standard for undervoltage protection of induction motors. Table 6.2 shows the voltage recovery time for each load combination for the time interval 29-33 seconds. It’s worth to note that for the case without the SVC, it can be seen that the minimum voltage sag is 0.71 p.u. while in Figure 6.1 it was 0.5 p.u, This increase in the voltage is due to the switched shunts that were added to the network in the steady state power flow in order to make the SVC model to work in the dynamic simulation.

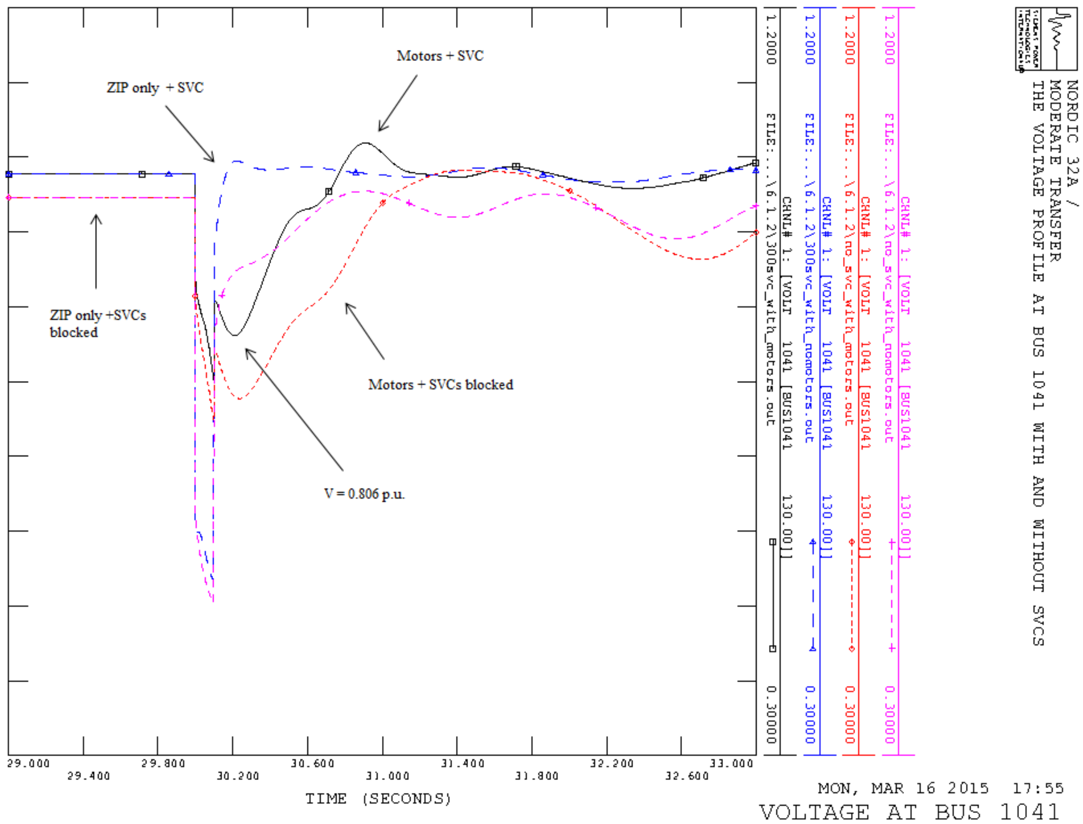

Figure 6.3: The VRT with different load combination with and without SVC at T= 29-33 seconds

Table 6.2: The voltage recovery time for different load combinations

Load combinations	**Minimum post-fault voltage sag (pu)**	**Voltage recovery time (seconds)**
ZIP + SVC	1	0.057
Motors + SVC	0.8	0.665
ZIP + SVC Blocked	0.85	0.667
Motors + SVC Blocked	0.71	0.9

The second fault occurred at T=130 seconds which caused the transmission line 4042-4043 to trip. Figure 6.4 below shows the slips of induction machine at bus 1041 and the voltages during the time interval 130 seconds at which the second fault has occurred. The voltage dip in the case with SVC is more significant than the first dip at T=30 seconds, this is due to the system being heavily stressed. However, Compared to the previous case in section 5.5 in which the SVCs were not installed, no cascaded trippings have occurred so far which shows the role of the SVCs in maintaining voltage stability. It can also be observed that the slip of the IM was quickly restored to nominal value compared to the case without SVC.

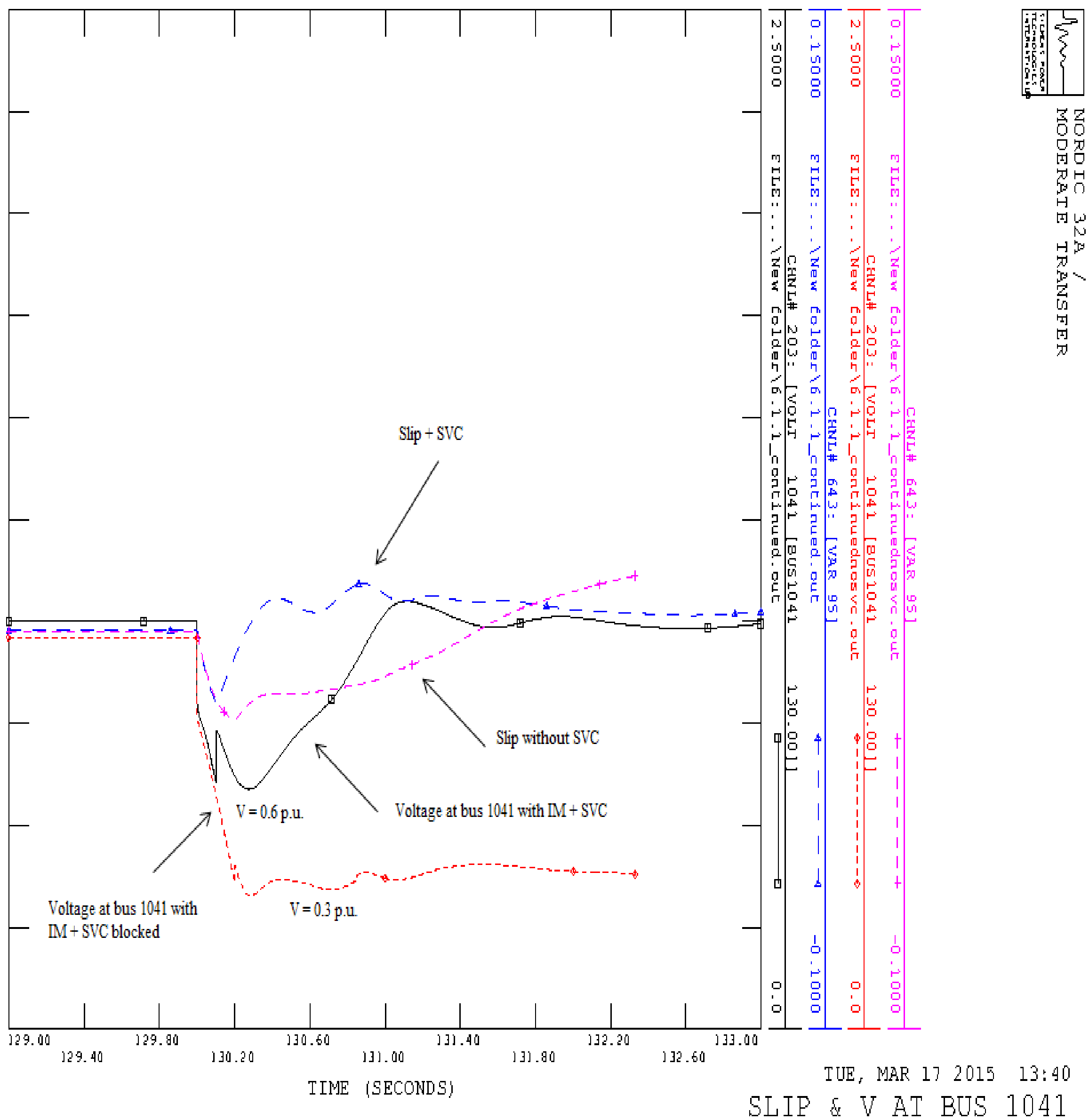

Figure 6.4: The slip of the induction motor load and voltages at bus 1041 at T=130 seconds.

At T= 230 seconds, circuit 2 of the transmission line 4031-4041 tripped due to a fault that has led to several cascaded trappings that eventually led to a voltage collapse. Figure 6.5 below shows the voltage profile of bus 1041 during the time interval 229-231 seconds at which cascading events has occurred that has led to the voltage collapse. The stalling of the induction motors worsened the situation by drawing huge amount of reactive power as it can be seen from the Figure. This has caused several transmission lines to be overloaded and eventually tripped.

The timings of the distance relay operation are shown in the Table 6.3 below. It can be seen that seven transmission lines have to be tripped before a voltage collapse occurs compared to the case without SVC in section 5.5 where only four transmission lines had to be tripped before the voltage collapse occurred.

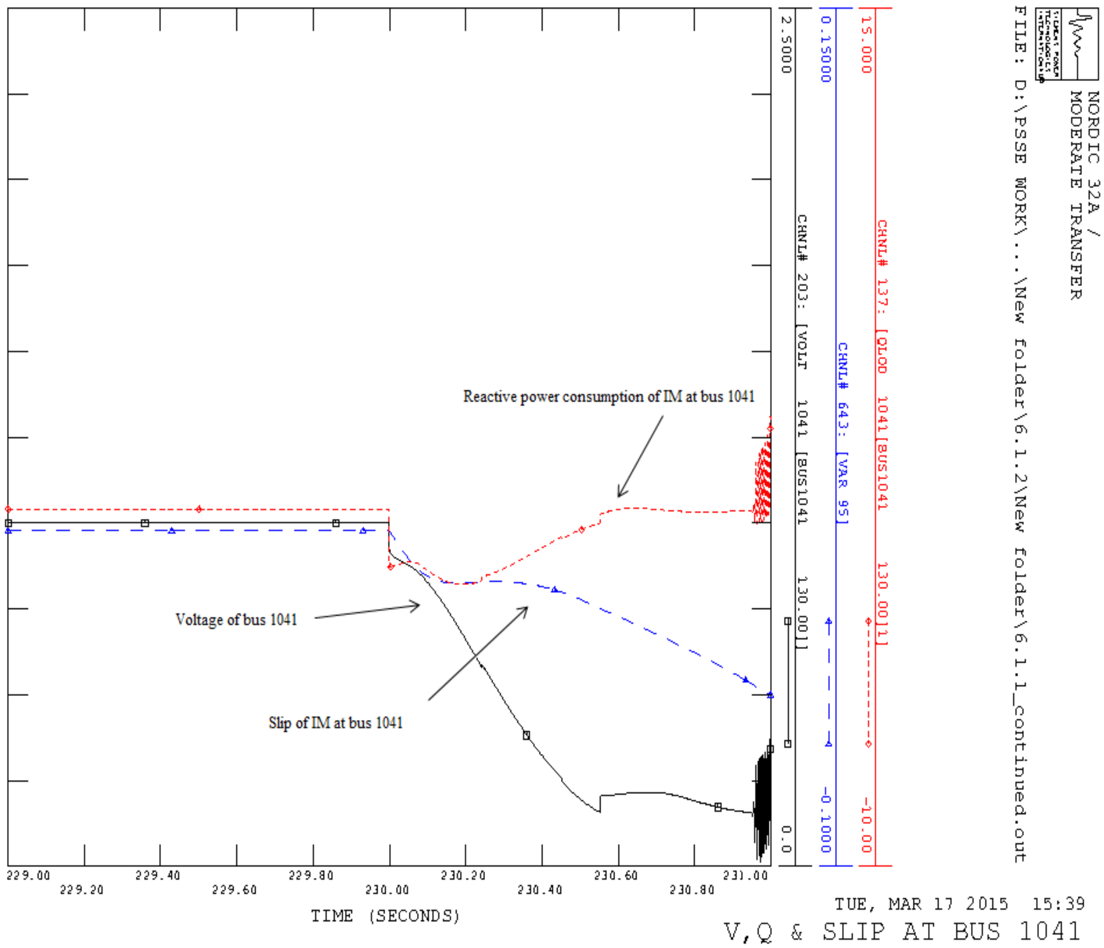

Figure 6.5: The voltage profile at bus 1041 at T= 229-231 seconds

Table 6.3: The timings of distance relay operation

			Pick up Times (Seconds)			Timed Out (Seconds)			
Event No.	**Transmission line**	**Fault initiation time (Seconds)**	**Zone 1**	**Zone 2**	**Zone 3**	**Zone 1**	**Zone 2**	**Zone 3**	**CB operating time (Seconds)**
1	4032-4044	30	30			30.05			30.1
2	4042-4043	130	130			130.05			130.1
3	4031-4041-2	230	230			230.05			230.1
4	4022-4031-1	Cascaded trip		230			230.3		230.351
5	4022-4031-2	Cascaded trip		230			230.3		230.351
6	4031-4032-1	Cascaded trip	230.31			230.36			230.41
7	4042-4044	Cascaded trip	230.452			230.502			230.552

Figure 6.6 below shows the distance relay 4042-4044 characteristics. Compared to the previous case in section 5.5 without the utilization of SVCs , the apparent impedance has entered zone 2 but quickly moved out of the tripping zones before finally resting in zone 1 at T= 230.452 seconds.

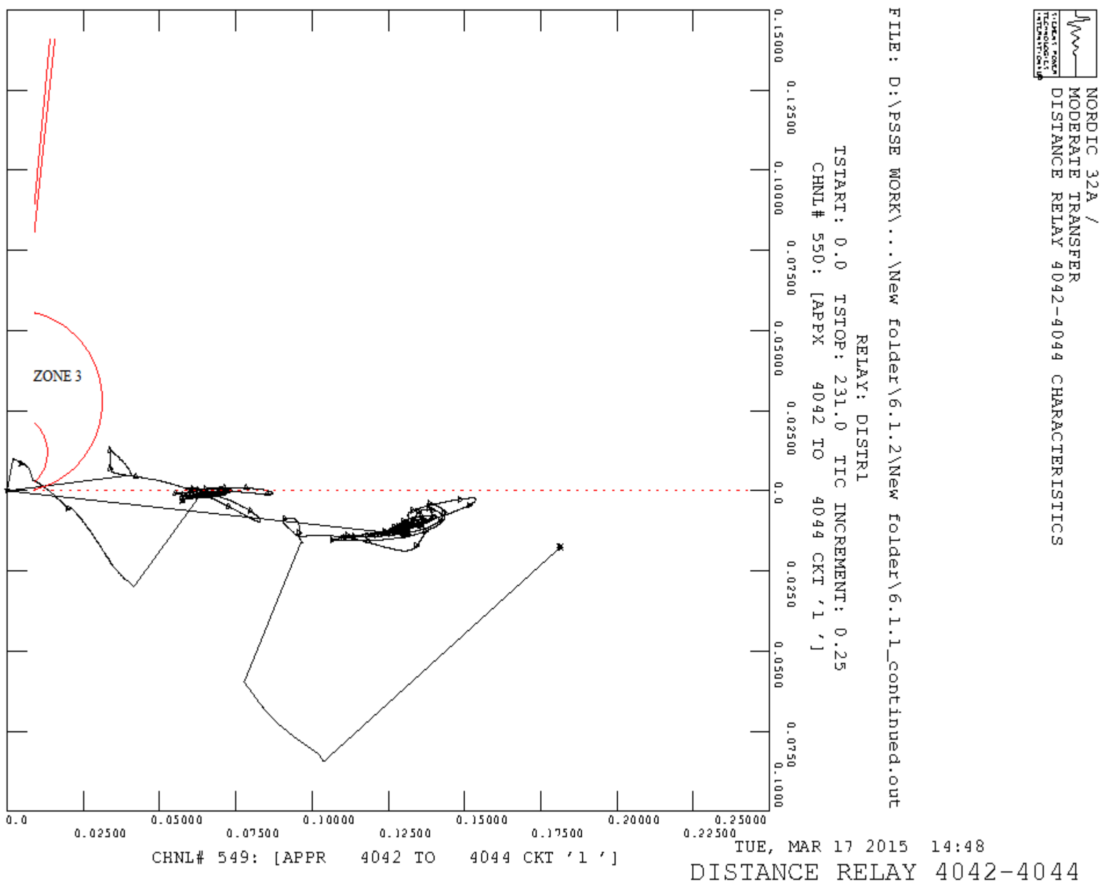

Figure 6.6: The characteristics of the distance relay at the transmission line 4042-4044.

6.2 Improvement of Voltage Stability Through STATCOM

STATCOMs has the capability to supply full reactive power regardless of the system's voltage in addition to the fast switching of the IGBT (insulated-gate bipolar transistors) which are employed in the voltage source converter. STATCOMs will be the ultimate tool to mitigate the post-fault VRT phenomena. In this section, the performance of the STATCOM in mitigating VRT will be investigated and will be compared to the SVC performance.

6.2.1 STATCOM rating and location

The methodology for selecting the rating of STATCOMs for our system will be the same as the SVC in section 6.1.1. However, STATCOMs always have symmetrical ratings i.e. the capacitive and the inductive ratings of a STATCOM are always the same. Therefore, the rating of the STATCOM devices is ±300 Mvar which will be placed at each of the weak buses in the system that already have induction motor. Also, unlike SVCs, STATCOMS have 125%-150% transient overloading capability. Therefore, in our case 125% transient overloading rating has been assumed. It's worth to note that high rated STATCOM devices are less desirable in real world situations due to the high losses associated with the voltage source converter which can go above 1% but the PSS/E model **CSTCNT** which will used to model STATCOMs in this study is losses. The parameters of the STATCOM model CSTCNT are shown in the Appendix F1 and further details about the model can be found in [41].

6.2.2 Voltage recovery time analysis with and without STATCOM

The simulation procedure will be the same as in the SVC section in section 6.1.2. Figure 6.7 below shows the voltages at bus 1041 with the STATCOM. As it has been predicted before, the voltage recovery time with STATCOM is significantly faster than that of the SVC in addition to the voltage didn't sag as much as that of that in the case of SVC. The voltage recovery times for each case are shown in Table 6.4.

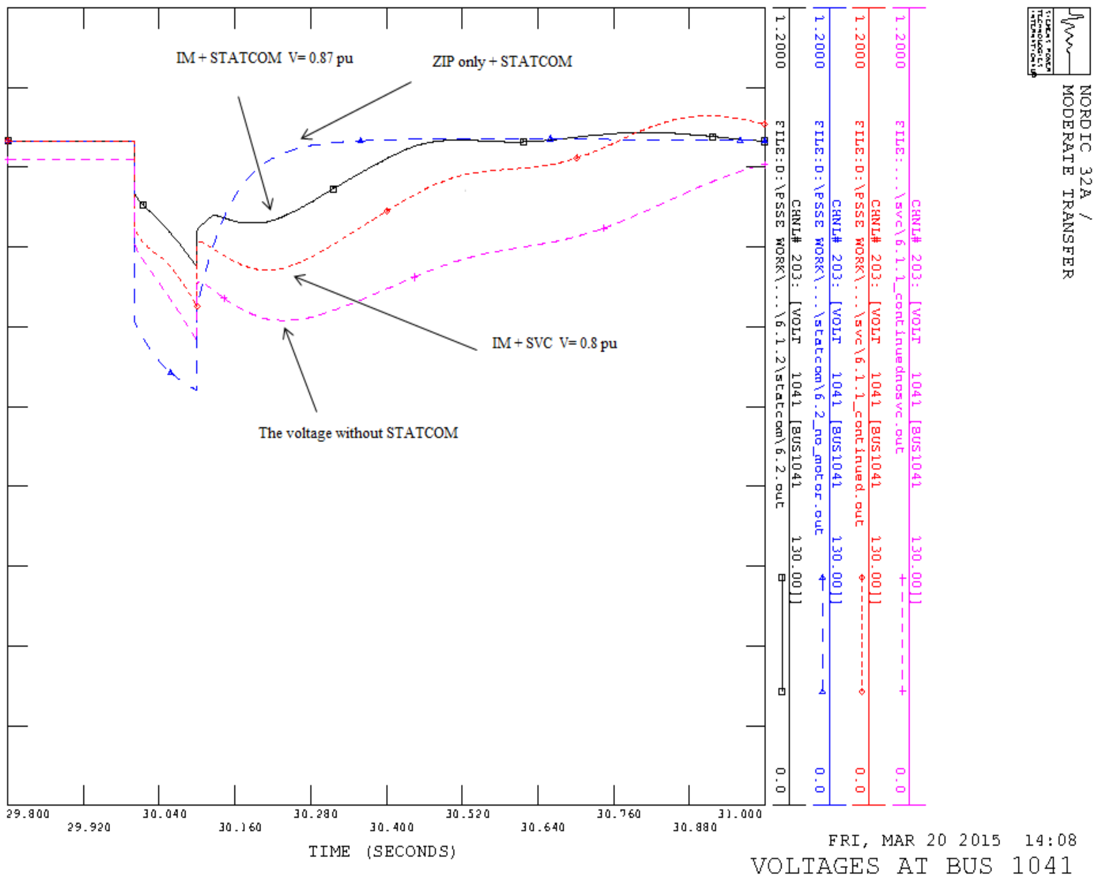

Figure 6.7: Voltages at bus 1041 with STATCOMs and SVCs

Table 6.4: The voltage recovery time for the time interval T= 29-33 seconds

Load combinations	Minimum post-fault voltage sag (pu)	Voltage recovery time (seconds)
ZIP + STATCOM	1	0.06
Motors + STATCOM	0.87	0.364
Motors + SVC	0.85	0.665
Motors + STATCOM blocked	0.71	0.9

Figure 6.8 below show the simulation results for the time interval 129-132 seconds where the second fault occurred in the transmission line 4042-4043. It can be seen the superior voltage recovery performance of the STATCOM compared to the SVC. In addition, unlike the SVC, the slip of the induction motor at bus 1041 was maintained to nominal value (near synchronous speed) and didn't deviate much during and post-fault time interval.

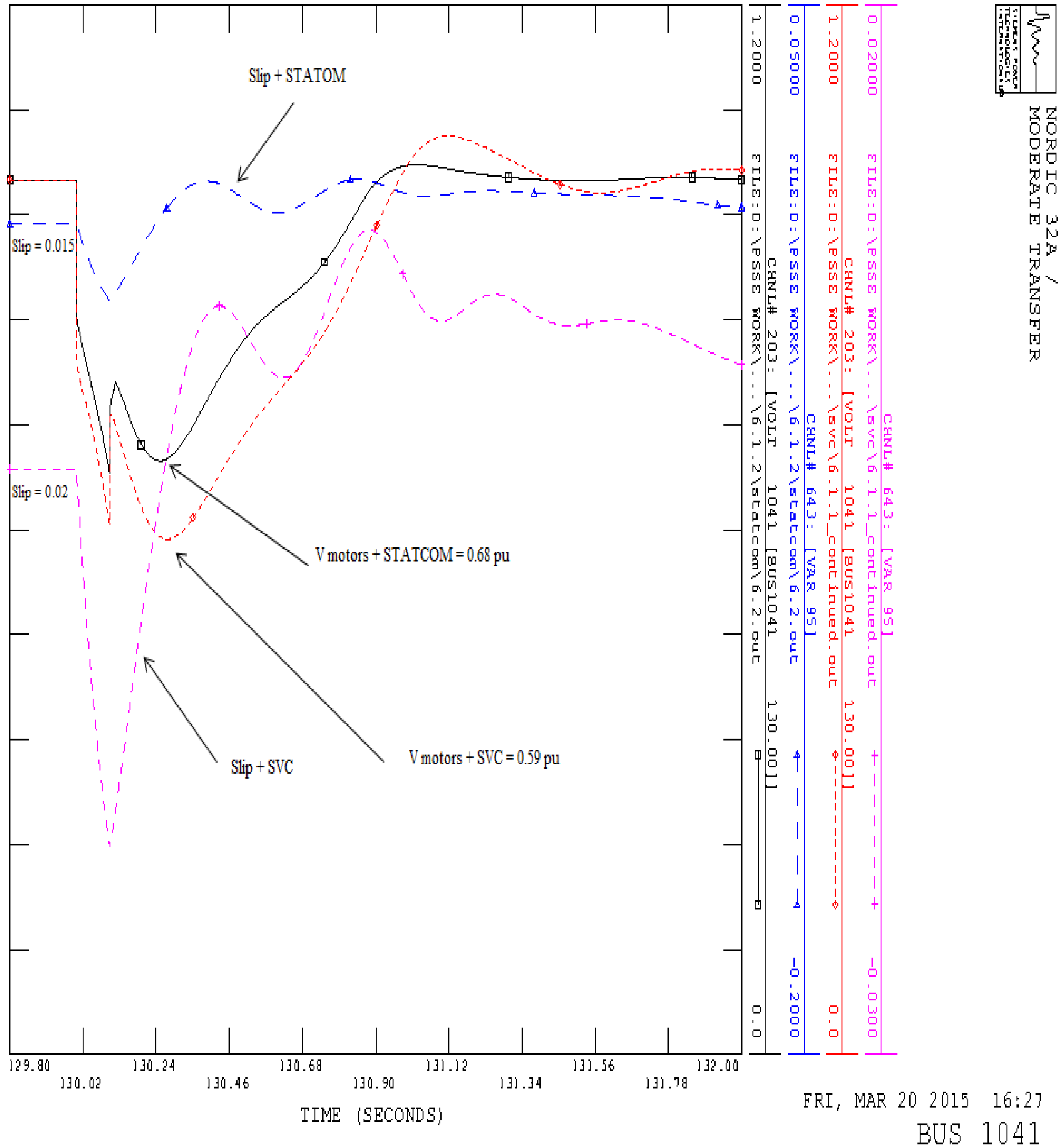

Figure 6.8: The induction motor slip and voltages at bus 1041.

The voltages and slips at bus 1041 during the time interval 229-232 seconds are shown below in Figure 6.9 in which a fault was introduced into the transmission line 4031-4041-2 that caused the transmission line to trip. The Figure shows the performance of the STATCOM compared to the SVC. It can be seen that the voltage collapse was delayed by 0.4 seconds compared to the case of SVC so does the stalling of the induction machines. It can be also seen that the voltage collapse occurred after the induction motors have stalled compared to the case of SVC. The timings of the distance relays are shown in the Table 6.5.

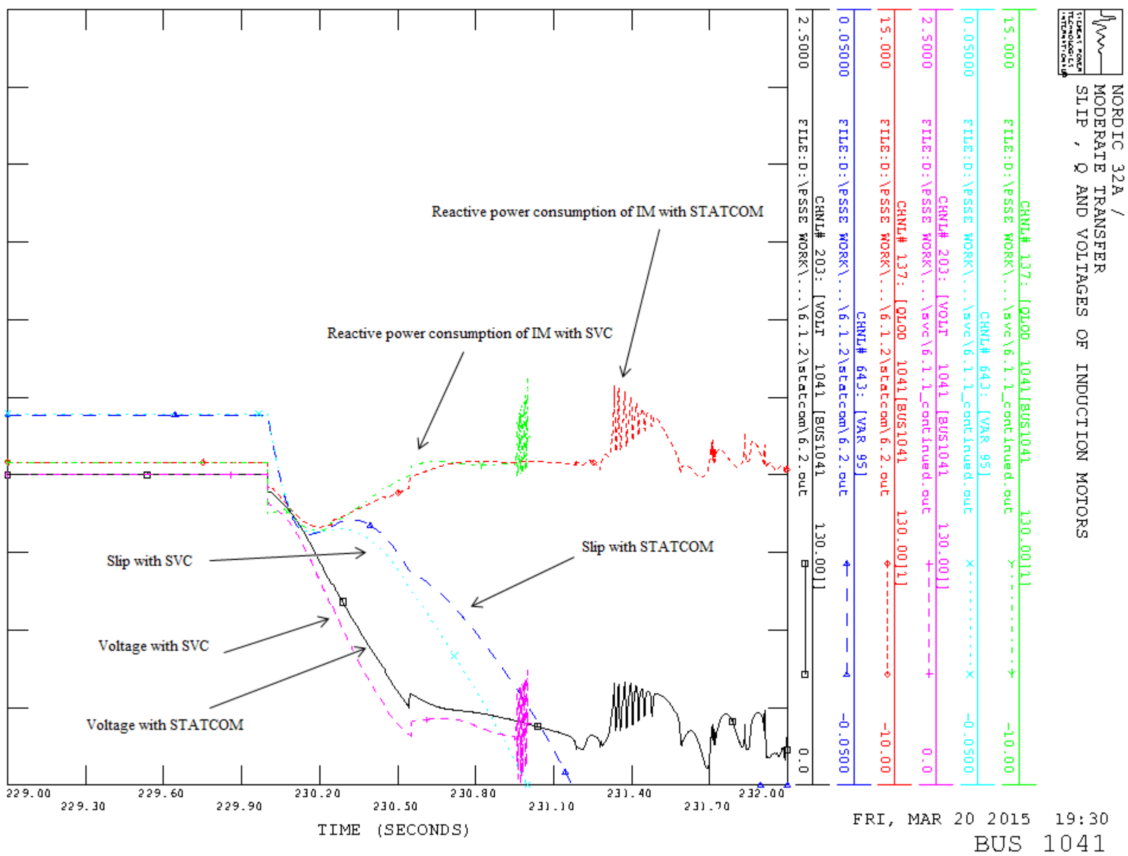

Figure 6.9: The slip and voltages at bus 1041.

Table 6.5: The timings of the distance relay operation

			Pick up Times (Seconds)			**Timed Out (Seconds)**			
Event No.	**Transmission line**	**Fault initiation time (Seconds)**	**Zone 1**	**Zone 2**	**Zone 3**	**Zone 1**	**Zone 2**	**Zone 3**	**CB operating time (Seconds)**
1	4032-4044	30	30			30.05			30.1
2	4042-4043	130	130			130.05			130.1
3	4031-4041-2	230	230			230.05			230.1
4	4022-4031-1	Cascaded trip		230			230.3		230.351
5	4022-4031-2	Cascaded trip		230			230.3		230.351
6	4031-4032-1	Cascaded trip	230.31			230.36			230.452
7	4042-4044	Cascaded trip	230.452			230.502			230.552
8	4041-4061	Cascaded trip		230.853			231.153		231.204

Compared to the case of the SVC in section 6.1, eight transmission lines had to be tripped (three tripped due to faults and five tripped due to overloading) before the voltage collapse occurred which is an indication of superior performance of STATCOMS over SVC in mitigating voltage collapses. The loadings on the transmission lines during the cascaded tripping events are shown in Figure 6.10.

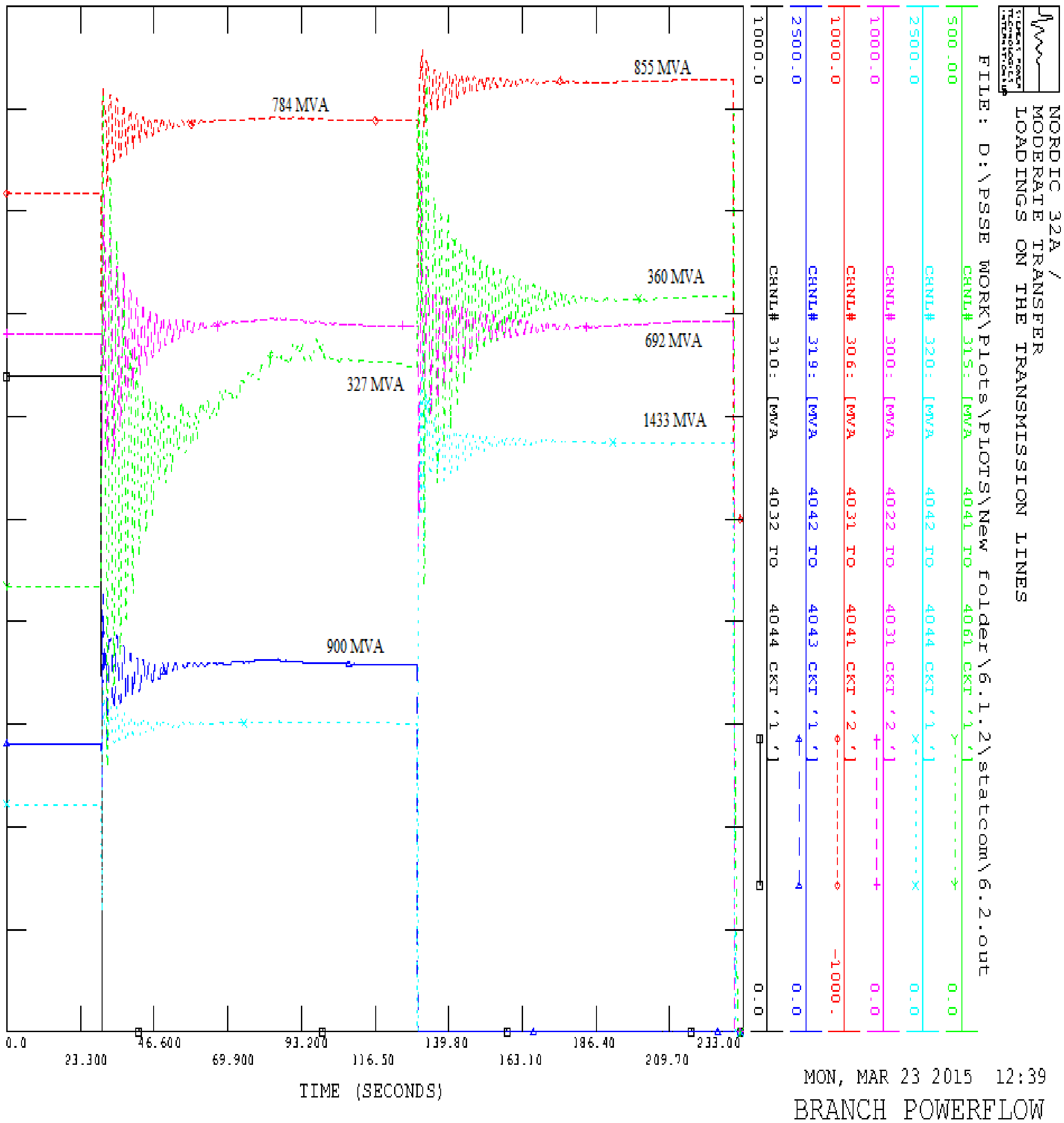

Figure 6.10: The loading of the critical lines

7

Impacts of Large Scale Integration of Solar PV Plants on Voltage Stability

Sweden's latitude is very high and it's known that the sunlight at higher latitudes vary greatly throughout the whole year and gets very limited during the winter time. However, through the utilization of sun tracking systems, the output power generated from solar PV plants can increase significantly in some parts in Sweden up to the point where large scale integration solar PV plants is both technically and economically feasible [43]. This chapter will begin by determining the optimal placement of solar PV plants, the maximum allowable PV penetration level, the effects of the changes of the irradiance on the voltage stability and finally the effects of solar PV integration on the voltage recovery time.

7.1 Solar PV Plant Location

In order to utilize solar PV plants effectively, they need to be located at a place that is exposed to the highest level of average solar Irradiance throughout the year. The Joint Research Centre of the European Commission (JRC) [43] has established the solar irradiance map of a PV panel with two-axis sun tracking system as shown in Figure 7.1 below. It can be seen from the Figure that the locations with highest sun-hours are located in the north eastern part in a suburb called Piteå and in the southern eastern part in a suburb called Öregrund. Therefore, in the Nordic-32 system, several buses will be introduced to mimic these regions and those buses will represent an aggregate of solar PV power plants which will be connected to the grid through high voltage 400 kV transmission lines. It's also worth to note that the PV plants are represented as separate buses because the PSS/E model of the PV plants only work if the PV plants are placed in separated bus.

The single line diagram of the Nordic-32 system with the addition of several buses for PV plants is shown in Figure 7.2. The maximum number of PV buses will be determined after the determination of the maximum allowable PV penetration which will be shown in section 7.4.

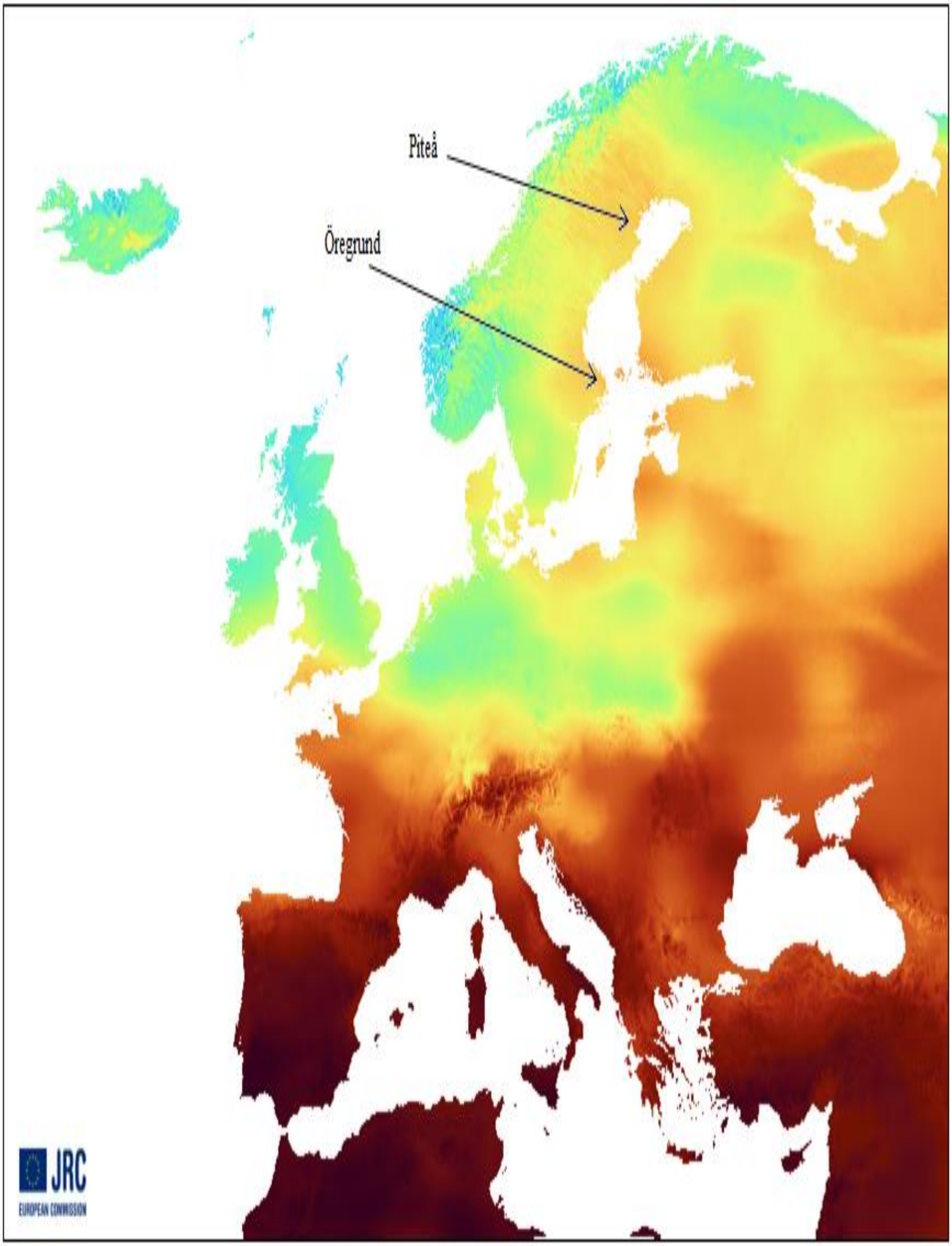

Figure 7.1: Solar irradiance map according to JRC [43]

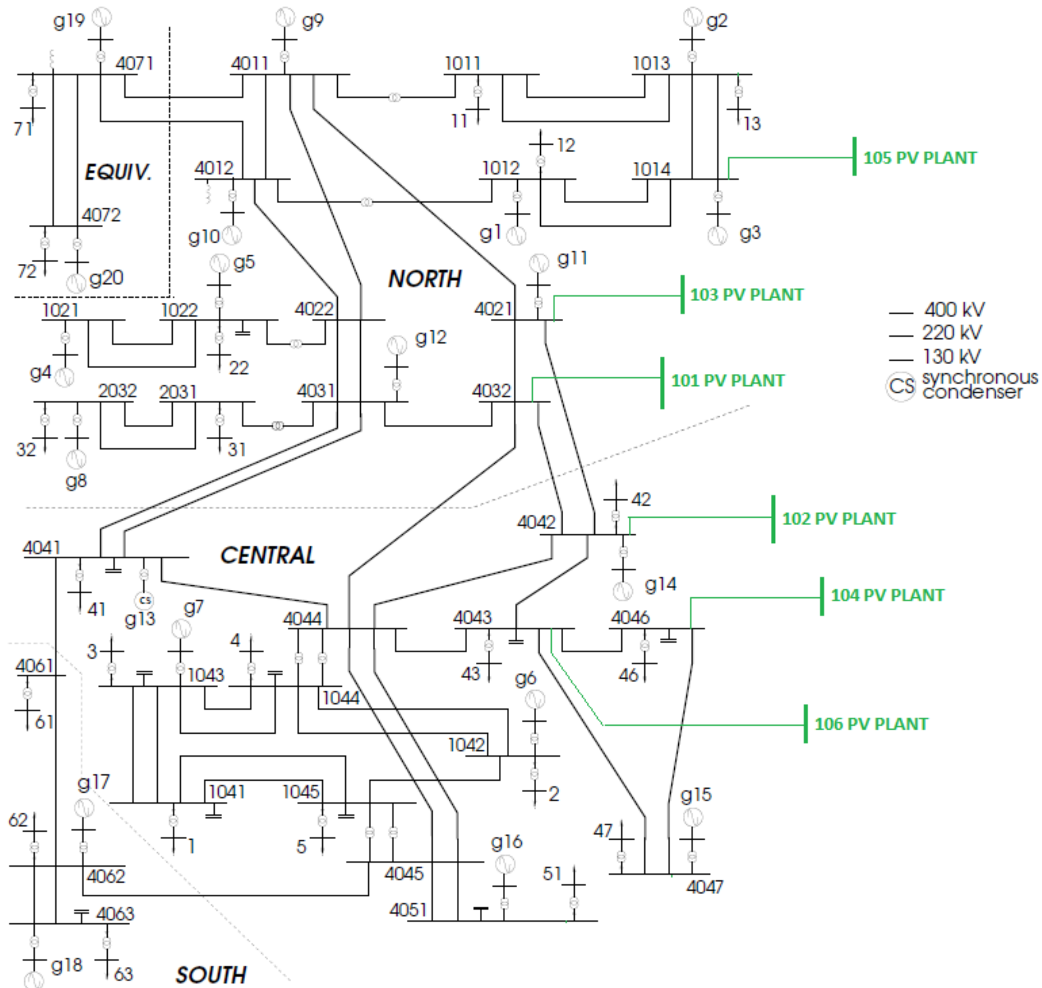

Figure 7.2: Nordic-32 bus system with PV plants buses [33]

7.2 Modifications to Nordic 32 System

As conventional generating units have been removed from the system and replaced by the PV power plants, the reactive power support of the system becomes weak since the PV plants are located far away from the load center in the south of the network and the power flow in the steady state will not converge. Therefore, in the steady state analysis, switched shunts were placed at the buses at which there were conventional generating units with a reactive power rating same as those of the conventional generating units. The switched shunt models will not be included in any dynamic simulation and in this case when the dynamic simulation initializes, it will consider switched shunts as a fixed shunt with the same rating that was adjusted by the program after performing the steady state power flow.

The other modification that has been done on the system is that the inertia constant of the conventional generators has been increased and the frequency controller (the governors) have been added to all of the conventional generating units (refer to Appendix A). This has been done in order to avoid huge frequency deviations when a disturbance occurs since PV plants lack the inertia. This will be further illustrated in section 7.4.

7.3 Solar PV Sizing Methodology

The first step in the large scale implementation of the PV plants is to determine the percentage of their penetration. The percentage of PV penetration will be calculated according to the following assumptions:

- The penetration percentage is based on the total active power generation of Nordic-32 system at normal base case loading.
- The maximum output active power of a solar PV plant is 600 MW when having an irradiance of 600 MW/m^2 (the maximum irradiance average measured at Piteå and Öregrund).
- The maximum output reactive power is 1/3 of the active power (that is ± 200 Mvar) and it is mainly dependent on voltage level at the PV plant bus.
- The PV plants will be installed at the proposed locations which are shown in Figure 7.2 in section 7.1 (the green buses).

As it has be seen from Figure 4.3 in chapter 4, the total active power generation is the sum of all connected loads and the system losses and can be given by equation (7.1). Table 7.1 shows the 10%, 20% and 30% active and reactive power generation for each PV penetration level:

$$P_{generation} = P_{load} + P_{losses} = 10940 + 311.32 = 11251.32 \text{ MW} \tag{7.1}$$

Table 7.1: the generation of each of the solar PV penetration level

Percentage of solar PV penetration	Active Power (MW)
10% PV Penetration	1125.13
20% PV Penetration	2250.3
30% PV Penetration	3375.4

7.4 Determination of Maximum Allowable Solar PV Penetration.

Solar power is beneficial up to a certain penetration level if the system at which it’s integrated to has many hydro and thermal units. This due to the fact that unlike conventional generating units PV plants do not have inertias. Therefore, when the system is subjected to a disturbance, the frequency of the system might deviate too much and that would cause the distance relay protection to trip and ultmately the system will be at much prone to voltage collapse. Hence, frequency deviation will be the basis on deciding the optimal solar PV penetration.

7.4.1 Dynamic simulation to determine the maximum PV penetration

According to the Nordic Grid Code [44], the maximum permissible frequency deviation is - 0.5 Hz due to the loss of one of the largest generating units and it’s known that PV power plants lack the interia which are associated with conventional generation units. Therefore, any disturbance in the system would cause a significant frequency deviation in the case of large scale integration of solar PV plants. Frequency deviations that occur due to the loss of loads could be easily avoided since the output of the generating units could be reduced readily. However, frequency deviations that occur due to the loss of generation are difficult to handle since generation reserves are limited. Therefore, limiting the frequency deviations due to the loss of generation is very important.

Dynamic simulation has been performed to determine the maximum solar PV penetration with the dynamic models of the solar PV shown in Appendix D. Figure 7.3 below shows the post-disturbance frequency deviation due to the tripping of one of the largest thermal generation units in the southern area of the Nordic-32 bus system. The selected unit for tripping was 4051-1 which was scheduled to produce 500 MW before tripping.

The frequency deviation analysis were done for 10% , 25% and 30% solar PV penetrations and as it can noted from Figure 7.3 that all of the cases are within the threshold. For the base case the deviation was -0.45 Hz. The 10% solar PV penetration frequency deviation was -0.5 Hz while for the 25% PV penetration the deviation was -0.6 Hz and for the 30% it was -0.65 Hz. The 30% PV penetration will be the maximum allowable PV penetration level, although the frequency deviation exceeded the threshold set by the Nordic Grid Code, the 30% PV penetration level will be considerd for the subsequent voltage stability analysis of the system in order observe the effects of the large scale PV plants on the voltage stability.

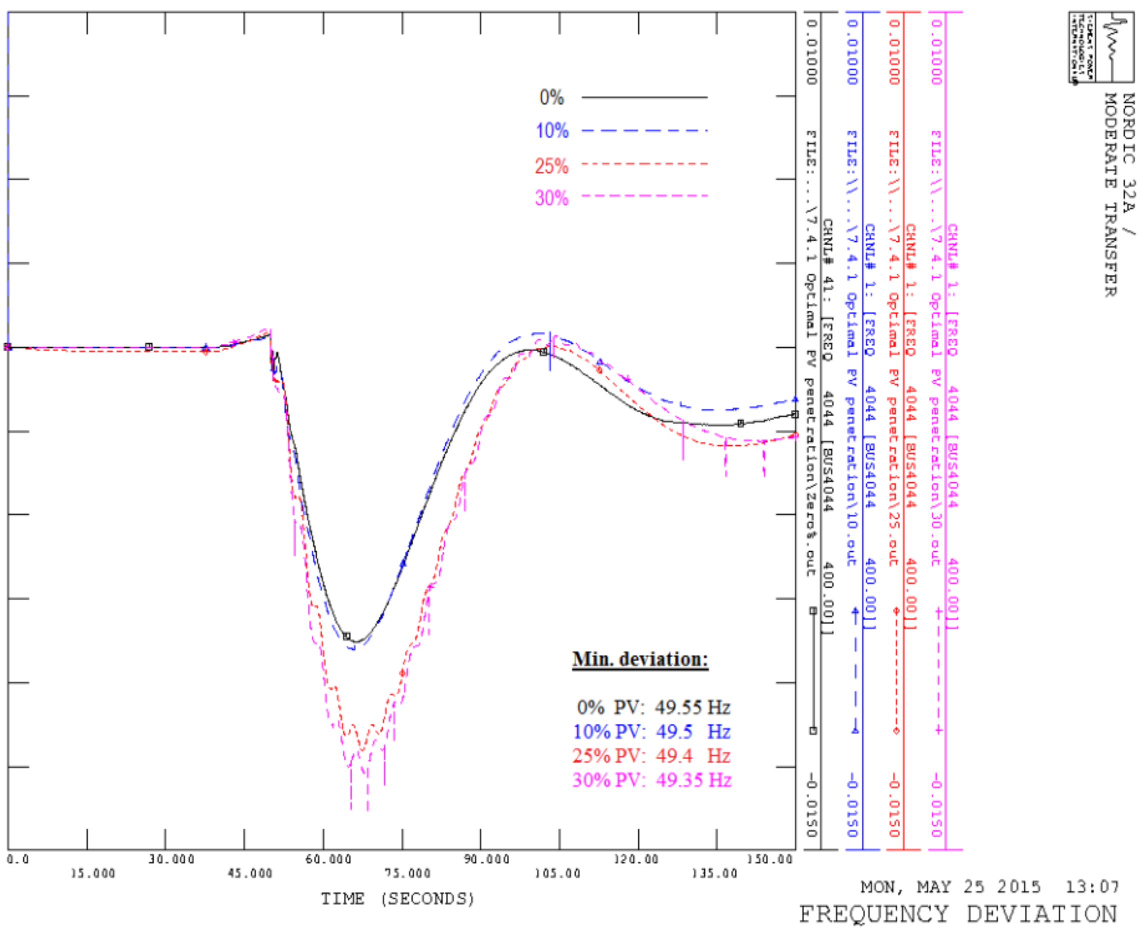

Figure 7.3: Frequency deviation for 0%, 10%, 25% and 30% PV penetration when tripping 4051-1G

7.4.2 P-V Curve analysis with different solar PV penetration levels

P-V curve analysis has been made to get an overview of the effects of large scale PV penetration on the voltage stability. The P-V analysis considered the generation from the northern portion of the network and the PV plants to the loads at the southern portion of the network. Figure 7.4 below shows the P-V curve for different solar PV penetration levels. It can be seen from the Figure that the base case and the 10% PV penetration are almost identical. However, for the 20% and 30% solar PV penetration levels, the voltage stability critical point became lower than that of the 10% and the base case. This is due to the fact that the solar PV power plants are concentrated at the eastern part of the network as shown in Figure 7.2 where the average of the solar irradiance is maximum. Therefore, the power generated from the PV plants has to travel very long distances to supply the loads at the western part of the network and that would increase the losses within the system in addition to the fact that the output power of the PV plants is limited to the availability of the solar Irradiance. Hence the position of large scale PV plants have a significant effect on the voltage stability.

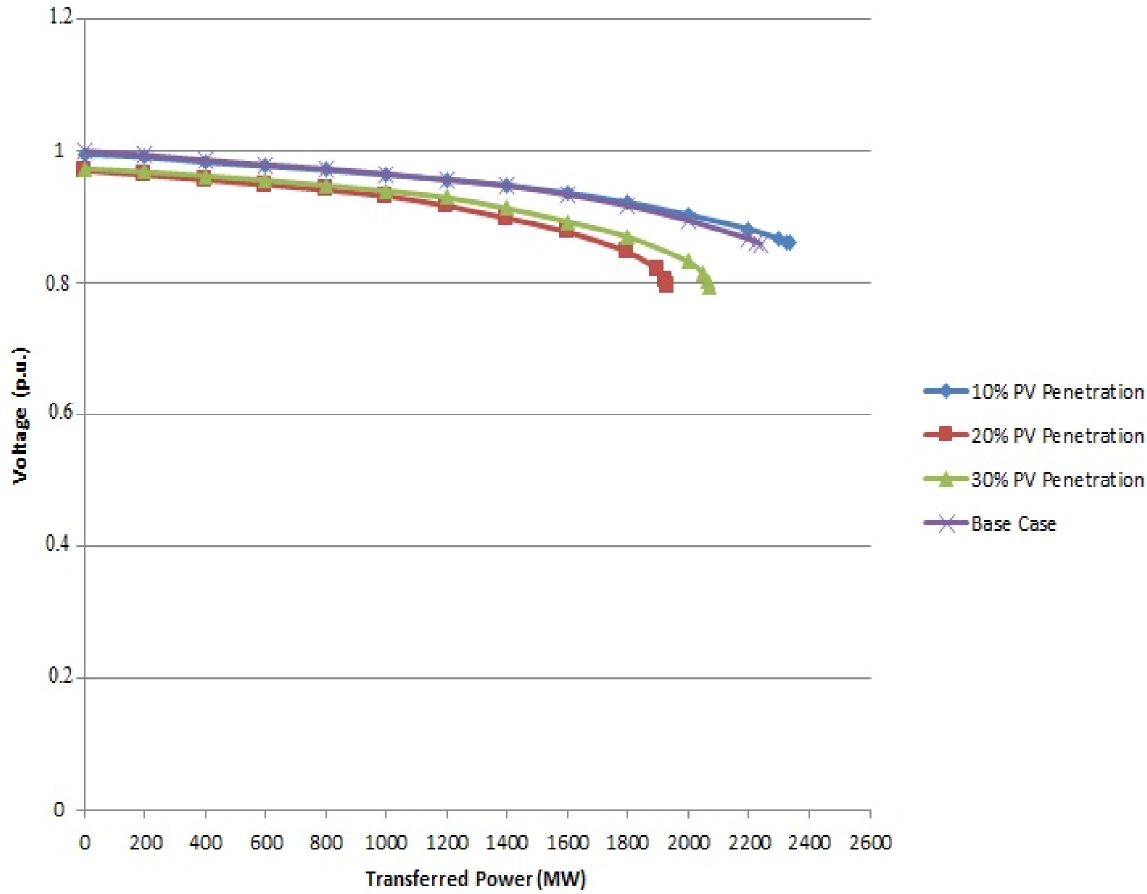

Figure 7.4: Power-voltage (P-V) curves for Nordic-32 systems with different PV penetration

7.5 Impacts of Load Profile and Irradiance Changes on Voltage Stability

The effect of the solar irradiance changes on the voltage stability will be investigated through performing dynamic analysis at 6, 9, 12, 15, 18 and 21 hour at the 15th day from each of the four seasons with the load profile of the system during each of those periods as shown in Figure 7.5. The simulation will mimic the periods where the solar irradiance is maximum and lowest. The average irradiance value at each hour was taken from NASA [45] and in order to achieve irradiance value changes within an hour, normal distribution function was used to sample 10 irradiance values that has an avergae equal to NASA irradiance value at that hour. The ten values were then distributed over 550 seconds with 50 seconds in between in order to run PV models in the dynamic simulation and investigate how the voltage behaves when changing the irradiance values. The irradiance changes and values for the specified hours are shown in Figure 7.6 and in Tables E1 and E2 in Appendix E.

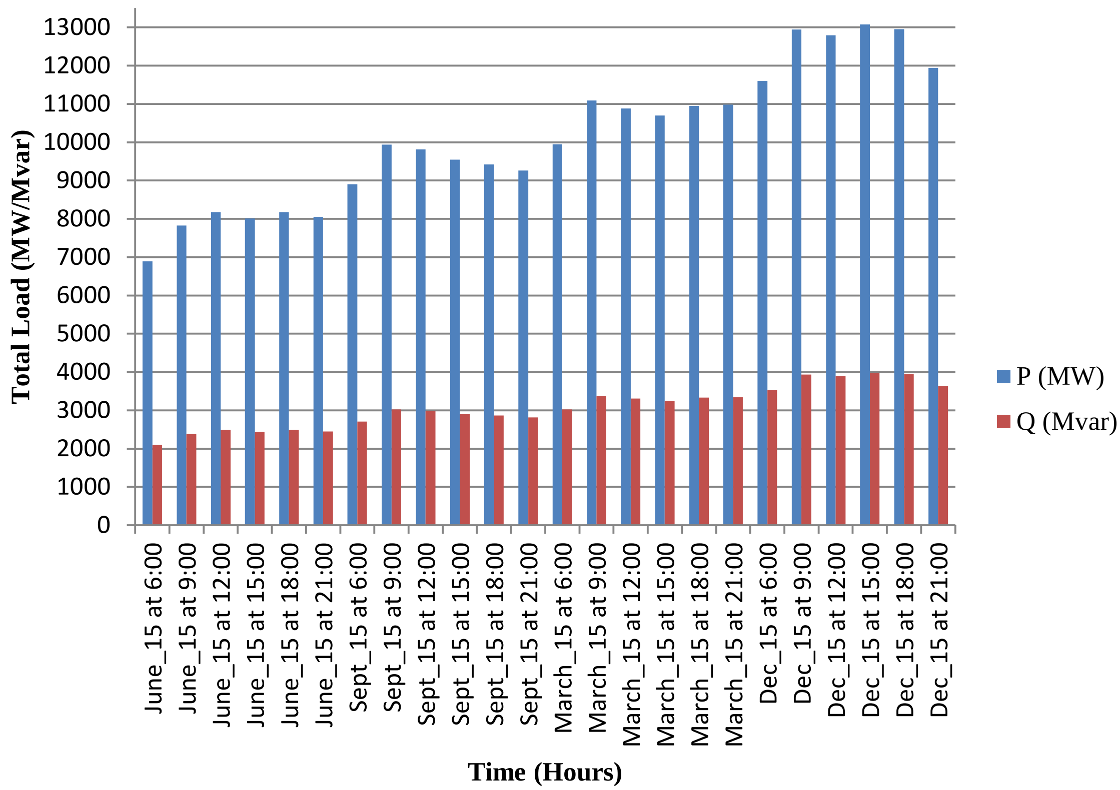

Figure 7.5: Load profile of the Nordic-32 system during the specified hours

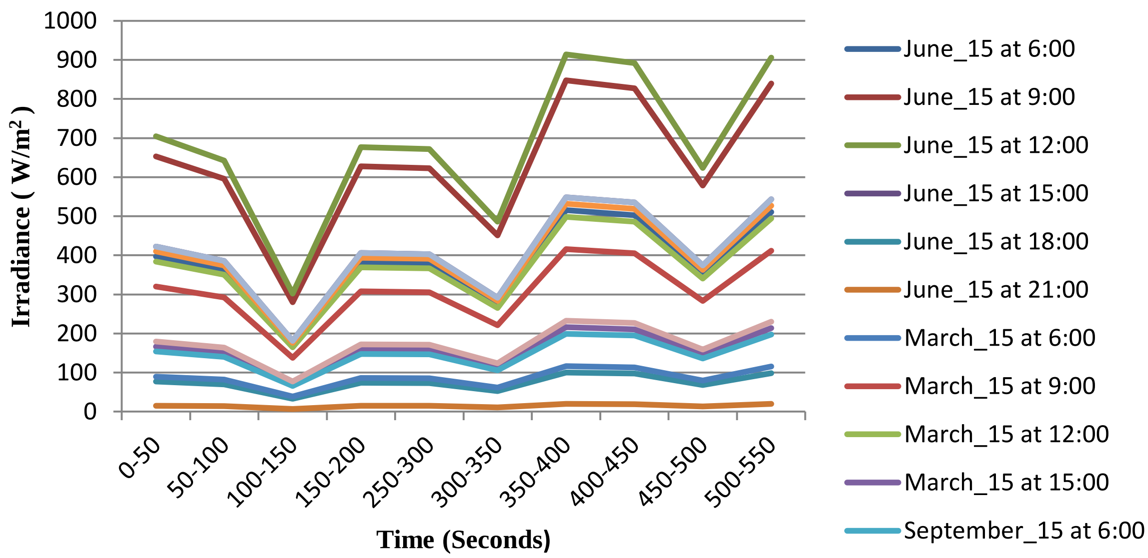

Figure 7.6: Irradiance values changes at the specified hours

7.5.1 Solar PV plant output power in relation to irradiance

Solar PV plants are sized according to the average solar irradiance available at the site of the PV. Therefore, in this analysis, a solar irradiance of 400 W/m^2 will yield 95% of the rated power of the PV plant which is 600 MW and an irradiance of 200 W/m^2 will yeild 50% of the rated power. The solar PV model will find the suitable output power for any of values of irradiance between the two irradiance values specified earlier.

The existing thermal generation units will be available on demand except those who have been shut down to be replaced by the PV plants, the dynamic simulation will force the PV plants to produce their rated power according to the irradiance and all of the output powers of the conventional generating units will be reduced and if the output power of the PV plants changes, the thermal generation units will be dispatch accordingly to compensate the power loss due the low irradiance levels. The analysis will be made through 30% PV penetration in the base case. However, as the load profile changes through the months, but the size and the number of the PV plants will be the same as the base case. The contribution of the solar PV power plant to the total generation of the system in the steady state power flow during the months is shown in the Figure 7.7.

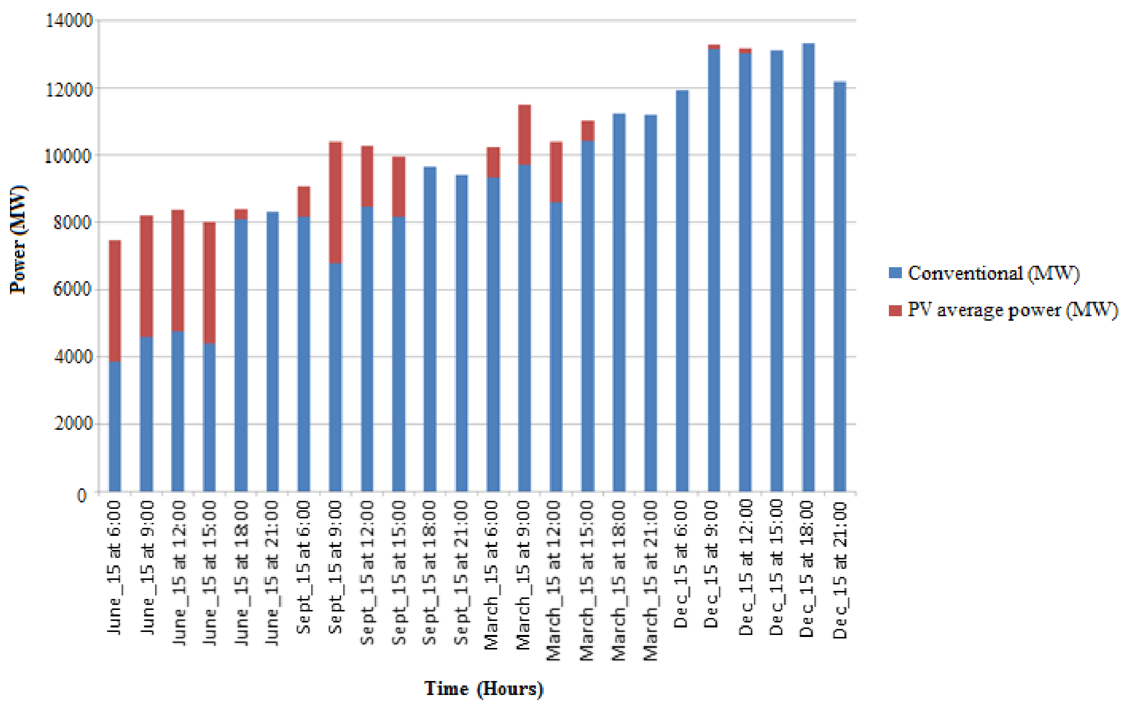

Figure 7.7: Active power production of PV plants and conventional generators during the specified hours

7.5.2 Dynamic simulation to investigate the impacts of load profile and irradince changes on voltage stability.

The procedure for the dynamic simulation will run as follows:

- The simulation will be run for 550 seconds. Every 50 seconds the irradiance value will change as shown in the Tables in Appendix E.
- Faults will be induced in the transmission line 4032-4044 at T= 100 seconds and the transmission line 4042-4044 at T= 200 and the transmission line 4031-4041-1 at T=300 seconds and the transmission line 4042-4043 at T = 400 seconds.

The voltage profiles at bus 1041 for hour 6 a.m. at a day of each of the months June , September , March and December are shown in Figure 7.8 below. It can be seen from the Figure that a voltage collapse has occurred after the fourth line fault (t = 400 seconds) in all seasons except in June. This is due to the fact that in June at 6 a.m. the the load profile is lowest compared to the rest of the months as it can be seen from the load profile Figure 7.8.

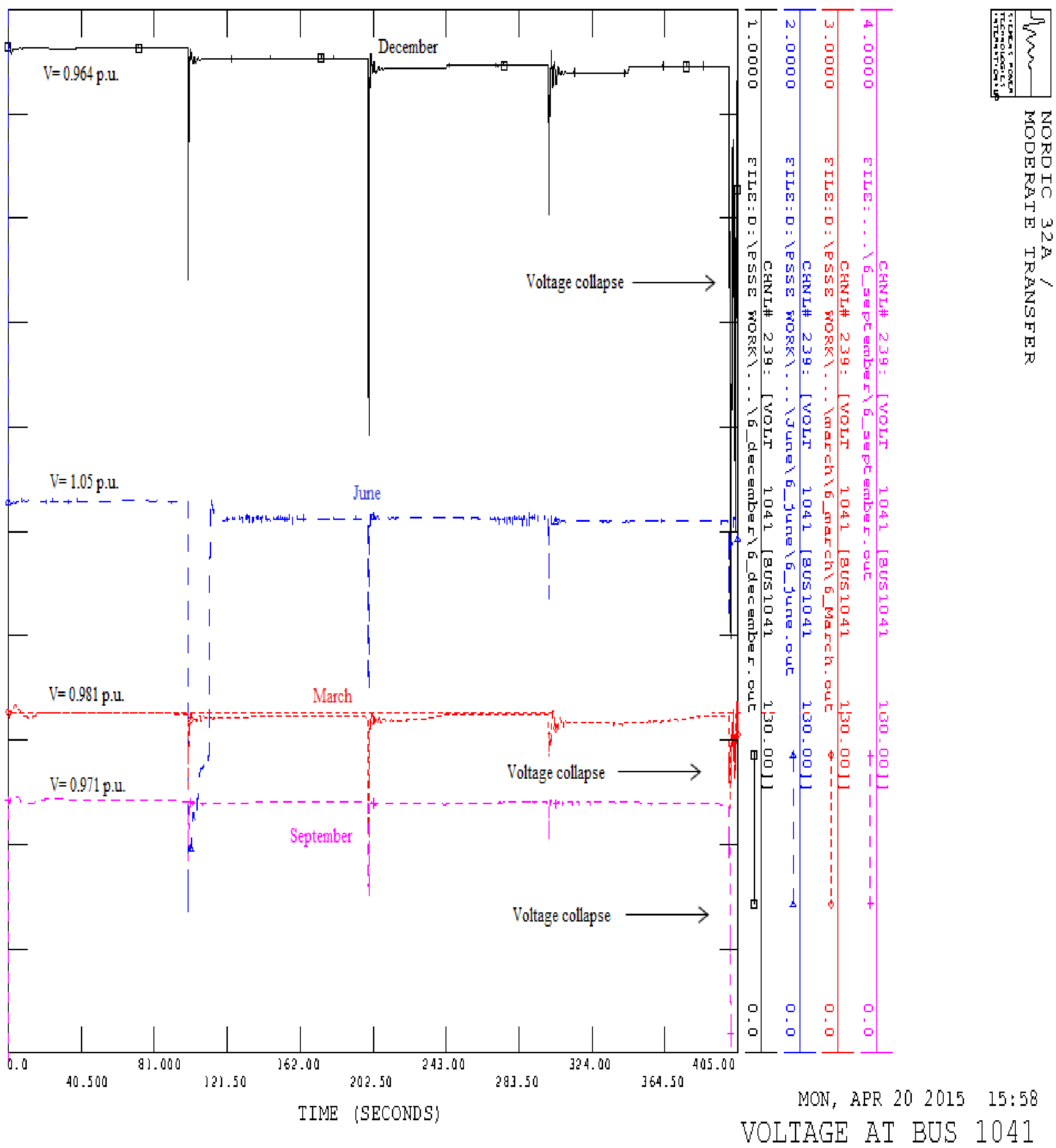

Figure 7.8: The voltage profile at 6 a.m. for all of the months

The voltage profiles at bus 1041 for hour 9 a.m. for each of the months are shown in Figure 7.9 below. From the Figure it can be observed that a voltage collapse has occurred immediately after the first fault (t = 100 seconds) for June and the september months but after the forth fault (t = 400 seconds) for March and December.

This is because at 9.a.m in June and september the loads has increased significantly than 6 a.m. while the PV power plants produce their maximum power. Moreover, most of the conventional generating units in the south were shutdown as it can be seen from Figure 7.8. during the these two months and this resulted in significant reactive power losses through the transmission lines as it has been observed in the P-V curves in section 7.4.2.

This is further illustrated in Table 7.2 which shows the losses for 9 a.m. in June where most of the generated power comes from the PV plants and the load demand is low and the losses for 9 p.m. in march where most of the generation comes from the conventional generating units which are dispirsed throughout the system. Despite that the load demand in march at 9 p.m. is higher than that of June, the losses is still lower than in the case of June at 9 a.m. This is due to the location of the PV plants which are installed far away from the load centre in the eastern part of the network where the irradiance is highest.

Table 7.2 Losses in the transmission lines for different hours

	Losses of June 9 a.m.			**Losses of March 9 p.m.**		
Level Branches	MW	Mvar	MVA	MW	Mvar	MVA
400 kV	198	2003	2012.76	140.00	1588.00	1594.16
220 kV	22	166	167.45	15.00	115.00	115.97
130 kV	51	344	347.76	55.00	374.00	378.02
Total losses	271	2513	2527.57	210.00	2077.00	2087.59

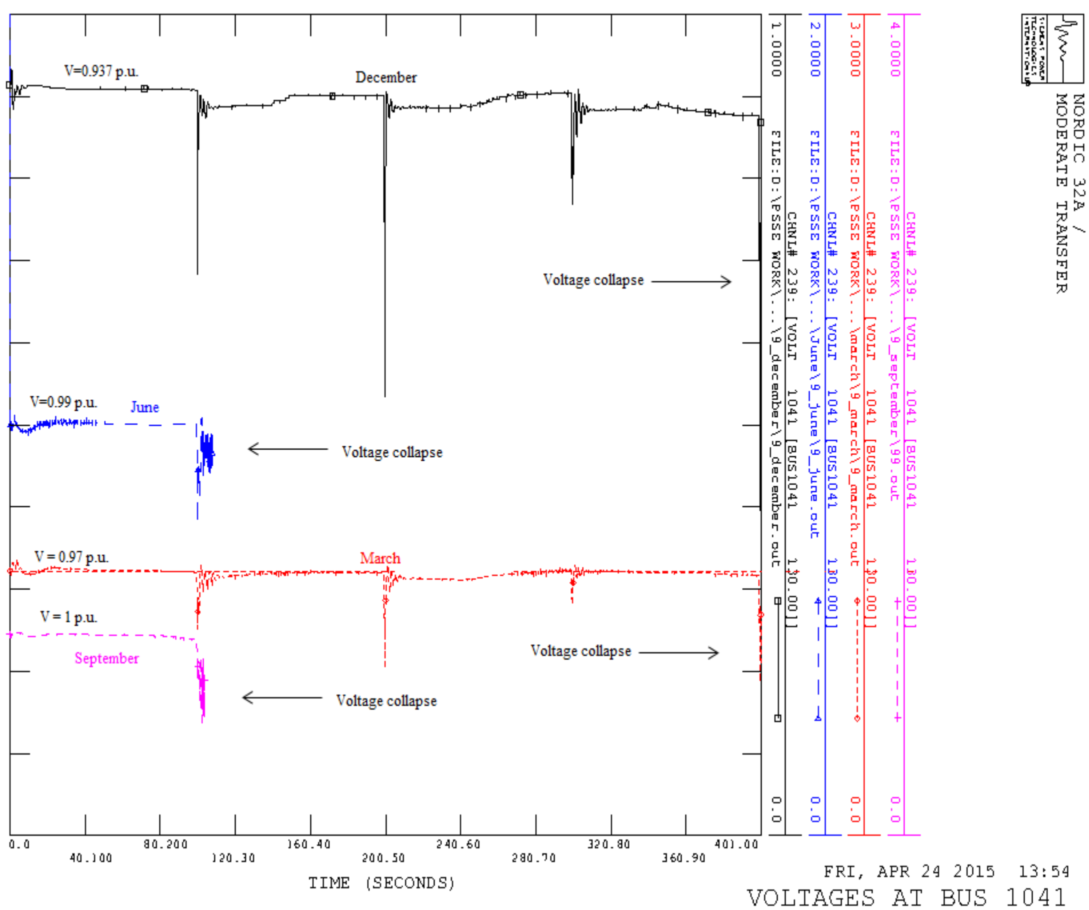

Figure 7.9: The voltage profile at 9 a.m. for all of the months

The analysis of hours 12:00 and 15:00 are shown in Figures 7.10 and 7.11 respectively. The voltage collapse for both hours cases occurred after the fourth fault (t = 400 seconds) for all months except for the month of June when the voltage collapse occurred after the first fault (t = 100 seconds). This early collapse in June was due to the same reasons that were explained earlier for 9 a.m.

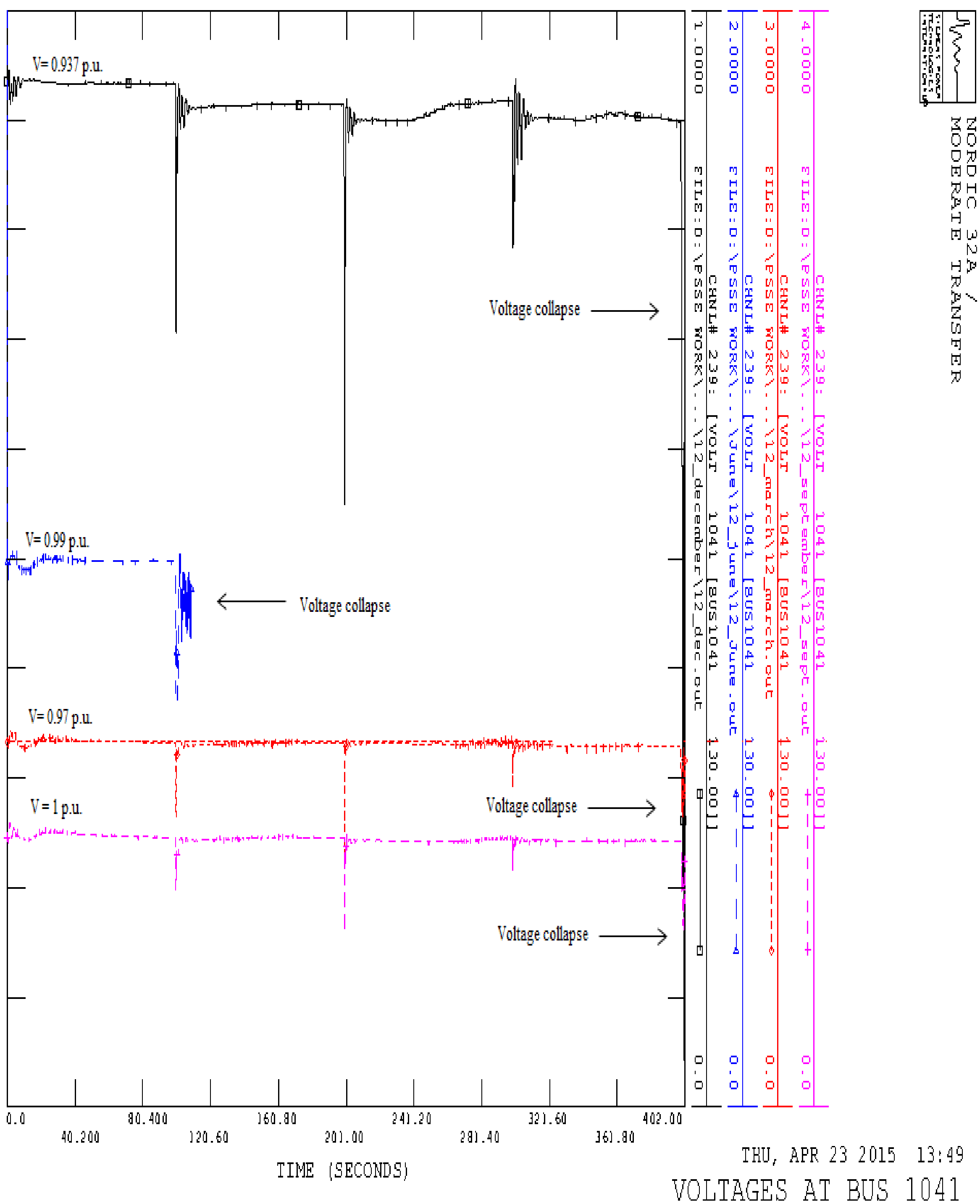

Figure 7.10: The voltage profile at 12:00. for all of the months

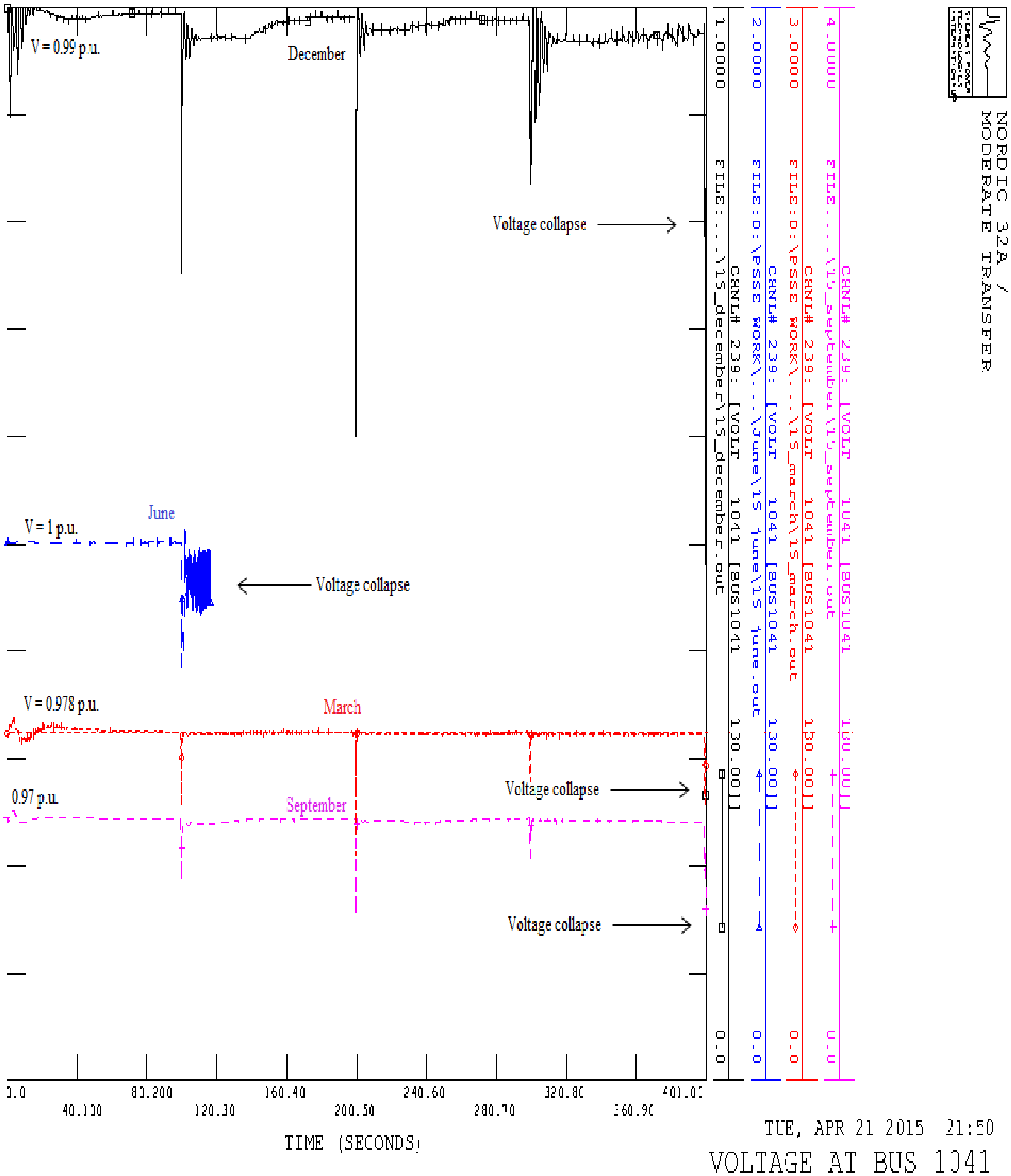

Figure 7.11: The voltage profile at 15:00 for all of the months

For hour 18:00, the voltage profiles in Figure 7.12 show that the voltage collapse occurred after the fourth line fault (t = 400 seconds) for all months cases except in December where it occuered after the third fault (t = 300 seconds). The results are different than the prevoius hours because in this case the solar irradiance has been reduced almost to zero for all of the months. Hence solar PV power plants produce zero power but they still provide reactive power support and the system is mainly dependent on conventional generation. In December, the voltage collapse occurred after the third fault since the load is at its peak as can be observed in Figure 7.12.

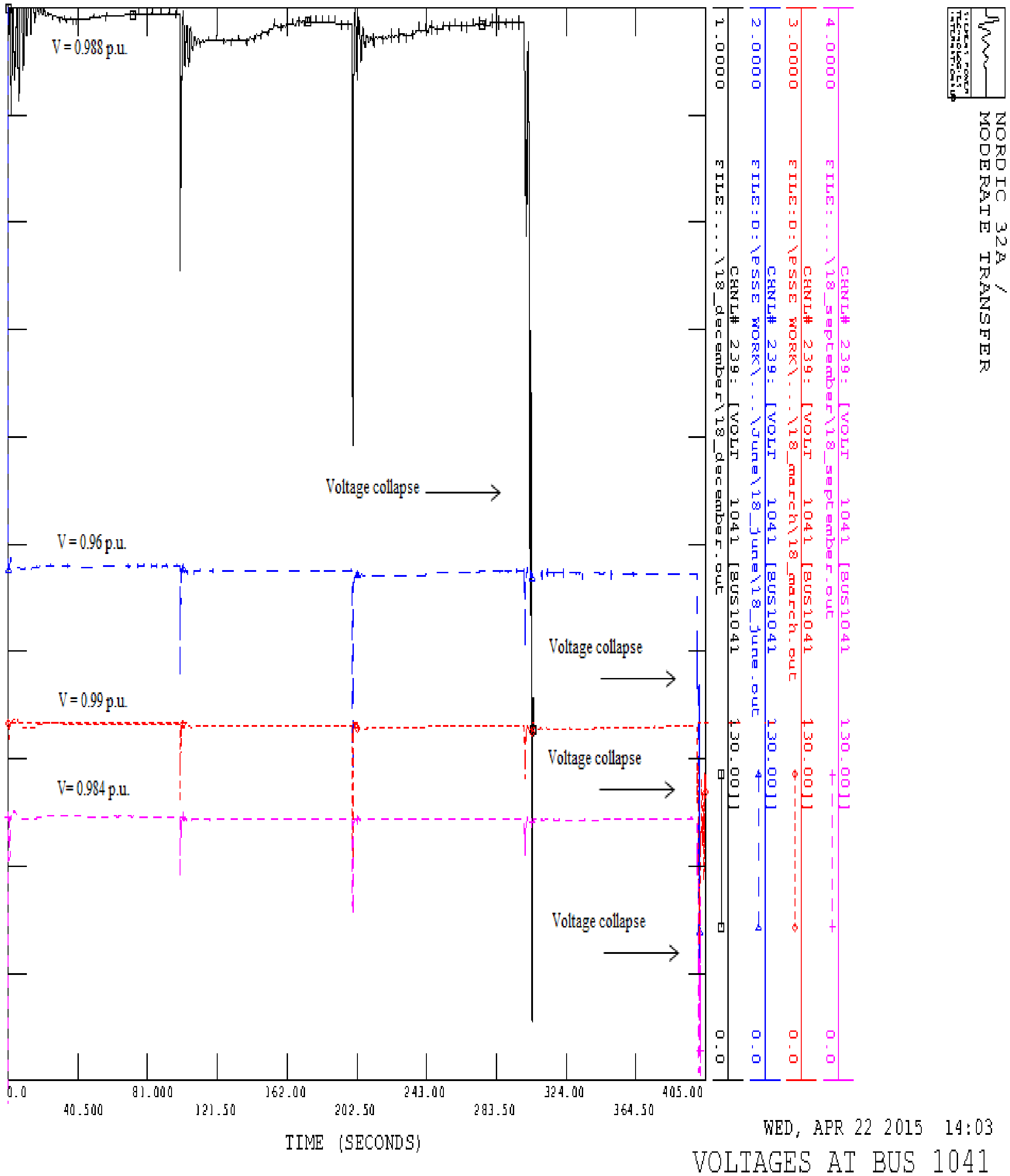

Figure 7.12: The voltage profile at 18:00. for all of the months

For the hour 21:00, the voltage profiles are shown in Figure 7.13. At this time, none of the PV power plants produce active power but the reactive power is still maintained. Also, the loads are slightly lower than the hour 18:00 and the voltage collapse occurred immediately after the forth faults (t = 400 seconds) for all of the months.

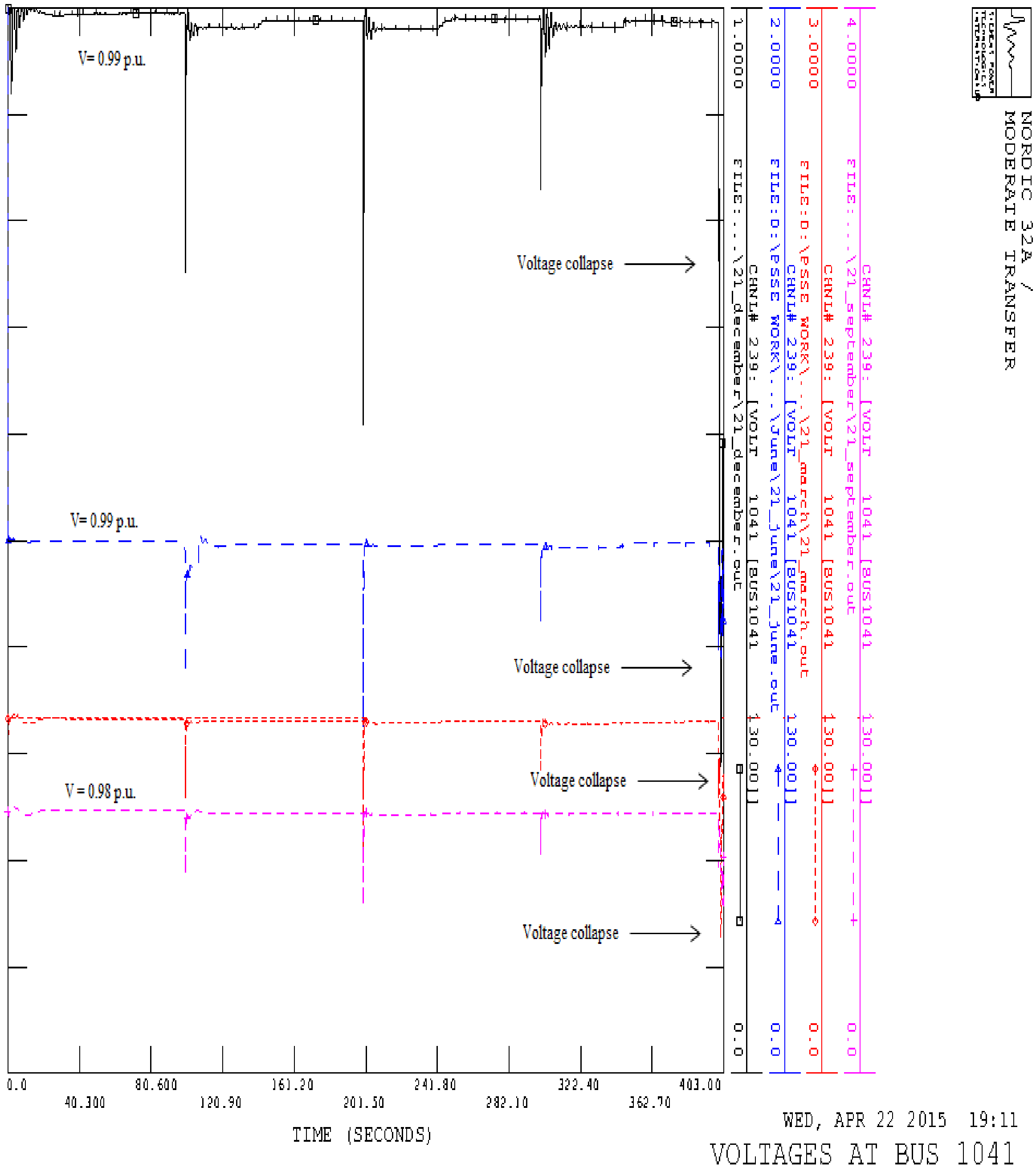

Figure 7.13: The voltage profile at 21:00 for all of the months

It can be concluded that the penetration level of the solar PV plants is a major factor that affects the voltage stability. From the previous cases, it can be seen that during the months where the PV plant's contribution to the total power generation of the system was greatest and the load profile was high, the system was more prone to a voltage collapse. The system in these cases becomes voltage instable as a single disturbance would cause a voltage collapse while for the cases where the contribution of the PV plants to the total generation is lowest, the system was N-3 which means three faults had to be occurred in the system before it goes into voltage collapse scenario that is because during the periods with low irradiance, the PV plants generate reactive power along with the conventional generating units as it demonstrated by Figure 7.14 below which shows the reactive power production during the period of heavy demand at hour 18 in December and hour 12 in September. It can be seen that the PV plant produces a significant amount of reactive power during the night to meet the reactive power demand.

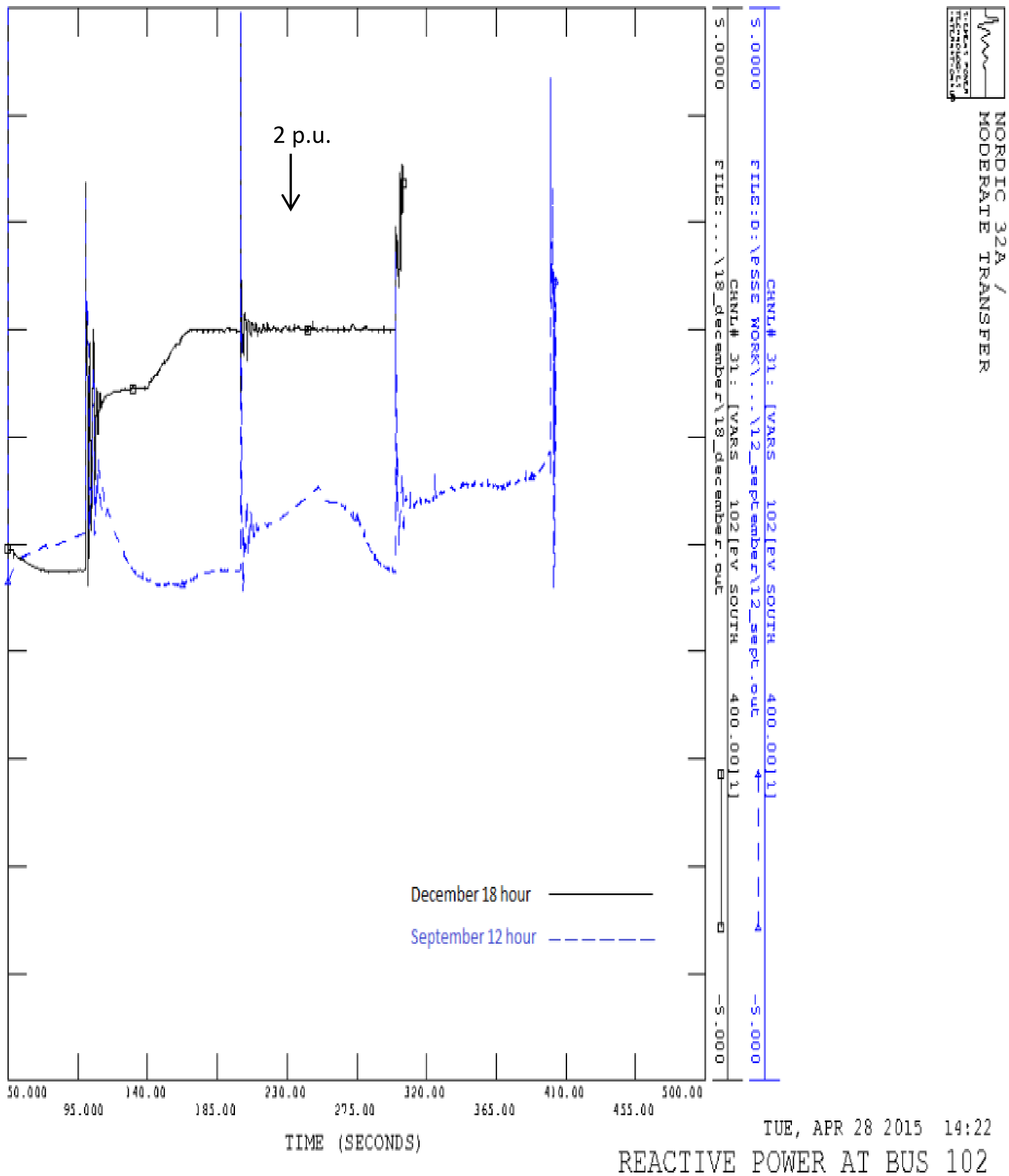

Figure 7.14: Reactive power production at PV plant 102 for two different hours

7.6 Voltage Recovery Time Analysis with Large Scale PV Penetration

This section demonstrates the voltage stability after applying a series of faults on the lines connecting the north area of the Nordic-32 system with the central and southern areas. These faults were applied on two systems: one without PV penetration and the other one is accompanied with 30% penetration as explained earlier. The aim is to study how the voltage is affected in terms of voltage drop and in terms of recovery time and whether there will be oscillations in bus voltages or not. This study was done with induction motor loads equals to 20% of all of the weak buses that were determined in chapter 4.

Figure 7.15 shows the voltage profile at bus 1041. The dynamic simulation is run till T= 100 seconds where a fault was induced at the transmission line 4032-4042. It can be noticed from the figure that the voltage recovery time worsens when having PV in the system. This can be explained by the fact that solar PV plants are installed far away from load center which resulted in high reactive power losses as explained in section 7.5.2. In addition, the time constant for conventional generators exciters is less than that of the PV model. Once there is fault in one of the lines, then there is a need for reactive power support in order to rescue the system from voltage collapse. Reactive power support is the major factor that is responsible for stabilizing the voltage at a bus.

For conventional generators, the time constant is equal to 0.1 seconds while it is 0.3 for the PV models. Therefore, the PV plant is slower in response to reactive power need than the conventional generators. Below is brief about time constants and lags of the PV models:

- PVGU1 model time constant = 0.02 seconds
- PVEU1 model time constant = 0.15 seconds (voltage regulator filter time constant) + 0.05 seconds (time lag in WindVar controller) + 0.08 seconds (controller feedback time constant).

Also, it can be observed that the steady state voltage associated with the 30% PV penetration system is less than that of the 0% PV penetration system as can be seen from Figure 7.16. This can be explained by the fact that all PV plants where most of the power is drawn are installed exclusively at the east while the loads are distributed among all most of the buses in all regions. This resulted in voltage drop in the lines connecting the PV plants that are installed away from the loads.

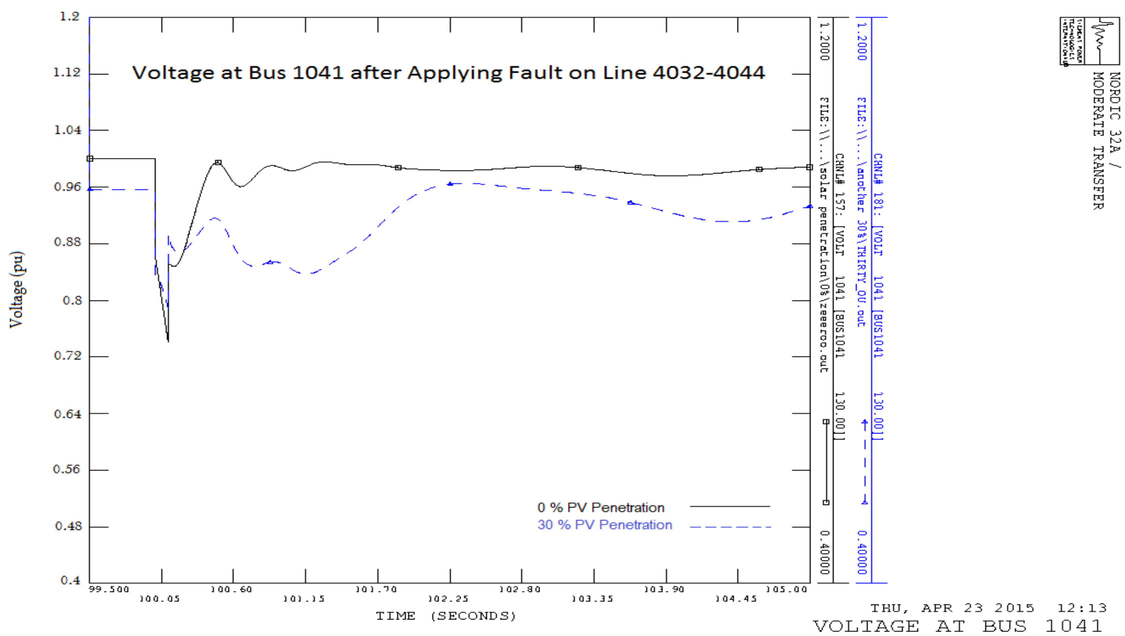

Figure 7.15: Bus 1041 voltage for 0% and 30% PV penetration during the first fault

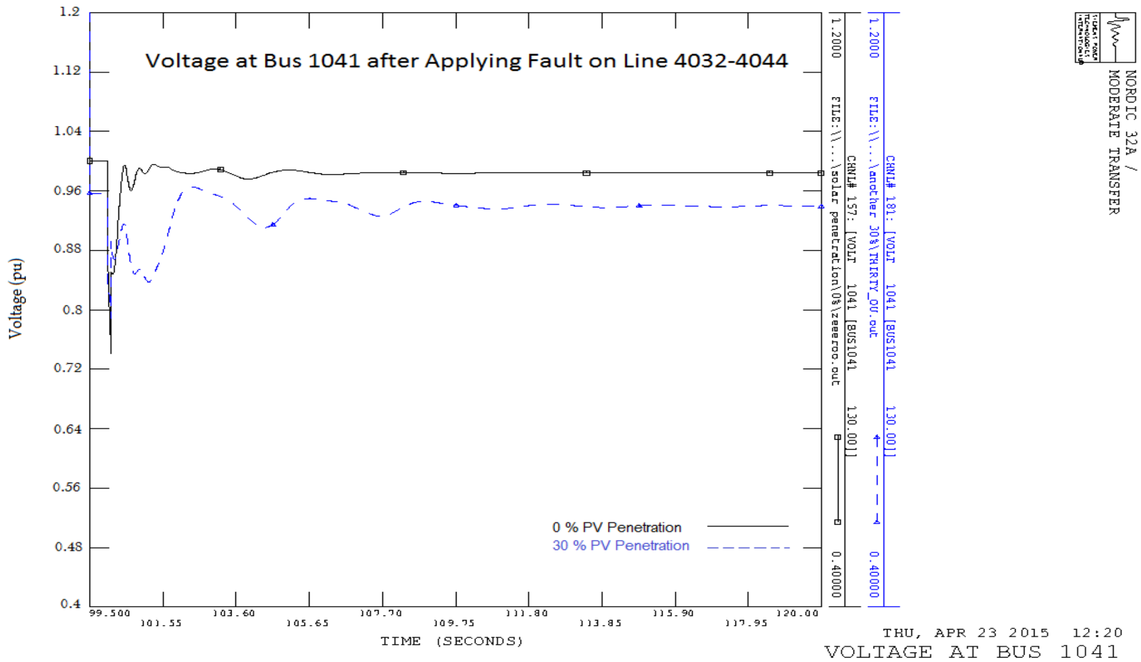

Figure 7.16: Bus 1041 voltage for 0% and 30% PV penetration during the first fault (extended)

Figure 7.17 demonstrates the frequency deviation before, during and after the fault. It can be seen that for both system, the deviation did not exceed 1 Hz which is the threshold for the load shedding frequency relays. The deviation of the 30% PV penetration system is slightly higher due to the lack of the required inertia compared to the case without PV where only conventional generators exist.

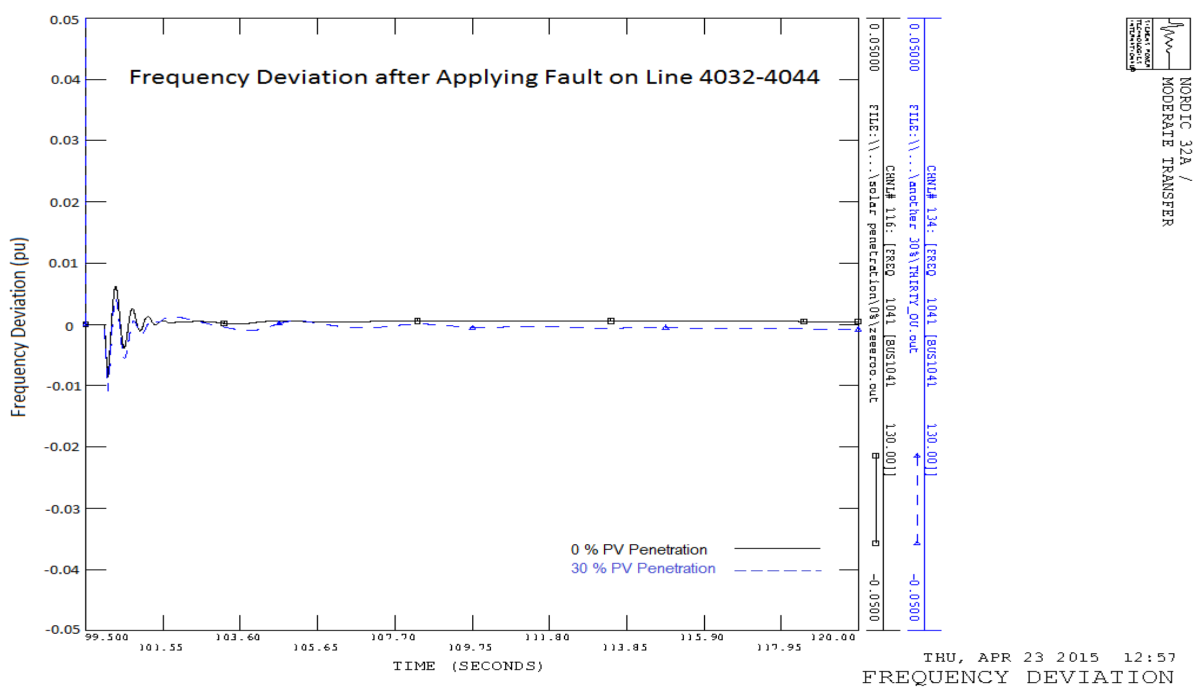

Figure 7.17: Frequency deviation due to the first fault

Figures 7.18 and 7.19 demonstrate the voltage plot before, during and after applying a fault on line 4042-4044 at t = 200s. It can be noticed that the system without PV plants sustained the fault and the voltage was recovered to its pre-fault value. However, the 30% PV penetration system was exposed to a voltage collapse as shown in Figure 7.18. The voltage collapse forced the system to operate out of stability and control which can be observed in the voltage curve in Figures 7.18 and 7.19. After the distance relay of line 4042-4044 cleared the fault in the 30% PV penetration system, three distance relays operated and tripped lines 4032-4042, 4041-4044 and 4041-4061. In Figure 7.20, one can notice that the frequency deviation of the 30% PV penetration system increased significantly at almost t = 202 second causing a collapse in the system as explained earlier.

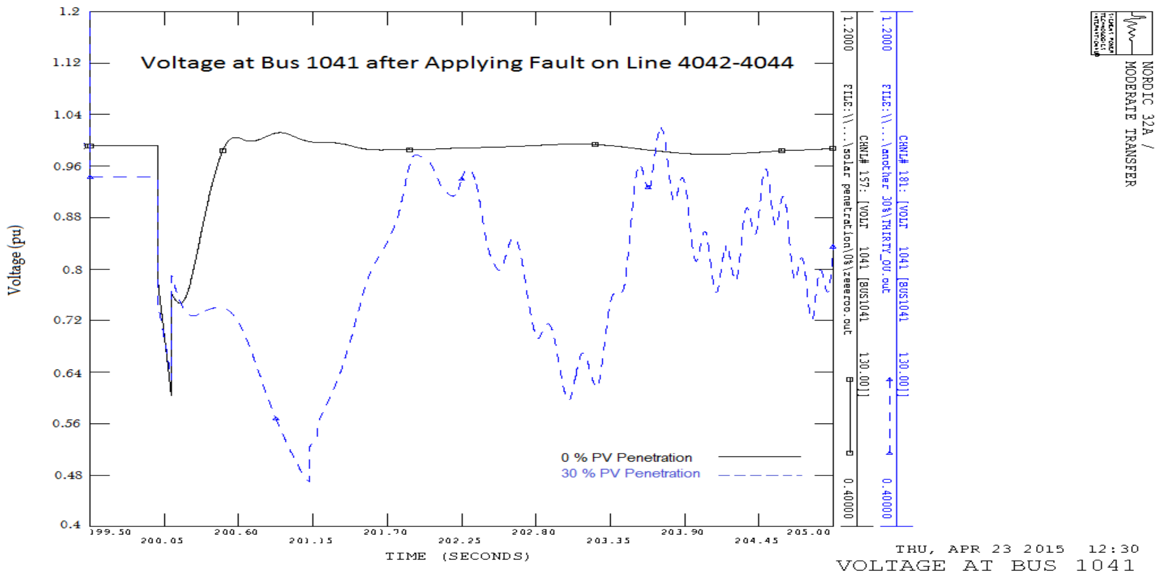

Figure 7.18: Bus 1041 voltage for 0% and 30% PV penetration during the second fault

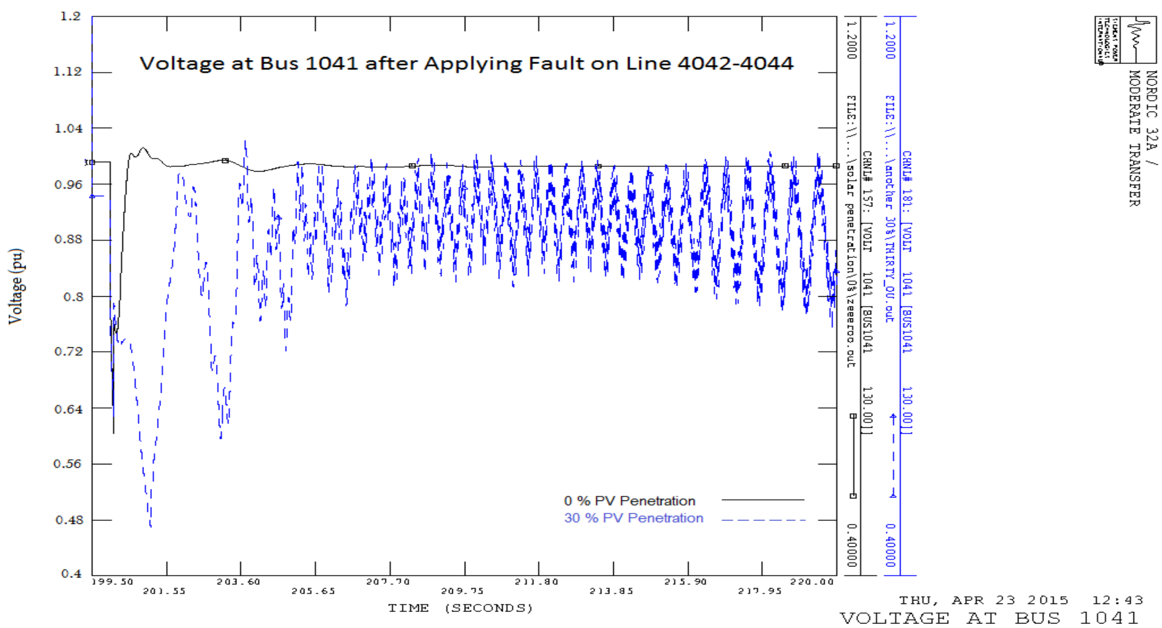

Figure 7.19: Bus 1041 voltage for 0% and 30% PV penetration during the second fault (extended)

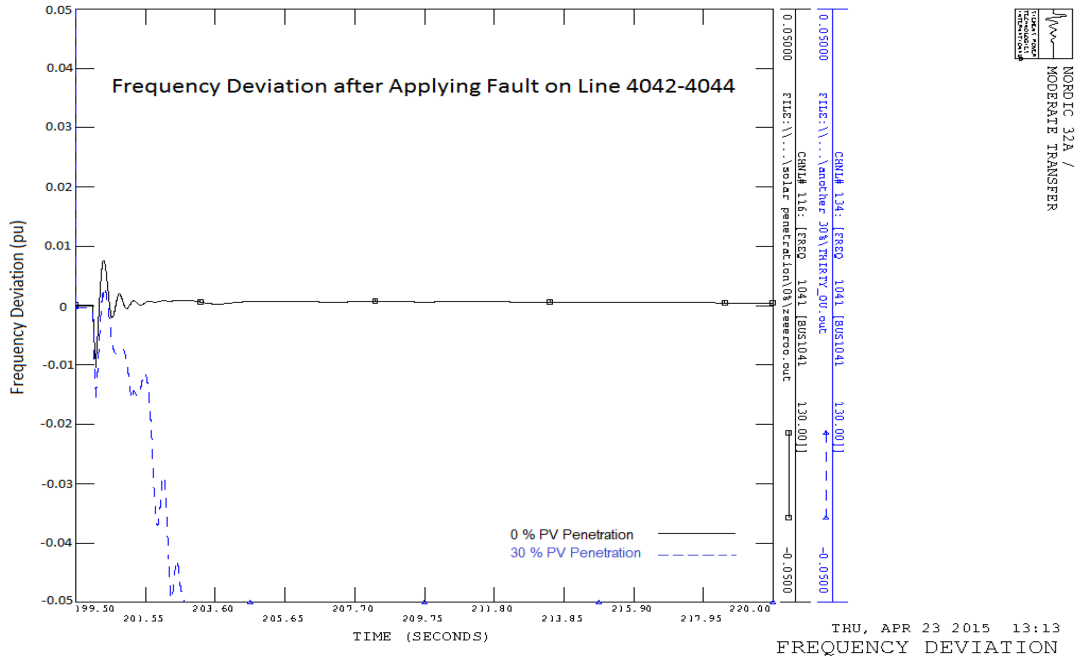

Figure 7.20: Frequency deviation during the second fault

The analysis continued for the 0% PV penetration system and the following two faults were applied on lines 4031-4041-1 and 4042-4043 at times t = 300s and t = 400s respectively. After the latter fault, a voltage and frequency collapse occurred. Moreover, the distance relay of the last line connecting the northern area to the central and southern tripped causing full islanding. Figures 7.21 and 7.22 show the voltage at bus 1041 and the frequency deviation during the period where the two faults occurred. It can be noticed that in this case, the system became more voltage stable than the case in chapter 5 in section 5.5. This is due the modifications that have been done in the system through increasing the inertia constants of the generators (more details in section 7.2).

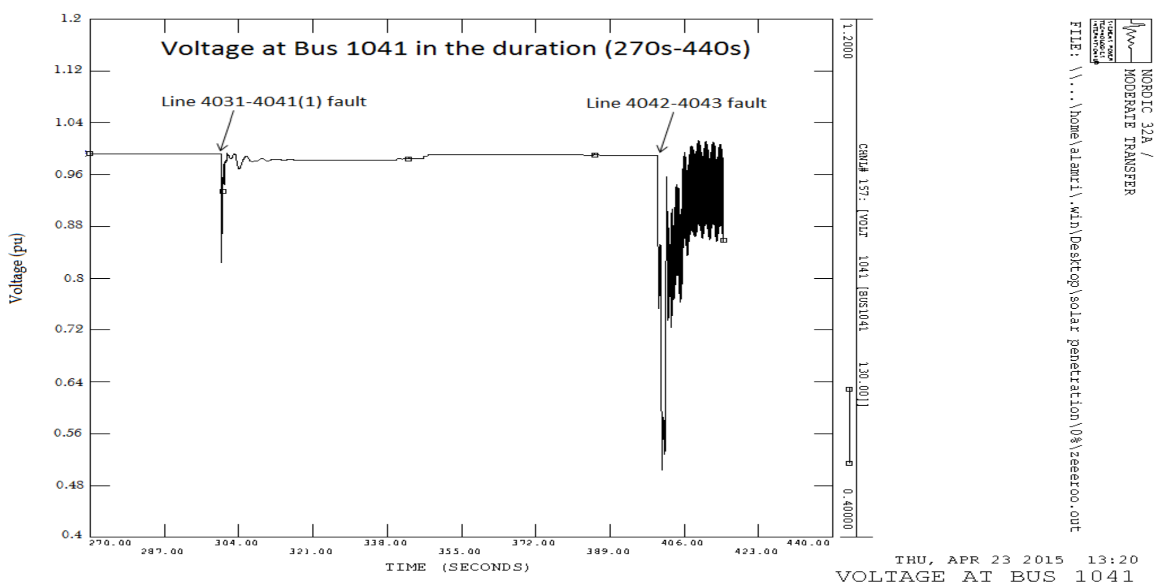

Figure 7.21: Voltage at bus 1041 of the 0% PV penetration system in the duration (270s-440s)

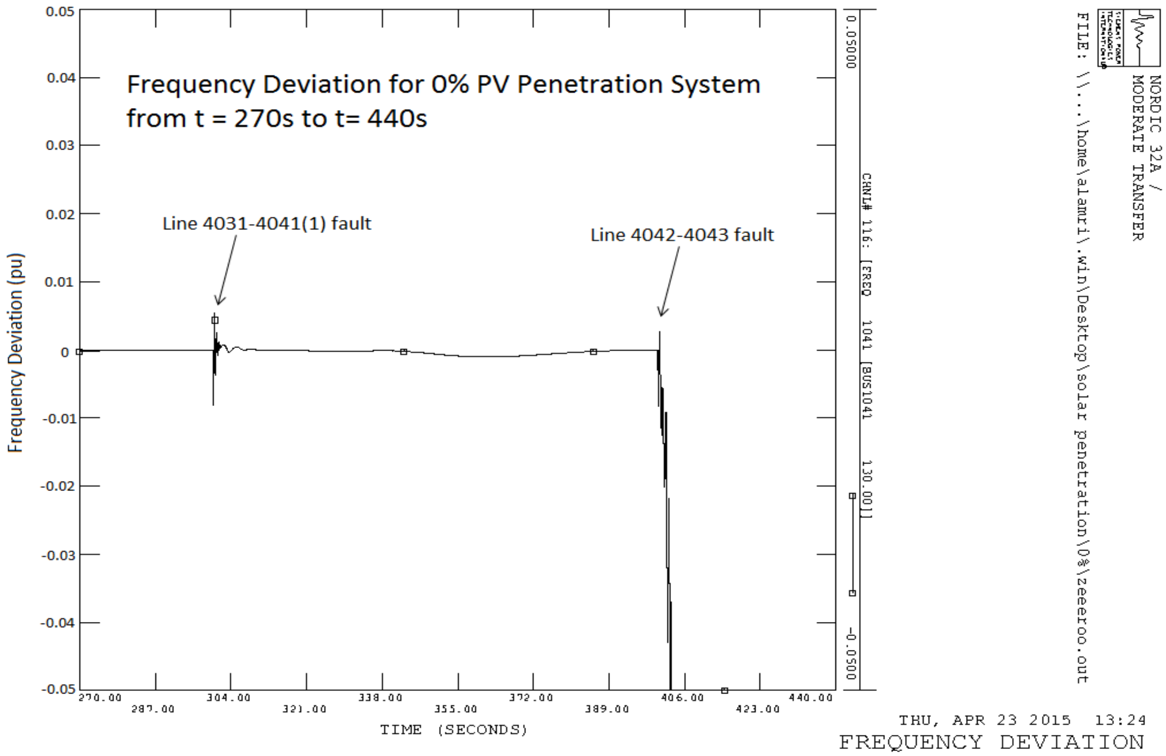

Figure 7.22: Frequency deviation of the 0% PV penetration system in the duration (270s-440s)

8

Conclusions and Future Work

8.1 Conclusions

With the regard to the effects of the loads on the voltage stability, the following has been concluded:

- It can be concluded that with increasing the induction motor loads, the voltage stability worsens due to the increase in the voltage recovery time. By distributing the induction motor loads among the weakest buses in the system, the voltage recovery time has increased even more than the case where they were aggregated at a single bus.
- With regard to the improvement of the voltage stability, it has been found that the STATCOM was superior over the SVC in improving the voltage stability of the system through improving the voltage recovery time. The STATCOMs were able to reduce the voltage recovery time by 60% compared to the SVCs where they only reduced the voltage recovery time by 29% for the same rating for both the SVC and the STATCOM.

With the regard to the effects of large scale integration of solar photovoltaics, the following has been concluded:

- The maximum percentage of PV penetration was determined to be 30% based on frequency deviation due to tripping one of the largest generation units located at the load centre. It was observed that this deviation increases as the PV penetration increases while deactivating an equavelant size of conventional generation. This is due to the fact that unlike conventional generating units, PV plants do not have inertias.
- According to the comparison that was done between the 0% and 30% PV penetration systems to investigate the voltage recovery time after applying a fault on one of the critical lines. It was noticed that the voltage recovery time worsens when having solar PV in the system. This is mainly due to the significant reactive power losses that occurs through the transmission lines as the PV plants in this case are installed in the eastern part of the network far away from the load center. Also, the time constant of the exciters of the PV plants is higher than that of the conventional generating units.
- The effect of irradiance changes on voltage stability was investigated through performing dynamic analysis at different hours at a single day from each of the four seasons months with varying load profile. It has been found that the system was more prone to voltage instability during the periods when the Irradiance is maximum and the load profile is high. This is due to the huge reactive power losses in the transmission lines since in this case PV plants produce most of the power in the system and they are located far away from the load centre in the eastern part of the network where the irradiance is highest.

However, it has also been found that during the periods of low irradiance where the PV plants do not produce active power, the system was able to withstand severe disturbances.This is because PV plants provide reactive power support along with the conventional generation units that are in operation.

8.2 Future Work

The following has been suggested as a future work for this project:

- The modification of the existing built-in solar PV model in PSS/E or writing a user defined model to mimic the fast response of a real power electronic based voltage controller of a PV plant and conducting an investigation on the post-disturbance voltage recovery time with these new models.
- The integration of a large scale wind farm to the existing network with the solar PV plants and the investigation of voltage stability and the role solar PV plant's voltage controller in meeting the reactive power support for the wind farm in order to mitigate the flicker emissions.
- Conducting a cost-benefit analysis for such a large scale integration of solar PV plants.
- Updating the existing Nordic32 test system to better match today's power grid of the Nordic countries and meeting the requirements of the Nordic Grid Code.
- Investigating the effects of series connected FATCS devices on the effect on the voltage stability and the voltage recovery time.

References

[1] Photon International, The Solar Power Magazine, April, 2011, http:// www.photon-magazine.com.

[2] Y. T. Tan, D. S. Kirschen, and N. Jenkins, “A model of PV generation suitable for stability analysis,” IEEE Trans. Energy Conversion, vol. 19, no. 4, pp. 748-755, 2004.

[3] P. Kundur, Power system stability and control. New York: McGraw-Hill, 1994.

[4] Venkat Krishnan and James D. McCalley, "Role of Induction Motors in Voltage Instability and Coordinated Reactive Power Planning". INTECH Open Access Publisher, 2012.

[5] B. Lee and K. Lee, ”Dynamic and static voltage stability enhancement of power systems”, IEEE Transactions on Power Systems, vol. 8, no. 1, pp. 231-238, 1993.

[6] S. Bhaladhare, A. Telang and P. Bedekar, ”P-V, Q-V Curve – A Novel Approach for Voltage Stability Analysis”, International Journal of Computer Applications® (IJCA), 2013.

[7] Corsi S. and Taranto, G.N., "Voltage instability - the different shapes of the “Nose”," *Bulk Power System Dynamics and Control - VII. Revitalizing Operational Reliability, 2007 iREP Symposium* , vol., no., pp.1,16, 19-24 Aug. 2007.

[8] I. Romero Navarro, ”Dynamic Load Models for Power Systems: Estimation of Time-Varying Parameters during Normal Operation”, Department of Industrial Electrical Engineering and Automation, Lund University, Lund, Sweden, 2002.

[9] K. Lindén and I. Segerqvist, ”Modelling of Load Devices and Studying Load/System Characteristics”, Department of Electrical Power Systems, Chalmers University of Technology, Göteborg, Sweden, 1992.

[10] ”Load representation for dynamic performance analysis (of power systems)”, IEEE Transactions on Power Systems, vol. 8, no. 2, pp. 472-482, 1993.

[11] A. Hughes, Electric motors and drives. Amsterdam: Elsevier/Newnes, 2006.

[12] N. Hingorani and L. Gyugyi, Understanding FACTS. New York: IEEE Press, 2000.

[13] Baghaee H.R., Jannati M., Vahidi B., Hosseinian S.H. and Rastegar H., "Improvement of voltage stability and reduce power system losses by optimal GA-based allocation of multi-type FACTS devices," *Optimization of Electrical and Electronic Equipment, 2008. OPTIM 2008. 11th International Conference on , vol., no., pp.209,214, 22-24 May 2008*.

[14] Sung-Hwan Song, Jung-Uk Lim and Seung-Il Moon, "FACTS operation scheme for enhancement of power system security," *Power Tech Conference Proceedings, 2003 IEEE Bologna* , vol.3, no., pp.36,41 Vol.3, 23-26 June 2003

[15] Amin, M.R. and Roy, R.B., "Design of microcontroller based Thyristor Controlled three-phase static volt-ampere reactive compensator," *Informatics, Electronics & Vision (ICIEV), 2014 International Conference on , vol., no., pp.1,6, 23-24 May 2014.*

[16] Shen ZhiJian, Jin Jing, Xiong XiaoFu and Ouyang Jinxin, "Influence of SVC on fault component directional protection and its improvement approach," *Advanced Power System Automation and Protection (APAP), 2011 International Conference on* , vol.3, no., pp.1845,1850, 16-20 Oct. 2011.

[17] B. Singh, S. Murthy and S. Gupta, ”Analysis and Design of STATCOM-Based Voltage Regulator for Self-Excited Induction Generators”, IEEE Trans. On Energy Conversion, vol. 19, no. 4, pp. 783-790, 2004.

[18] K. Mahajmra, A. Ghosh and S. Doradla, ”Simplified Model for Control Design of STATCOM Using Three-Level Inverter”, IEEE, no. 0-7803-4886-998, 1998.

[19] H. Abdel-Gawad and V. Sood, "Overview of connection topologies for grid-connected PV systems," Electrical and Computer Engineering (CCECE), 2014 IEEE 27th Canadian Conference on , vol., no., pp.1,8, 4-7 May 2014.

[20] M. Rashid, Power electronics handbook. Burlington, MA: Butterworth-Heinemann, 2011.

[21] Aree P., "Effects of Large Induction Motors on Voltage Sag," *Power and Energy Engineering Conference (APPEEC), 2012 Asia-Pacific* , vol., no., pp.1,4, 27-29 March 2012

[22] Perez J.J., Cortes C.A. and Gomez, A., "A study of voltage sags in electric motors," *Electrical Power Quality and Utilisation, 2007. EPQU 2007. 9th International Conference on* , vol., no., pp.1,6, 9-11 Oct. 2007

[23] Bollen M.H.J., Hager Mats and Roxenius C., "Effect of induction motors and other loads on voltage dips: theory and measurements," *Power Tech Conference Proceedings, 2003 IEEE Bologna* , vol.3, no., pp.6 pp. Vol.3,, 23-26 June 2003.

[24] G. K. Stefopoulos and A. P. Meliopoulos, "Induction Motor Load Dynamics: Impact on Voltage Recovery Phenomena," Transmission and Distribution Conference and Exhibition, 2005/2006 IEEE PES , vol., no., pp.752,759, 21-24 May 2006.

[25] M. Gordon, "Impact of load behavior on transient stability and power transfer limitations," Power & Energy Society General Meeting, 2009. PES ”09. IEEE , vol., no., pp.1,8, 26-30 July 2009

[26] S. Kabir, M. Nadarajah and R. Bansal, "Impact of large scale photovoltaic system on static voltage stability in sub-transmission network," ECCE Asia Downunder (ECCE Asia), 2013 IEEE , vol., no., pp.468,473, 3-6 June 2013

[27] Amarasekara H.W.K.M., Meegahapola L., Agalgaonkar A.P and Perera, S., "Impact of renewable power integration on VQ stability margin," *Power Engineering Conference (AUPEC), 2013 Australasian Universities* , vol., no., pp.1,6, Sept. 29 2013-Oct. 3 2013

[28] X. Xiaoyan, H. Yuehui, H. Guoqing, Z. Haixiang and W. Weisheng, ”Modeling of large grid-integrated PV station and analysis its impact on grid voltage”, IEEE, no. 978-1-4244-4934-7, 2009.

[29] S. Kabir, O. Krause and S. Bartlett, "Impact of large-scale photovoltaic system on short and long term voltage stability in sub-transmission network," *Power Engineering Conference (AUPEC), 2013 Australasian Universities* , vol., no., pp.1,6, Sept. 29 2013-Oct. 3 2013

[30] H. Li, Y. Xu, S. Adhikari, D. Tom Rizy, F. Li and P. Irminger, "Real and reactive power control of a three-phase single-stage PV system and PV voltage stability," Power and Energy Society General Meeting, 2012 IEEE , vol., no., pp.1,8, 22-26 July 2012

[31] Y. Mitsugi and A. Yokoyama, "Phase angle and voltage stability assessment in multi-machine power system with massive integration of PV considering PV"s FRT requirements and dynamic load characteristics," Power System Technology (POWERCON), 2014 International Conference on , vol., no., pp.1112,1119, 20-22 Oct. 2014

[32] R. Yan and T. Kumar Saha, "Investigation of Voltage Stability for Residential Customers Due to High Photovoltaic Penetrations," Power Systems, IEEE Transactions on , vol.27, no.2, pp.651,662, May 2012

[33] T. VAN CUTSEM and L. PAPANGELIS, Description, Modeling and Simulation Results of a Test System for Voltage Stability Analysis, 6th ed. Liège: University of Liège., 2013.

[34] K. Walve, "Nordic32-A CIGRE test system for simulation of transient stability and long term dynamics," Svenska Kraftnät, Sweden, Tech. Rep., 1993

[35] Siemens Industry, Inc., PSS/E PROGRAM APPLICATION GUIDE VOLUME 2. New York: Siemens Power Technologies International, 2013.

[36] P. Chen, Models for Tap-Changing Transformers. Gothenburg: Chalmers University of Technology, 2013.

[37] Mathur, R. and Varma, R. (2002). *Thyristor-based FACTS controllers for electrical transmission systems*. Piscataway, NJ: IEEE.

[38] Siemens Industry, Inc., PSS/E MODEL LIBRARY. New York: Siemens Power Technologies International, 2013.

[39] L. Lima and J. Feltes, "PSS®E Test System for Voltage Collapse Analysis", *Siemens Power Technology*, 2009.[Online].Available:http://w3.usa.siemens.com/datapool/us/SmartGrid/docs/pti/2009July/PDFs/PSSE_System_Test_for_Voltage_Collapse_Analysis.pdf. [Accessed: 05- Apr- 2015].

[40] R. Koessler, "Dynamic simulation of static VAR compensators in distribution systems", IEEE Transactions on Power Systems, vol. 7, no. 3, pp. 1285-1291, 1992.

[41] M. Jorge and B. Marques, "Steady State Analysis of the Interconnection of Offshore Energy Parks", Universidade de Lisboa, Lisboa, 2010.

[42] "IEEE Guide for AC Motor Protection," IEEE Std C37.96-2000, p. i, 2000.

[43] JRC, "JRC Science Hub - European Commission", JRC Science Hub, 2015. [Online]. Available: https://ec.europa.eu/jrc/. [Accessed: 30- Apr- 2015].

[44] European network of transmission system operators for electricity, "The Nordic Grid Code", European network of transmission system operators for electricity, 2007. [Online]. Available:

https://www.entsoe.eu/fileadmin/user_upload/_library/publications/nordic/planning/070115_entsoe_nordic_NordicGridCode.pdf. [Accessed: 30- Apr- 2015].

[45] Eosweb.larc.nasa.gov, ”Surface meteorology and Solar Energy”, 2015. [Online]. Available: https://eosweb.larc.nasa.gov/sse/. [Accessed: 30- Apr- 2015].

Appendix A

Modified Generator Dynamic Models

```
4042 'GENSAL' 1 5 .05     .1  9.99 0 1.1 .7 .25  .2 .15 .1 .3/
4047 'GENSAL' 1 5 .05     .1  9.99 0 1.1 .7 .25  .2 .15 .1 .3/
4047 'GENSAL' 2 5 .05     .1  9.99 0 1.1 .7 .25  .2 .15 .1 .3/
4051 'GENSAL' 1 5 .05     .1  9.99 0 1.1 .7 .25  .2 .15 .1 .3/
4051 'GENSAL' 2 5 .05     .1  9.99 0 1.1 .7 .25  .2 .15 .1 .3/
4062 'GENSAL' 1 5 .05     .1  9.99 0 1.1 .7 .25  .2 .15 .1 .3/
4063 'GENSAL' 1 5 .05     .1  9.99 0 1.1 .7 .25  .2 .15 .1 .3/
4063 'GENSAL' 2 5 .05     .1  9.99 0 1.1 .7 .25  .2 .15 .1 .3/
1042 'GENSAL' 1 5 .05     .1  9.99 0 1.1 .7 .25  .2 .15 .1 .3/
1043 'GENSAL' 1 5 .05     .1  9.99 0 1.1 .7 .25  .2 .15 .1 .3/
4011 'GENSAL' 1 5 .05     .1  9.99 0 1.1 .7 .25  .2 .15 .1 .3/
4012 'GENSAL' 1 5 .05     .1  9.99 0 1.1 .7 .25  .2 .15 .1 .3/
4021 'GENSAL' 1 5 .05     .1  9.99 0 1.1 .7 .25  .2 .15 .1 .3/
4031 'GENSAL' 1 5 .05     .1  9.99 0 1.1 .7 .25  .2 .15 .1 .3/
4071 'GENSAL' 1 5 .05     .1  9.99 0 1.1 .7 .25  .2 .15 .1 .3/
4072 'GENSAL' 1 5 .05     .1  9.99 0 1.1 .7 .25  .2 .15 .1 .3/
1012 'GENSAL' 1 5 .05     .1  9.99 0 1.1 .7 .25  .2 .15 .1 .3/
1013 'GENSAL' 1 5 .05     .1  9.99 0 1.1 .7 .25  .2 .15 .1 .3/
1014 'GENSAL' 1 5 .05     .1  9.99 0 1.1 .7 .25  .2 .15 .1 .3/
4041 'GENSAL' 1 7 .05     .1  9.99 0 1.2 1 .3  .2 .15 .1 .3/
4071 'GENSAL' 1 5 .05     .1  9.99 0 1.1 .7 .25  .2 .15 .1 .3/
4072 'GENSAL' 1 5 .05     .1  9.99 0 1.1 .7 .25  .2 .15 .1 .3/
1012 'GENSAL' 1 5 .05     .1  9.99 0 1.1 .7 .25  .2 .15 .1 .3/
1013 'GENSAL' 1 5 .05     .1  9.99 0 1.1 .7 .25  .2 .15 .1 .3/
1014 'GENSAL' 1 5 .05     .1  9.99 0 1.1 .7 .25  .2 .15 .1 .3/
1021 'GENSAL' 1 5 .05     .1  9.99 0 1.1 .7 .25  .2 .15 .1 .3/
1022 'GENSAL' 1 5 .05     .1  9.99 0 1.1 .7 .25  .2 .15 .1 .3/
2032 'GENSAL' 1 5 .05     .1  9.99 0 1.1 .7 .25  .2 .15 .1 .3/
```

Appendix B

Load characteristics models

Induction motors have been installed on buses 1041,61,42,42 and 62. The Torque Speed Characteristics of each of the motors are shown below with the corresponding equivalent circuit parameters. Note that the ratings of the induction motor loads in these models is dependent on the loads that already exist in the network since it converts the loads that already exists in the network data into induction motor loads.

B1: Induction Motor Characteristics (Bus 1041)

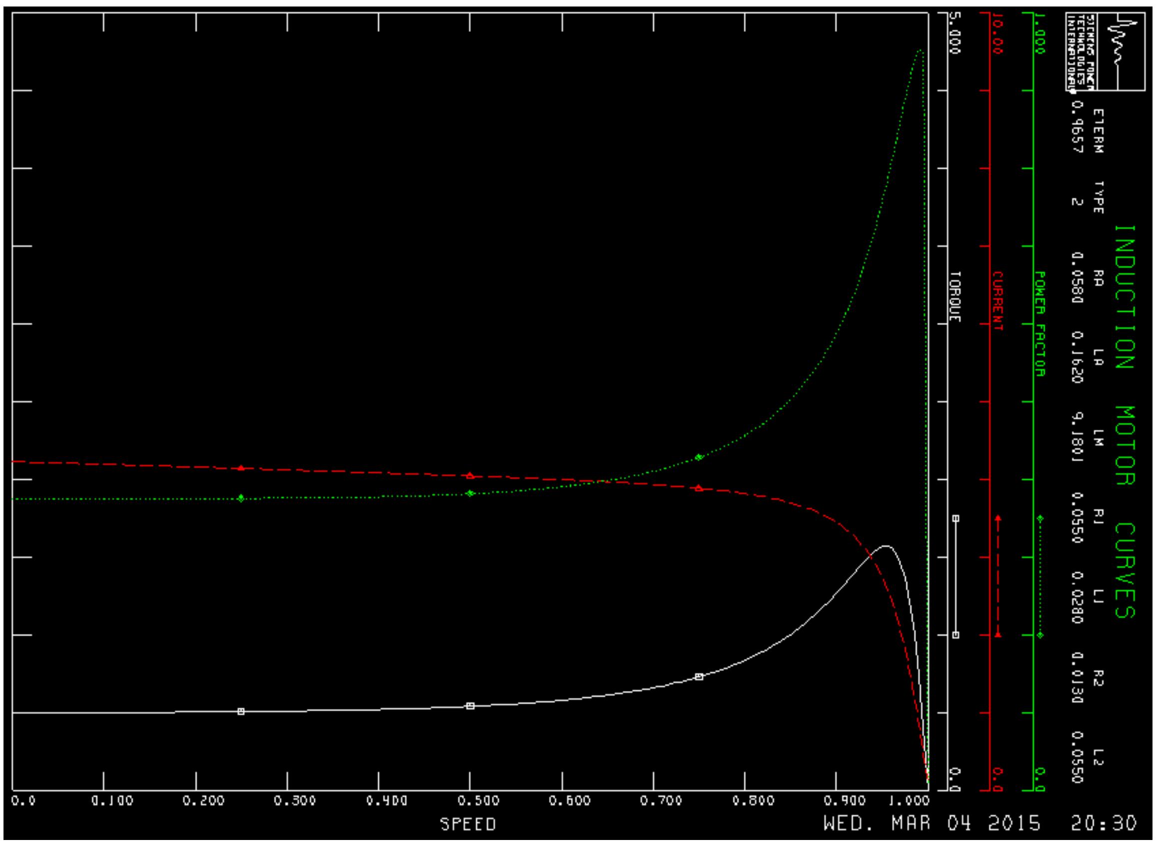

Torque-Speed Characteristics of the induction motor load at bus 1041

1041 'CIM5BL' 1 2
0.58000E-01 0.16200 9.1801 0.55000E-01 0.28000E-01
0.13000E-01 0.55000E-01 1.0000 0.25000E-01 5.0000
0.50000 632.46 0.0000 1.0000 0.0000
0.0000 0.0000 1.0000 0.0000 /

B2: Induction Motor Characteristics (Bus 61)

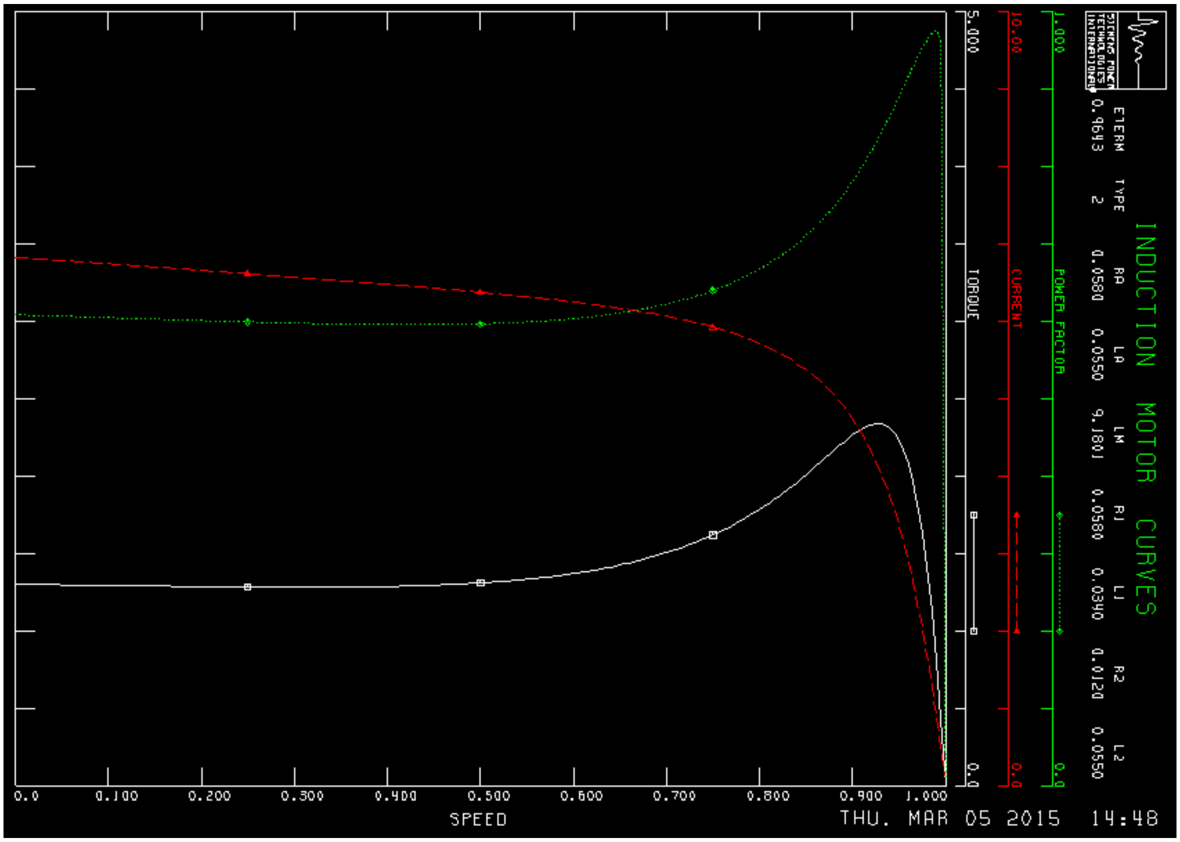

Torque-Speed Characteristics of the induction motor load at bus 61

61 'CIM5BL' 1 2
0.58000E-01 0.55000E-01 9.1801 0.58000E-01 0.34000E-01
0.12000E-01 0.55000E-01 1.0000 0.25000E-01 5.0000
0.50000 512.46 0.0000 1.0000 0.0000
0.0000 0.0000 1.0000 0.0000 /

B3: Induction Motor Characteristics (Bus 46)

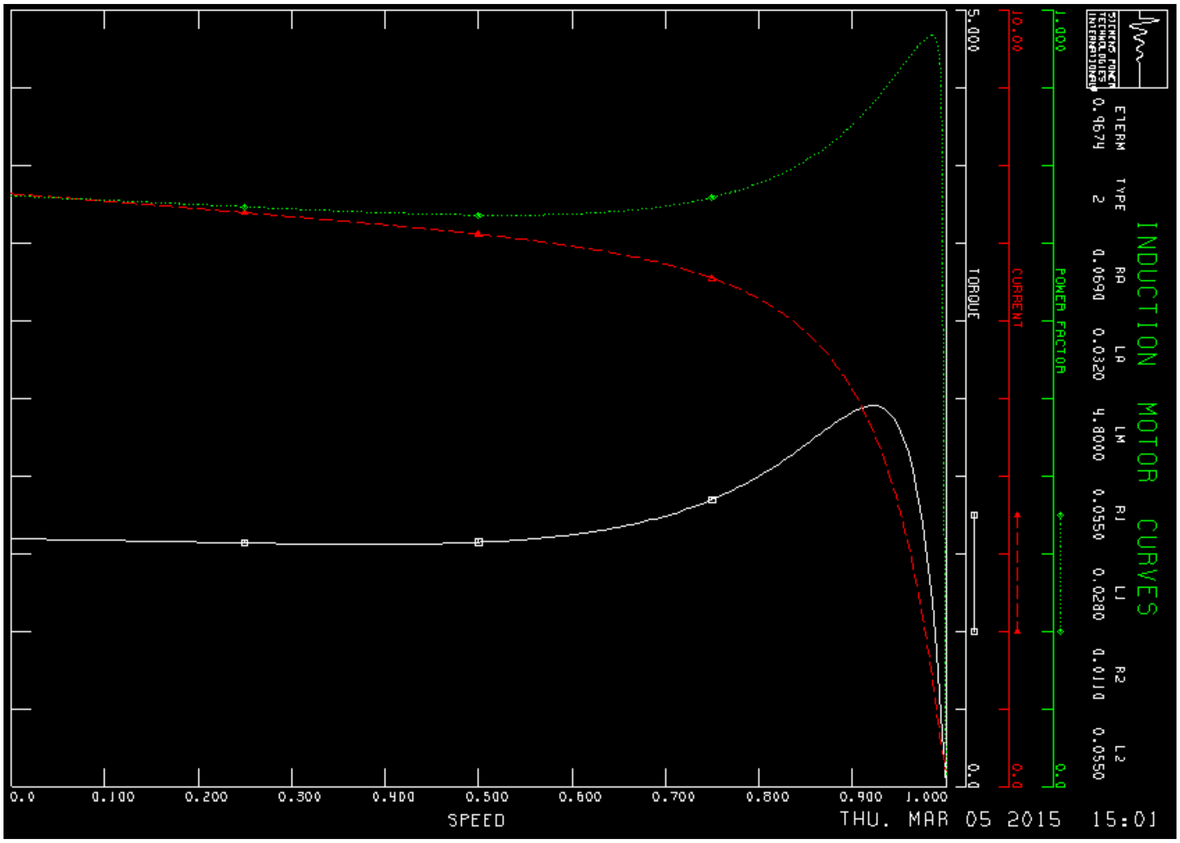

Torque-Speed Characteristics of the induction motor load at bus 46

```
46 'CIM5BL'        1        2
  0.69000E-01  0.32000E-01   4.8000     0.55000E-01  0.28000E-01
  0.11000E-01  0.55000E-01   1.0000     0.25000E-01   5.0000
  0.50000      726.31      0.0000      1.0000      0.0000
   0.0000      0.0000      1.0000      0.0000    /
```

B4: Induction Motor Characteristics (Bus 43)

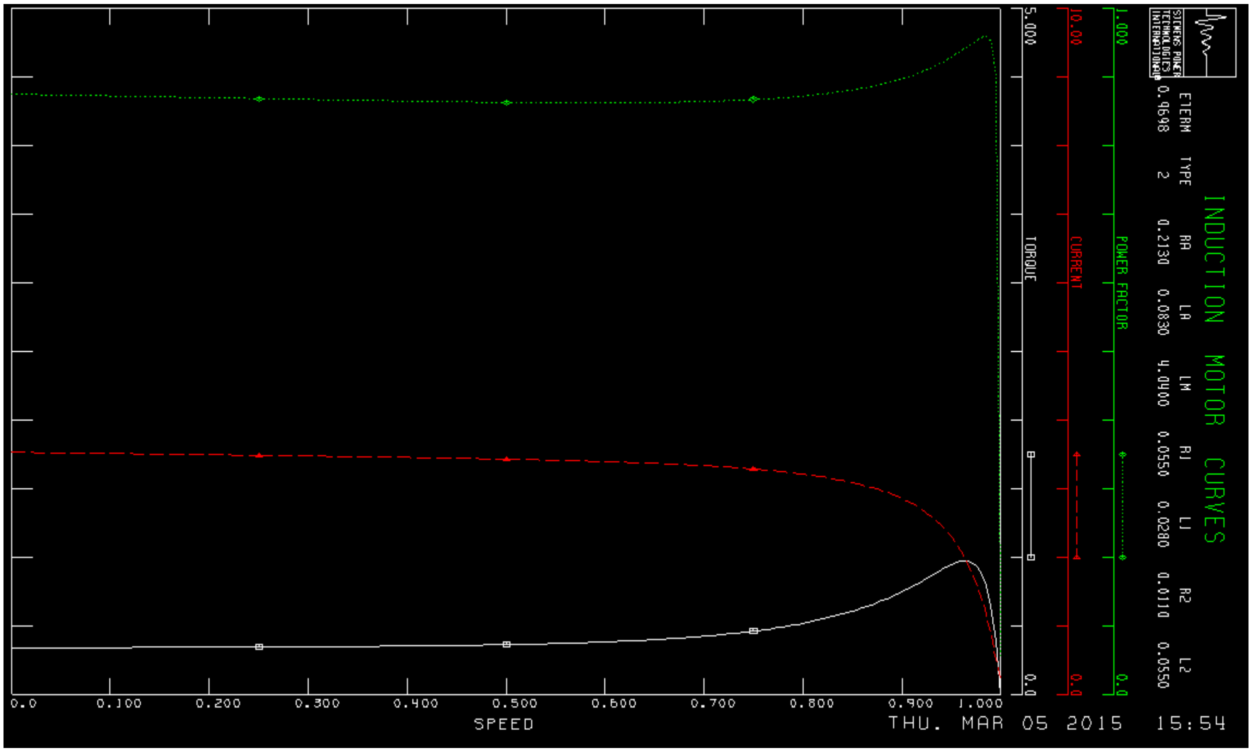

Torque-Speed Characteristics of the induction motor load at bus 43

```
43 'CIM5BL'        1        2
   0.21300    0.83000E-01  4.0400     0.55000E-01  0.28000E-01
   0.11000E-01  0.55000E-01  1.0000     0.25000E-01  5.0000
   0.50000     931.15     0.0000     1.0000     0.0000
    0.0000     0.0000     1.0000     0.0000    /
```

B5: Induction Motor Characteristics (Bus 62)

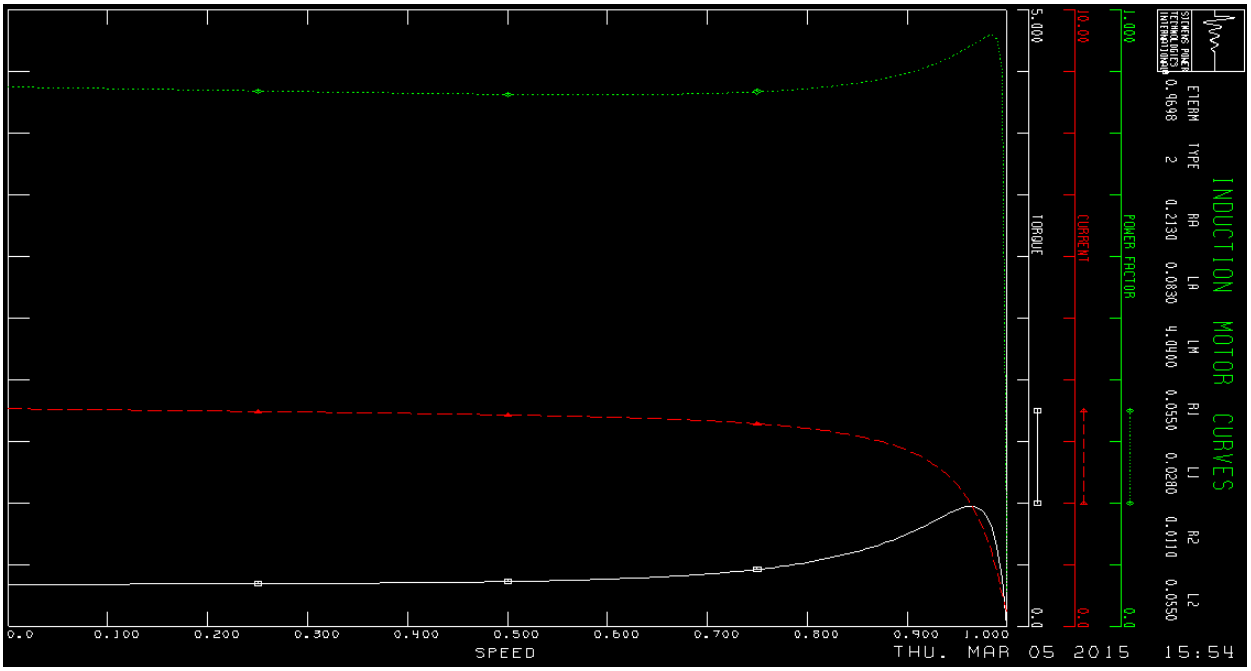

Torque-Speed Characteristics of the induction motor load at bus 62

```
62 'CIM5BL'          1          2
      0.15900     0.83000E-01   5.9900     0.55000E-01  0.28000E-01
      0.12000E-01  0.55000E-01   1.0000     0.25000E-01   5.0000
      0.50000      310.49      0.0000      1.0000      0.0000
       0.0000      0.0000      1.0000      0.0000    /
```

Appendix C

Distance Relay Dynamic Models

C1: Mho Distance Relay (DISTR1) settings

				Zone one settings (pu)			Zone two settings (pu)			Zone three settings (pu)		
Relay placement	Reach coverage	Branch No.	Type	Z magnitude	The angle	Radius of reach	Z magnitude	The angle	Radius of reach	Z magnitude	The angle	Radius of reach
4047	4043-4044-1044	1	Distance Relay (Mho)	0.016	84.289	0.008	0.018	84.289	0.009	0.046	86.765	0.023
4011	4021-4032-4044	1	Distance Relay (Mho)	0.012	86.186	0.006	0.069	84.289	0.034	0.112	81.113	0.056
4011	4022-4031-4041	1	Distance Relay (Mho)	0.040	84.289	0.020	0.048	84.289	0.024	0.088	84.032	0.044
4012	4022-4031-4042	1	Distance Relay (Mho)	0.028	83.480	0.014	0.043	83.630	0.022	0.116	83.059	0.058
4021	4032-4042-4044	1	Distance Relay (Mho)	0.032	84.289	0.016	0.048	82.875	0.010	0.083	74.610	0.041
4022	4031-4041-4061	1	Distance Relay (Mho)	0.032	84.289	0.016	0.048	83.817	0.024	0.090	82.827	0.045
4022	4031-4041-4062	2	Distance Relay (Mho)	0.032	84.289	0.016	0.048	83.817	0.024	0.090	82.827	0.045
4031	4032-4042-4045	1	Distance Relay (Mho)	0.008	84.289	0.004	0.020	83.723	0.010	0.064	83.405	0.032
4031	4041-4044-4051	1	Distance Relay (Mho)	0.032	81.469	0.016	0.046	81.835	0.023	0.075	82.761	0.037
4031	4041-4044-4051	2	Distance Relay (Mho)	0.032	81.469	0.016	0.046	81.835	0.023	0.075	82.761	0.037
4032	4042-4043-4046	1	Distance Relay (Mho)	0.033	75.964	0.016	0.044	76.4035	0.022	0.058	77.9190	0.029
4032	4044-4043-4046	1	Distance Relay (Mho)	0.040	83.157	0.020	0.052	83.2007	0.026	0.062	83.3760	0.031
4041	4044-4043-4046	1	Distance Relay (Mho)	0.024	84.289	0.012	0.032	84.2894	0.016	0.042	84.2894	0.021
4041	4061-4062-4063	1	Distance Relay (Mho)	0.009	82.405	0.005	0.049	82.559	0.025	0.072	83.094	0.036
4042	4044-4045-4062	1	Distance Relay (Mho)	0.016	84.289	0.008	0.024	84.289	0.012	0.056	83.682	0.028
4042	4043-4046-4047	1	Distance Relay (Mho)	0.012	82.405	0.006	0.017	82.626	0.008	0.028	83.480	0.014

C2: Mho Distance Relay (DISTR1) dynamic model codes

4047 'DISTR1' 4043 1 1 1 1 0 0 0 0 0 0 0 0 0 0 2.5 0.016079 84.28941 0.008039 15 0.018089776 84.2894 0.009044888 30 0.046073 86.765 0.0230365 0 1 2.5 0 0 0 0 0 0 0 0 0/
4011 'DISTR1' 4021 1 1 1 1 0 0 0 0 0 0 0 0 0 0 2.5 0.012026637 86.18592517 0.006013319 15 0.068545465 84.2894 0.034272732 30 0.111602053 81.113 0.055801026 0 1 2.5 0 0 0 0 0 0 0 0 0/
4011 'DISTR1' 4022 1 1 1 1 0 0 0 0 0 0 0 0 0 0 2.5 0.040199502 84.28940686 0.020099751 15 0.048239403 84.2894 0.024119701 30 0.08848 84.0317 0.04424 0 1 2.5 0 0 0 0 0 0 0 0 0/
4012 'DISTR1' 4022 1 1 1 1 0 0 0 0 0 0 0 0 0 0 2.5 0.028182264 83.48019825 0.014091132 15 0.043267 83.63 0.0216335 30 0.115849 83.059 0.0579245 0 1 2.5 0 0 0 0 0 0 0 0 0/
4021 'DISTR1' 4032 1 1 1 1 0 0 0 0 0 0 0 0 0 0 2.5 0.032159602 84.28940686 0.016079801 15 0.048374 82.875 0.0096748 30 0.082975 74.61 0.0414875 0 1 2.5 0 0 0 0 0 0 0 0 0/
4022 'DISTR1' 4031 1 1 1 1 0 0 0 0 0 0 0 0 0 0 2.5 0.032159602 84.28940686 0.016079801 15 0.048289002 83.8171 0.024144501 30 0.089702 82.8274 0.044851 0 1 2.5 0 0 0 0 0 0 0 0 0/
4022 'DISTR1' 4031 2 1 1 1 0 0 0 0 0 0 0 0 0 0 2.5 0.032159602 84.28940686 0.016079801 15 0.048289002 83.8171 0.024144501 30 0.089702 82.8274 0.044851 0 1 2.5 0 0 0 0 0 0 0 0 0/
4031 'DISTR1' 4032 1 1 1 1 0 0 0 0 0 0 0 0 0 0 2.5 0.0080399 84.28940686 0.00401995 15 0.020121 83.7227 0.0100605 30 0.064426 83.4045 0.032213 0 1 2.5 0 0 0 0 0 0 0 0 0/
4031 'DISTR1' 4041 1 1 1 1 0 0 0 0 0 0 0 0 0 0 2.5 0.032357997 81.46923439 0.016178999 15 0.046471 81.835 0.0232355 30 0.074595 82.7607 0.0372975 0 1 2.5 0 0 0 0 0 0 0 0 0/
4031 'DISTR1' 4041 2 1 1 1 0 0 0 0 0 0 0 0 0 0 2.5 0.032357997 81.46923439 0.016178999 15 0.046471 81.835 0.0232355 30 0.074595 82.7607 0.0372975 0 1 2.5 0 0 0 0 0 0 0 0 0/
4032 'DISTR1' 4042 1 1 1 1 0 0 0 0 0 0 0 0 0 0 2.5 0.032984845 75.96375653 0.016492423 15 0.044257605 76.4035 0.022128803 30 0.0583 77.9190 0.02915 0 1 2.5 0 0 0 0 0 0 0 0 0/
4032 'DISTR1' 4044 1 1 1 1 0 0 0 0 0 0 0 0 0 0 2.5 0.040286971 83.15722659 0.020143485 15 0.0524 83.2007 0.0262 30 0.0624 83.3760 0.0312 0 1 2.5 0 0 0 0 0 0 0 0 0/
4041 'DISTR1' 4044 1 1 1 1 0 0 0 0 0 0 0 0 0 0 2.5 0.024119701 84.28940686 0.012059851 15 0.0322 84.2894 0.0161 30 0.0422 84.2894 0.0211 0 1 2.5 0 0 0 0 0 0 0 0 0/
4041 'DISTR1' 4061 1 1 1 1 0 0 0 0 0 0 0 0 0 0 2.5 0.009079648 82.40535663 0.004539824 15 0.049416

82.5586 0.024708 30 0.071519 83.0936 0.0357595 0 1 2.5 0 0 0 0 0 0 0 0 0 0/
4042 'DISTR1' 4044 1 1 1 1 0 0 0 0 0 0 0 0 0 0 2.5 0.016079801 84.28940686 0.0080399 15 0.02412 84.2894 0.01206 30 0.056342 83.6823 0.028171 0 1 2.5 0 0 0 0 0 0 0 0 0 0/
4042 'DISTR1' 4043 1 1 1 1 0 0 0 0 0 0 0 0 0 0 2.5 0.012106 82.402 0.006053 15 0.016537411 82.62623 0.0082687 30 0.02818 83.48 0.01409 0 1 2.5 0 0 0 0 0 0 0 0 0 0/

Appendix D

Solar PV Plants Models

All of the parameters in the PV models except the irradiance and the rated power are based on [35].

<u>D1: Plant 101</u>

101 'USRMDL' 1 'PVGU1' 101 1 0 9 3 3 0.20000E-01 0.20000E-01 0.40000 0.90000 1.1100 1.2000 2.0000 2.0000 0.20000E-01 /
101 'USRMDL' 1 'PVEU1' 102 0 4 24 10 4 101 0 1 0 0.15000 18.000 5.0000 0.50000E-01 0.10000 0.0000 0.80000E-01 0.2856 -0.2856 1.1000 0.0000 0.50000 -0.50000 0.50000E-01 0.10000 0.90000 1.1000 120.00 0.50000E-01 0.50000E-01 1.7000 1.1100 1.1100 600/
101 'USRMDL' 1 'PANELU1' 103 0 0 5 0 1 0.5 0.95 1 1 1/
101 'USRMDL' 1 'IRRADU1' 104 0 1 20 0 1 1 1 700 60 700 130 700 250 700 320 700 399 700 490 700 590 700 690 700 850 700/

<u>D2: Plant 102</u>

102 'USRMDL' 1 'PVGU1' 101 1 0 9 3 3 0.20000E-01 0.20000E-01 0.40000 0.90000 1.1100 1.2000 2.0000 2.0000 0.20000E-01 /
102 'USRMDL' 1 'PVEU1' 102 0 4 24 10 4 102 0 1 0 0.15000 18.000 5.0000 0.50000E-01 0.10000 0.0000 0.80000E-01 0.2856 -0.2856 1.1000 0.0000 0.50000 -0.50000 0.50000E-01 0.10000 0.90000 1.1000 120.00 0.50000E-01 0.50000E-01 1.7000 1.1100 1.1100 600/
102 'USRMDL' 1 'PANELU1' 103 0 0 5 0 1 0.5 0.95 1 1 1/
102 'USRMDL' 1 'IRRADU1' 104 0 1 20 0 1 1 1 700 60 700 130 700 250 700 320 700 399 700 490 700 590 700 690 700 850 700/

<u>D3: Plant 103</u>

103 'USRMDL' 1 'PVGU1' 101 1 0 9 3 3 0.20000E-01 0.20000E-01 0.40000 0.90000 1.1100 1.2000 2.0000 2.0000 0.20000E-01 /
103 'USRMDL' 1 'PVEU1' 102 0 4 24 10 4 103 0 1 0 0.15000 18.000 5.0000 0.50000E-01 0.10000 0.0000 0.80000E-01 0.2856 -0.2856 1.1000 0.0000 0.50000 -0.50000 0.50000E-01 0.10000 0.90000 1.1000 120.00 0.50000E-01 0.50000E-01 1.7000 1.1100 1.1100 600/
103 'USRMDL' 1 'PANELU1' 103 0 0 5 0 1 0.5 0.95 1 1 1/
103 'USRMDL' 1 'IRRADU1' 104 0 1 20 0 1 1 1 700 60 700 130 700 250 700 320 700 399 700 490 700 590 700 690 700 850 700/

<u>D4: Plant 104</u>

104 'USRMDL' 1 'PVGU1' 101 1 0 9 3 3 0.20000E-01 0.20000E-01 0.40000 0.90000 1.1100 1.2000 2.0000 2.0000 0.20000E-01 /
104 'USRMDL' 1 'PVEU1' 102 0 4 24 10 4 104 0 1 0 0.15000 18.000 5.0000 0.50000E-01 0.10000 0.0000 0.80000E-01 0.2856 -0.2856 1.1000 0.0000 0.50000 -0.50000 0.50000E-01 0.10000 0.90000 1.1000 120.00 0.50000E-01 0.50000E-01 1.7000 1.1100 1.1100 600/
104 'USRMDL' 1 'PANELU1' 103 0 0 5 0 1 0.5 0.95 1 1 1/
104 'USRMDL' 1 'IRRADU1' 104 0 1 20 0 1 1 1 700 60 700 130 700 250 700 320 700 399 700 490 700 590 700 690 700 850 700/

D5: Plant 105

105 'USRMDL' 1 'PVGU1' 101 1 0 9 3 3 0.20000E-01 0.20000E-01 0.40000 0.90000 1.1100 1.2000 2.0000 2.0000 0.20000E-01 /
105 'USRMDL' 1 'PVEU1' 102 0 4 24 10 4 105 0 1 0 0.15000 18.000 5.0000 0.50000E-01 0.10000 0.0000 0.80000E-01 0.2856 -0.2856 1.1000 0.0000 0.50000 -0.50000 0.50000E-01 0.10000 0.90000 1.1000 120.00 0.50000E-01 0.50000E-01 1.7000 1.1100 1.1100 600/
105 'USRMDL' 1 'PANELU1' 103 0 0 5 0 1 0.5 0.95 1 1 1/
105 'USRMDL' 1 'IRRADU1' 104 0 1 20 0 1 1 1 700 60 700 130 700 250 700 320 700 399 700 490 700 590 700 690 700 850 700/

D6: Plant 106

106 'USRMDL' 1 'PVGU1' 101 1 0 9 3 3 0.20000E-01 0.20000E-01 0.40000 0.90000 1.1100 1.2000 2.0000 2.0000 0.20000E-01 /
106 'USRMDL' 1 'PVEU1' 102 0 4 24 10 4 106 0 1 0 0.15000 18.000 5.0000 0.50000E-01 0.10000 0.0000 0.80000E-01 0.2856 -0.2856 1.1000 0.0000 0.50000 -0.50000 0.50000E-01 0.10000 0.90000 1.1000 120.00 0.50000E-01 0.50000E-01 1.7000 1.1100 1.1100 600/
106 'USRMDL' 1 'PANELU1' 103 0 0 5 0 1 0.5 0.95 1 1 1/
106 'USRMDL' 1 'IRRADU1' 104 0 1 20 0 1 1 1 700 60 700 130 700 250 700 320 700 399 700 490 700 590 700 690 700 850 700/

Appendix E

Irradiance Values

The Irradiance data has been obtained from [45].

Table E1: Irradiance Values in the Southern Part of Sweden

South of Sweden			Seconds									
Month	Time	e Irradiance	0-50	50-100	100-150	150-200	250-300	300-350	350-400	400-450	450-500	500-550
June	6	387.5	397.1875	362.3125	170.5	381.6875	378.78125	274.15625	515.375	502.78125	351.65625	510.53125
June	9	637.5	653.4375	596.0625	280.5	627.9375	623.15625	451.03125	847.875	827.15625	578.53125	839.90625
June	12	687.5	704.6875	642.8125	302.5	677.1875	672.03125	486.40625	914.375	892.03125	623.90625	905.78125
June	15	412.5	422.8125	385.6875	181.5	406.3125	403.21875	291.84375	548.625	535.21875	374.34375	543.46875
June	18	75	76.875	70.125	33	73.875	73.3125	53.0625	99.75	97.3125	68.0625	98.8125
June	21	0	15.375	14.025	6.6	14.775	14.6625	10.6125	19.95	19.4625	13.6125	19.7625
March	6	87.5	89.6875	81.8125	38.5	86.1875	85.53125	61.90625	116.375	113.53125	79.40625	115.28125
March	9	280	320.3125	292.1875	137.5	307.8125	305.46875	221.09375	415.625	405.46875	283.59375	411.71875
March	12	375	384.375	350.625	165	369.375	366.5625	265.3125	498.75	486.5625	340.3125	494.0625
March	15	162.5	166.5625	151.9375	71.5	160.0625	158.84375	114.96875	216.125	210.84375	147.46875	214.09375
March	18	0	0	0	0	0	0	0	0	0	0	0
March	21	0	0	0	0	0	0	0	0	0	0	0
September	6	150	153.75	140.25	66	147.75	146.625	106.125	199.5	194.625	136.125	197.625
September	9	400	410	374	176	394	391	283	532	519	363	527
September	12	412.5	422.8125	385.6875	181.5	406.3125	403.21875	291.84375	548.625	535.21875	374.34375	543.46875
September	15	175	179.375	163.625	77	172.375	171.0625	123.8125	232.75	227.0625	158.8125	230.5625
September	18	0	0	0	0	0	0	0	0	0	0	0
September	21	0	0	0	0	0	0	0	0	0	0	0
December	9	40	41	37.4	17.6	39.4	39.1	28.3	53.2	51.9	36.3	52.7
December	12	40	41	37.4	17.6	39.4	39.1	28.3	53.2	51.9	36.3	52.7

Table E2: Irradiance Values in the Northern Part of Sweden

North of Sweden			Seconds									
Month	Time	e Irradiance	0-50	50-100	100-150	150-200	250-300	300-350	350-400	400-450	450-500	500-550
June	6	400	410	374	176	394	391	283	532	519	363	527
June	9	587.5	602.1875	549.3125	258.5	578.6875	574.28125	415.65625	781.375	762.28125	533.15625	774.03125
June	12	550	563.75	514.25	242	541.75	537.625	389.125	731.5	713.625	499.125	724.625
June	15	375	384.375	350.625	165	369.375	366.5625	265.3125	498.75	486.5625	340.3125	494.0625
June	18	137.5	140.9375	128.5625	60.5	135.4375	134.40625	97.28125	182.875	178.40625	124.78125	181.15625
June	21	15	15.375	14.025	6.6	14.775	14.6625	10.6125	19.95	19.4625	13.6125	19.7625
March	6	75	76.875	70.125	33	73.875	73.3125	53.0625	99.75	97.3125	68.0625	98.8125
March	9	312.5	320.3125	292.1875	137.5	307.8125	305.46875	221.09375	415.625	405.46875	283.59375	411.71875
March	12	300	307.5	280.5	132	295.5	293.25	212.25	399	389.25	272.25	395.25
March	15	112.5	115.3125	105.1875	49.5	110.8125	109.96875	79.59375	149.625	145.96875	102.09375	148.21875
March	18	0	0	0	0	0	0	0	0	0	0	0
March	21	0	0	0	0	0	0	0	0	0	0	0
September	6	137.5	140.9375	128.5625	60.5	135.4375	134.40625	97.28125	182.875	178.40625	124.78125	181.15625
September	9	325	333.125	303.875	143	320.125	317.6875	229.9375	432.25	421.6875	294.9375	428.1875
September	12	325	333.125	303.875	143	320.125	317.6875	229.9375	432.25	421.6875	294.9375	428.1875
September	15	137.5	140.9375	128.5625	60.5	135.4375	134.40625	97.28125	182.875	178.40625	124.78125	181.15625
September	18	0	0	0	0	0	0	0	0	0	0	0
September	21	0	0	0	0	0	0	0	0	0	0	0
December	All	0	0	0	0	0	0	0	0	0	0	0

Appendix F

Reactive Compensators

All of the parameters in the STATCOM and SVC models except the rated power are based on [41] and [39] respectively.

F1: STATCOM Model

STATCOM model parameters is shown in the below Table followed by the dynamic model codes:

STATCOM Parameters	
Parameter	Value
T1 (S)	0.1
T2 (S)	0.1
T3 (S)	0.1
T4 (S)	0.1
K	25
Droop	0
Vmax	999
Vmin	-999
IcMax (PU)	1.25
Ilmax (PU)	1.25
Vcutout (pu)	0.2
Elimit (PU)	1.2
Xt (PU)	0.1
Acc	0.5
STBASE (Mvar)	300

'FACTS 1' 'CSTCNT' 0 0.1 0.1 0.1 0.1 25 0 999 -999 1.25 1.25 0.2 1.2 0.1 0.5 300/

'FACTS 2' 'CSTCNT' 0 0.1 0.1 0.1 0.1 25 0 999 -999 1.25 1.25 0.2 1.2 0.1 0.5 300/

'FACTS 3' 'CSTCNT' 0 0.1 0.1 0.1 0.1 25 0 999 -999 1.25 1.25 0.2 1.2 0.1 0.5 300/

'FACTS 4' 'CSTCNT' 0 0.1 0.1 0.1 0.1 25 0 999 -999 1.25 1.25 0.2 1.2 0.1 0.5 300/

'FACTS 5' 'CSTCNT' 0 0.1 0.1 0.1 0.1 25 0 999 -999 1.25 1.25 0.2 1.2 0.1 0.5 300/

Where FACTS 1, 2, 3, 4 and 5 are the names of the FACTS devices in the network data which corresponds to the buses 1041, 43, 46, 61 and 62.

F2: SVC Models

The model codes for Static Var compensators are shown below:

1041 'CSSCST' 0 52500 0 0 2.4 0 0.01 0 0 2/

43 'CSSCST' 0 52500 0 0 2.4 0 0.01 0 0 2/

46 'CSSCST' 0 52500 0 0 2.4 0 0.01 0 0 2/

61 'CSSCST' 0 52500 0 0 2.4 0 0.01 0 0 2/

62 'CSSCST' 0 52500 0 0 2.4 0 0.01 0 0 2/